


รายงานวิจัยฉบับสมบูรณ์

โครงการ การศึกษาการเร่งปฏิกิริยาการสลายพันธะระหว่างคาร์บอนและออกซิเจนในปฏิกิริยาไฮโดรเจนโนไลซิสของแอริลอีเทอร์ด้วยตัวเร่งปฏิกิริยานิกเกิลโดยวิธีทางเคมีคำนวณเพื่อหาความเป็นไปได้ในการย่อยสลายสารชีวมวลลิกนิน

Mechanistic Study of Nickel-Catalyzed C-O Bond Activation in Hydrogenolysis of Aryl Ethers by Density Functional Theory: A Potential Application for Lignin Degradation of Biomass

โดย ผศ.ดร.พนิดา สุรวัฒนาวงศ์

มิถุนายน 2557

สัญญาเลขที่ MRG5580117

รายงานวิจัยฉบับสมบูรณ์

โครงการ การศึกษาการเร่งปฏิกิริยาการสลายพันธะระหว่างคาร์บอนและออกซิเจนในปฏิกิริยาไฮโดรเจนโนไลซิสของแอริลอีเทอร์ด้วยตัวเร่งปฏิกิริยานิกเกิลโดยวิธีทางเคมีคำนวณเพื่อหาความเป็นไปได้ในการย่อยสลายสารชีวมวลลิกนิน

Mechanistic Study of Nickel-Catalyzed C-O Bond Activation in Hydrogenolysis of Aryl Ethers by Density Functional Theory: A Potential Application for Lignin Degradation of Biomass

ผศ.ดร.พนิดา สุรวัฒนาวงศ์
ภาควิชาเคมี คณะวิทยาศาสตร์ มหาวิทยาลัยมหิดล

สนับสนุนโดยสำนักงานกองทุนสนับสนุนการวิจัย

ABSTRACT

Project Code: MRG5580117

Project Title: Mechanistic Study of Nickel-Catalyzed C-O Bond Activation in Hydrogenolysis of Aryl Ethers by Density Functional Theory: A Potential Application for Lignin Degradation of Biomass

Investigator: Assist. Prof. Panida Surawatanawong
Department of Chemistry, Faculty of Science, Mahidol University
E-mail: panida.sur@mahidol.ac.th

Project Period: 2 years

Catalysts for aromatic C-O bond activation can be of potentially used for lignin degradation process. We investigated the mechanisms for the hydrogenolysis C-O bond activation of diphenyl ether by the nickel complex with *N*-heterocyclic carbene (SIPr) to obtain benzene and phenol as products. According to the calculation, the $Ni(COD)_2$ precursor undergoes SIPr ligand substitution to form Ni(SIPr)(η^6-PhOPh), which can easily rearrange to Ni(SIPr)(η^2-PhOPh), the active species for C-O bond activation.

The catalytic reaction includes three basic steps: (i) oxidative addition of Ni(SIPr)(η^2-PhOPh) to form $[Ni(SIPr)(OPh)(Ph)]^0$, (ii) σ-bond metathesis, in which H_2 binds to the nickel to form $[Ni(SIPr)(OPh)(Ph)(H_2)]^0$, then the phenol (or benzene) is eliminated, and (iii) reductive elimination of the benzene (or phenol) and binding of PhOPh to regenerate Ni(SIPr)(η^2-PhOPh). Diphenyl ether is not only a substrate but also serves as ligand to stabilize Ni-SIPr complex. The rate determining step is found at the oxidative addition (+24 kcal/mol).

The oxidative addition step was calculated for diaryl ether with trifluoromethyl electron withdrawing group ($PhOC_6H_4CF_3$). According to the free energy barrier, the C-O bond activation at the carbon adjacent to the aryl ring with electron withdrawing substituent is favorable, in agreement with the experiment that the major products are phenol and trifluoromethylbenzene. The hydrogenation products, e.g., cyclohexane, cyclohexadiene, were not observed in the experiment. We also showed that the hydrogenation of benzene via Ni(SIPr)(η^2-C_6H_6) requires high energy barrier (+40 kcal/mol).

Keywords: Nickel, N-Heterocyclic Carbene, C-O Bond Activation, Hydrogenolysis, Density Functional Theory,

บทคัดย่อ

รหัสโครงการ: MRG5580117

ชื่อโครงการ: การศึกษาการเร่งปฏิกิริยาการสลายพันธะระหว่างคาร์บอนและออกซิเจนในปฏิกิริยาไฮโดรเจนโนไลซิสของแอริลอีเทอร์ด้วยตัวเร่งปฏิกิริยานิกเกิลโดยวิธีทางเคมีคำนวณเพื่อหาความเป็นไปได้ในการย่อยสลายสารชีวมวลลิกนิน

ชื่อนักวิจัย: ผศ.ดร.พนิดา สุรวัฒนาวงศ์
ภาควิชาเคมี คณะวิทยาศาสตร์ มหาวิทยาลัยมหิดล

อีเมล์: panida.sur@mahidol.ac.th

ระยะเวลาโครงการ: 2 ปี

การศึกษาการเร่งปฏิกิริยาสลายพันธะระหว่างคาร์บอนและออกซิเจนสามารถนำไปสู่ประโยชน์ในการย่อยสลายสารชีวมวลลิกนินได้ เราได้ศึกษากลไกการเกิดปฏิกิริยาไฮโดรเจนโนไลซิสของไดฟีนิลอีเทอร์ให้เป็นเบนซีนกับฟีนอลด้วยตัวเร่งปฏิกิริยาสารเชิงซ้อนนิกเกิลกับเอ็นเฮเทอโรไซคลิกคาร์บีนลิแกนด์ (SIPr) จากการศึกษาคำนวณพบว่า ตัวเริ่มต้น $Ni(COD)_2$ สามารถแลกเปลี่ยนลิแกนด์กับ SIPr เกิดเป็น Ni(SIPr)(η^6-PhOPh) ซึ่งสามารถเปลี่ยนเป็น Ni(SIPr)(η^2-PhOPh) ได้ง่าย โดย Ni(SIPr)(η^2-PhOPh) เป็นโมเลกุลสำคัญต่อการสลายพันธะ C-O

กระบวนการเร่งปฏิกิริยามีสามขั้น คือ (i) ออกซิเดทีฟแอดดิชัน (oxidative addition) ของ Ni(SIPr)(η^2-PhOPh) เกิดเป็น $[Ni(SIPr)(OPh)(Ph)]^0$, (ii) ซิกมาบอนด์เมตาเทซิส (σ-bond metathesis) โดย H_2 จับกับนิกเกิลเกิดเป็น $[Ni(SIPr)(OPh)(Ph)(H_2)]^0$ จากนั้นฟีนอล (หรือเบนซีน) ถูกกำจัดออกไป, (iii) รีดักทีฟอีลิมิเนชัน (reductive elimination) ของเบนซีน (หรือฟีนอล) และจับกับไดฟีนิลอีเทอร์ เกิดเป็น Ni(SIPr)(η^2-PhOPh) อีกครั้ง จะเห็นได้ว่าไดฟีนิลอีเทอร์ไม่เพียงแต่เป็นสารตั้งต้น ยังทำทำหน้าที่ช่วยทำให้สารเชิงซ้อน Ni-SIPr มีความเสถียรด้วย เราพบว่า ขั้นกำหนดปฏิกิริยาอยู่ที่ ขั้นการเกิดออกซิเดทีฟแอดดิชัน (+24 kcal/mol)

เมื่อศึกษาเพิ่มเติมในการเกิดออกซิเดทีฟแอดดิชันของไดแอริลอีเทอร์ที่มีหมู่ไตรฟลูออโรเมทิลเป็นหมู่ดึงอิเล็กตรอน ($PhOC_6H_4CF_3$) พบว่า การสลายพันธะ C-O ที่ตำแหน่งใกล้กับวงแอริลที่หมู่ดึงอิเล็กตรอนเกิดได้ที่พลังงานต่ำกว่า สอดคล้องกับผลการทดลองที่พบผลิตภัณฑ์หลัก คือ ฟีนอลและไตรฟลูออโรเมทิลเบนซีน นอกจากนี้เราได้ศึกษาการเกิดไฮโดรจิเนชันของเบนซีน เริ่มจาก Ni(SIPr)(η^2-C_6H_6) พบว่า ปฏิกิริยาต้องข้ามผ่านพลังงานที่สูงมาก (+40 kcal/mol) จึงสอดคล้องกับผลการทดลองที่ไม่พบผลิตภัณฑ์จากการเกิดไฮโดรจิเนชัน เช่น ไซโคลเฮกซะไดอีน หรือไซโคลเฮกเซน

คำหลัก: นิกเกิล, เอ็นเฮเทอโรไซคลิกคาร์บีน, การสลายพันธะคาร์บอนออกซิเจน, ไฮโดรเจนโนไลซิส, ทฤษฎีฟังก์ชันความหนาแน่น

OBJECTIVES (วัตถุประสงค์)

The principal investigator (PI) aims to understand reaction mechanisms of the catalysts that have potential applications for alternative energy.

While the PI was conducting the study on nickel-catalyzed hydrogenolysis C-O bond activation of aryl ethers, trying to explain the reaction mechanism of this catalyst for its potential application in lignin degradation of biomass, the biocatalyst, i.e., flavoenzymes, came into attention through the collaboration with Prof. Pimchai Chaiyen. Flavoenzymes are useful as biocatalysts for chemical synthesis reactions and as bioelectrocatalysts for biofuel cell applications. Flavin derivatives were successfully used for catalytic water oxidation in a photochemical water splitting process. Understanding how flavoenzymes function is crucial to improve their applications and to develop biomimetic flavin derivatives for use as efficient biocatalysts and in biofuel cells.

With the resources funded by TRF-CHE, the PI can conduct the study on flavoenzyme reaction mechanism, in addition to the study of nickel-catalyzed hydrogenolysis C-O bond activation of aryl ethers. Density functional study was applied for both systems. Thus, there are two chapters for this research report with their objectives shown below.

CHAPTER 1: Mechanistic Study of Nickel-Catalyzed C-O Bond Activation in Hydrogenolysis of Aryl Ethers by Density Functional Theory

(1) To elucidate the most probable reaction pathways for the hydrogenolysis of aryl ethers to form aromatic and phenolic products through C-O bond activation by Ni-NHC catalyst complex.
(2) To determine the rate determining step in the catalytic reaction from the highest energy barrier in the calculated free energy profiles.

CHAPTER 2: Proton-Coupled Electron Transfer for C4a-Hydroperoxyflavin Formation and Stabilization in a Flavoenzyme

(1) To determine the role of protein side chains that involve in lowering the energy barriers and assisting in proton transfer in flavoenzymes.
(2) To understand the factors that support formation and stabilization of C4a-hydroperoxyflavin, the key intermediate for H_2O_2 elimination in flavoenzymes.

TABLE OF CONTENTS

CHAPTER 1

Mechanistic Study of Nickel-Catalyzed C-O Bond Activation in Hydrogenolysis of Aryl Ethers by Density Functional Theory

INTRODUCTION (บทนำ)

There are considerable concerns in using petroleum feedstock as a precursor in chemical industry since the crude oil resources are limited.[1] The alternate resource can be the abundant biomass, especially from agricultural wastes, as raw materials to generate chemical products. The major contents of agricultural residues are cellulose, hemicellulose, and lignin.[2] Depolymerization of these three main components plays a key role in their efficient use.

While cellulose and hemicelluloses can undergo degradation *via* hydrolysis,[3] lignin without hydrolysable linkage is more difficult to degrade and generally requires high temperature to process. Therefore, lignin degradation is the central attention for the efficient use of biomass.[4] To breakdown the highly complex structure of lignin, which is the heterogenous polymer with the diverse set of C-C and C-O cross-link units and aromatic C-O bonds,[5] the catalyst is needed to lower the processed temperature and to gain a control over the product distribution.

Catalysis of the aromatic C-O bond cleavage is significant for the conversion of lignin biomass to arene feedstocks.[6] Wenkert *et al*. first reported the cross-coupling reaction of aryl methyl ether and phenyl Grignard reagents using $NiCl_2(PPh_3)_2$ catalyst.[7] Apart from Grignard reagents,[8] other carbon nucleophiles, e.g., organozinc[9] and arylboronic reagents,[10] have been used for the C-O bond activation. Despite of being less reactive, hydrogen attracted much attention to be used as a substrate in place of the carbon nucleophile.

Hydrogenolysis of aromatic C-O bond can be done by heterogeneous Ni catalyst.[11] However, its high reactivity resulted in further hydrogenation and thus led to product mixtures of arenes and alcohols as well as cycloalkanes and cycloalkanols.[6a, 11] Recently, Sergeev and Hartwig[6b] have reported that the nickel complex with *N*-heterocyclic carbene ligand (SIPr) (Scheme 1) in the presence of NaO^tBu base can catalyze hydrogenolysis of diaryl ethers[6b] to obtain arenes and alcohols as the sole products. Diaryl ethers with electron withdrawing trifluoromethyl group showed the faster rate than unsubstituted diphenyl ether and diaryl ethers with electron donating group. In competition experiments with the presence of both diphenyl ether and 4-*tert*-butylphenyl

methyl ether, hydrogenolysis preferentially occurred for diphenyl ether (Scheme 1). This selective catalytic system presents highly promising application for degradation of lignin, which contains aromatic C-O bonds that are generally difficult to activate.

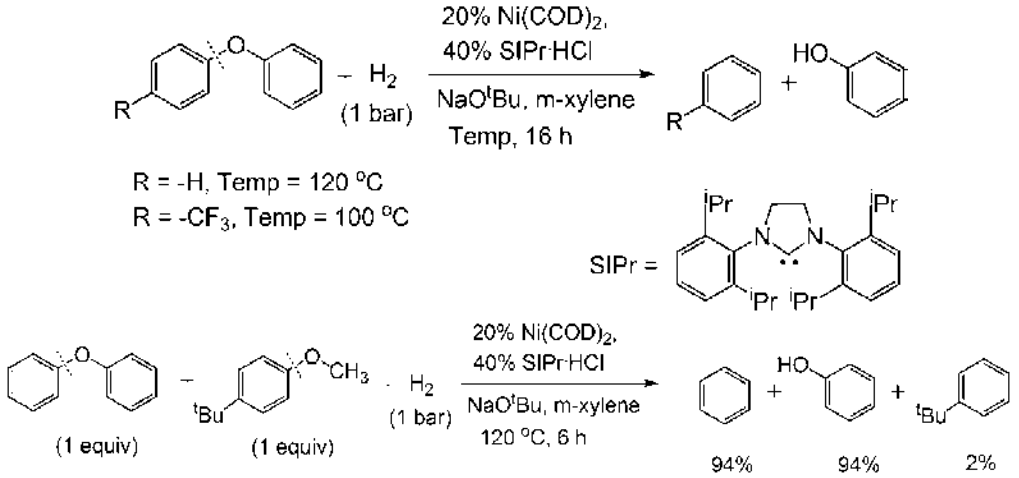

Scheme 1. Nickel catalyzed hydrogenolysis of diaryl ethers.

In complement to the experiment, density functional theory (DFT) can give insights into the reaction mechanisms of related C-O bond activation by Ni complexes.[12] Shi and coworkers[10a] have shown that $Ni(PCy_3)_2Cl_2$ can selectively activated aryl C-O bond (Ar-OAc) in a series of aryl esters to obtain the biaryl product from the arylboronic reagents although the acyl C-O bond (ArO-Ac) is weaker and normally perceived to be activated first. Liu and coworkers[13] performed density functional calculation to study the mechanisms and revealed that although the oxidative addition of ArO-Ac to the Ni^0 complex is more facile than the oxidative addition of Ar-OAc, the subsequent transmetalation step for the former requires higher energy to overcome.

In this study, we used density functional theory to study the mechanisms of the nickel complex with *N*-heterocyclic carbene (SIPr) ligand for the catalysis of hydrogenolysis C-O bond activation of diphenyl ether (PhOPh). From the $Ni(COD)_2$ precursor and the presence of SIPr ligand, the Ni(SIPr)(η^2-PhOPh) can be formed and serve as the active species for the catalytic reaction. The reaction mechanisms and the key species were investigated (Scheme 2). The catalytic cycle involves three steps: (i) oxidative addition of Ni(SIPr)(η^2-PhOPh) to form $[Ni(SIPr)(OPh)(Ph)]^0$, (ii) σ-bond

metathesis, in which H_2 binds to the nickel center and benzene is eliminated, and (iii) reductive elimination of phenol and rebinding of PhOPh to recover Ni(SIPr)(η^2-PhOPh). Understanding the reaction mechanisms of the nickel catalysts for hydrogenolysis C-O bond activation of diphenyl ether will provide guidance for the development of catalytic system to achieve the highest possible selectivity and efficiency in aromatic C-O bond activation. This can potentially apply for lignin degradation.

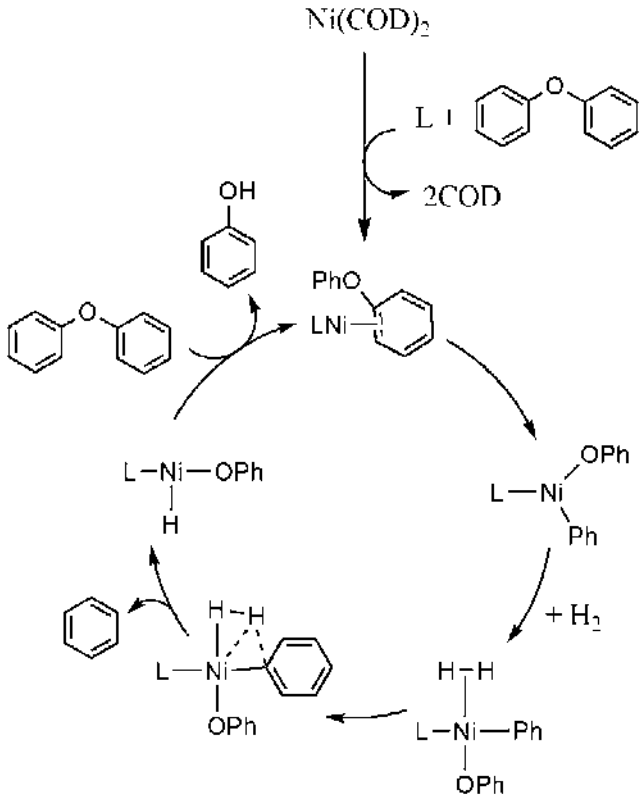

Scheme 2. Reaction mechanisms for hydrogenolysis C-O bond activation of diphenyl ether by the nickel complex with *N*-heterocyclic carbene ligand (L = SIPr).

METHODOLOGY (วิธีการทดลอง)

All calculations were performed with the Gaussian09 program.[14] All structures were fully optimized with default convergence criteria, and frequencies were calculated to ensure that there is no imaginary frequency for minima and only one imaginary frequency corresponding to the reaction coordinate for transition states. Zero-point energies and thermodynamic functions were calculated at 298.15 K and 1 atm. B3LYP[15] functional with basis set 1 (BS1) was used for all geometry optimization and frequency calculation. In BS1, Stuttgart relativistic small core (RSC) 1997 ECP basis set[16] was used for Ni; 6-31++G(d,p)[17] for N, C, O, and H on the five membered *N*-heterocyclic carbene ligand L (Scheme 1) and on the substrates, i.e., diphenyl ether and H_2; 6-31G[17] for all other atoms (the substituents on the ligand SIPr. As M06[18] has been successfully used for other Ni complex studies,[19] we carried out solvation free energy corrections by M06 with basis set 2 (BS2) on the gas-phase optimized structures using conductor-like polarizable continuum model (CPCM)[20] with Bondi atomic radii and solvation parameters corresponding to *m*-xylene (ε = 2.348). BS2 is the same as BS1 except that 6-31G(d),[17] was used for the substituents on the ligand SIPr. Unless specified otherwise, the energies mentioned throughout the article refer to the M06/BS2//B3LYP/BS1 relative free energies with solvent correction in *m*-xylene.

RESULTS AND DISCUSSION (ผลการทดลอง และ วิจารณ์ผลการทดลอง)

A. Formation of Ni(SIPr)(η^2-PhOPh) active species

In the presence of SIPr, the $Ni(COD)_2$ precursor can undergo SIPr ligand substitution to form Ni(SIPr)(COD), which is isoenergetic (-0.29 kcal/mol) (Figure 1). The structure of Ni(SIPr)(COD) shows that only one of the double bonds of COD binds to the nickel center (Figure 2). The SIPr ligand substitution on Ni(SIPr)(COD) leads to relatively stable $Ni(SIPr)_2$ (-9.63 kcal/mol). The Ni-C bond distance of $Ni(SIPr)_2$ is in good agreement with the X-ray crystal structure[21] within 0.03 Å.

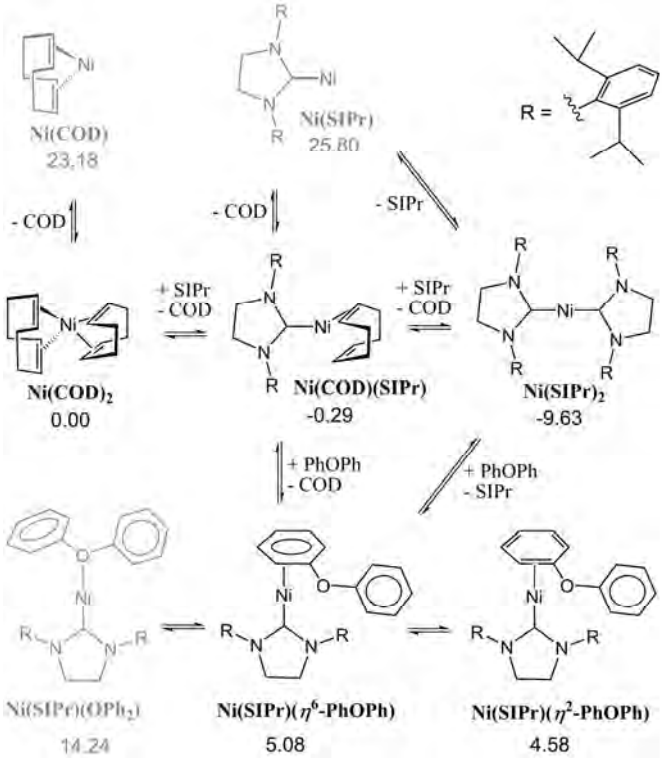

Figure 1. Formation of Ni(SIPr)(η^2-PhOPh). Solvent corrected relative free energies in *m*-xylene are given in kcal/mol.

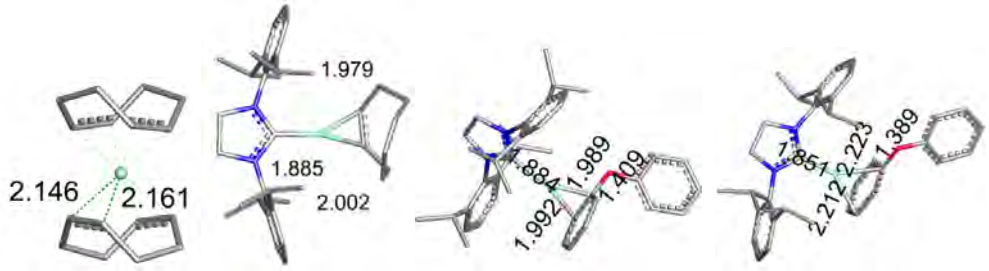

$Ni(COD)_2$ **Ni(SIPr)(COD)** **Ni(SIPr)(η^2-PhOPh)** **Ni(SIPr)(η^6-PhOPh)**

Figure 2. Selected optimized structures in the formation of Ni(SIPr)(η^2-PhOPh) from $Ni(COD)_2$ precursor. Calculated bond distances are shown in Å.

Several studies of palladium phosphine and nickel N-heterocyclic carbene[22] complexes showed that for the sterically hindered mono-dentate ligands, the oxidative addition of the substrate preferably occur on the mono-ligated metal complex rather than the di-ligated metal complex.[13, 23] Here, we tried to locate $[Ni^{II}(SIPr)_2(Ph)(OPh)]^0$ (**IN4**), the product for the oxidative addition of diphenyl ether on $Ni(SIPr)_2$, but all the attempts were not successful. Thus, the oxidative addition of diphenyl ether on $Ni(SIPr)_2$ is unlikely as the steric hindrance of SIPr hinders the substrate binding site.

Ogoshi and coworkers[24] showed that upon the addition of NHC (SIPr and IPr) in an arene solution under H_2, the hydrogenation of $Ni(COD)_2$ leads to Ni(NHC)(η^6-arene) complex, confirmed by X-ray crystal structure. While the COD dissociation from Ni(SIPr)(COD) to form Ni(SIPr) requires +26.09 kcal/mol, the diphenyl ether substitution on Ni(SIPr)(COD) to form Ni(SIPr)(η^6-PhOPh) is slightly endergonic (+5.08 kcal/mol) (Figure 1). We also explored other modes of diphenyl ether binding; O-bound Ni(SIPr)(OPh_2) has higher energy than Ni(SIPr)(η^6-PhOPh) by +9.16 kcal/mol (Figure 1) while η^2-bound Ni(SIPr)(η^2-PhOPh) has similar energy to Ni(SIPr)(η^6-PhOPh) (< 1 kcal/mol).

Therefore, from $Ni(COD)_2$, the Ni(SIPr)(η^6-PhOPh) can be formed and rearrange to Ni(SIPr)(η^2-PhOPh) to undergo C-O bond activation. Diphenyl ether is not only the substrate in the reaction but also serves as a ligand to stabilize Ni(SIPr) complex to form Ni(SIPr)(η^2-PhOPh).

B. Hydrogenolysis C-O bond activation

a) The Oxidative addition

The Ni(SIPr)(η^6-PhOPh) can rearrange to Ni(SIPr)(η^2-PhOPh), which undergo oxidative addition to form transition state **TS1** with the energy barrier of +24.01 kcal/mol, leading to $[Ni^{II}(SIPr)(Ph)(OPh)]^0$ (**IN3**) (Figure 3). The three-coordinate complex **IN3**, with the phenyl *trans* to the vacant site, can rearrange to **IN5** and **IN6**, with the phenolate and the SIPr ligand *trans* to the vacant site, respectively. Then, H_2 can bind to the vacant site of any of these three-coordinate isomers.

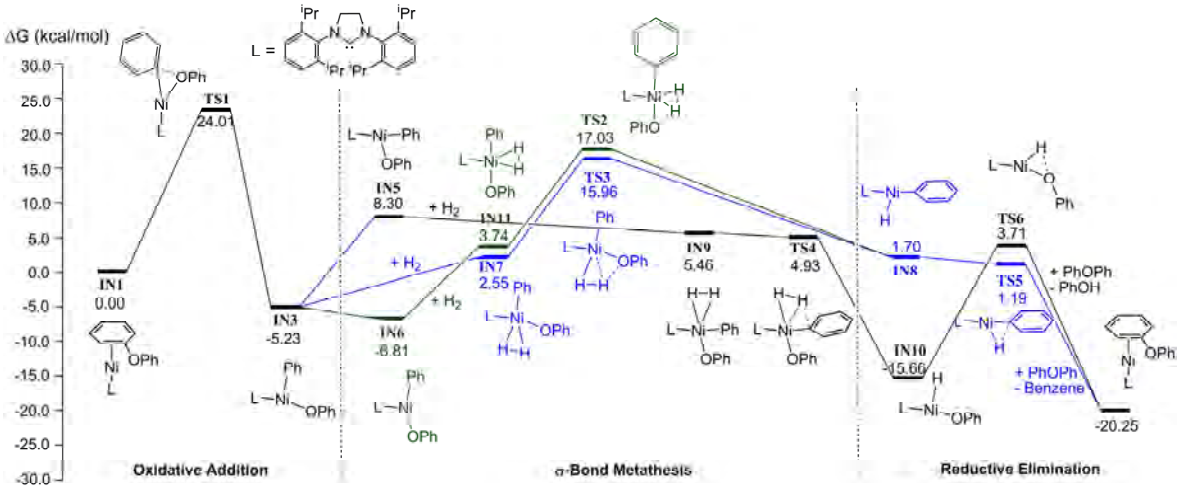

Figure 3. Free energy profiles for the overall mechanisms for the hydrogenolysis C-O bond activation of diphenyl ether. Solvent corrected relative free energies in benzene are given in kcal/mol.

b) The σ-Bond Metathesis

The H_2 binding to the vacant site of the three-coordinate complex $[Ni(SIPr)(Ph)(OPh)]^0$ (**IN3**, **IN5**, and **IN6**) leads to the H_2-complex $[Ni(H_2)(SIPr)(Ph)(OPh)]^0$ (**IN7**, **IN9**, and **IN11**) (Figure 3). Generally, dihydride complexes can be formed on the electron rich transition metal, which can provide π-backbonding to the binding H_2.[25] As expected, the dihydride complex $[Ni(H)(H)(SIPr)(Ph)(OPh)]^0$, the product from the oxidative addition of H_2 on $[Ni^{II}(SIPr)(Ph)(OPh)]^0$ is not found. Thus, we

consider the H_2-complex $[Ni(H_2)(SIPr)(Ph)(OPh)]^0$ undergo the O-H and C-H bond formations *via* σ-bond metathesis.

The H_2 binding at the vacant site of the three-coordinate complex **IN3** forms the H_2-complex **IN7**. The H_2 in **IN7** is perpendicular to the coordination plane. Nonetheless, the rotational barrier for H_2 is rather small (1-2 kcal/mol) according to the study by Eckert and coworkers[26] on metal H_2-complex. Thus, **IN7** can proceed to the σ-bond metathesis *via* transition state **TS3**, which involves a four-centered interaction (Figure 4). The O-H bond is formed and the H-H bond is weakened. Then, the T-shape nickel complex $[Ni^{II}(SIPr)(Ph)(H)]^0$ with the hydride *trans* to the empty site (**IN8**) is obtained and the phenol is eliminated as a product. The overall energy barrier is +21.19 kcal/mol. **IN3** can rearrange to slightly more stable **IN6** (-1.58 kcal/mol). Then, the H_2 binds at the vacant site *trans* to the SIPr ligand to form H_2-complex **IN11**. The σ-bond metathesis *via* **TS2** to form O-H bond also leads to the formation **IN8** with the elimination of phenol (Figure 3). The overall energy barrier (+23.84 kcal/mol) is slightly higher than that *via* **TS3**.

For **IN5**, H_2 binds at the vacant site *trans* to the phenolate to form H_2-complex **IN9**. Although the rearrangement of **IN3** to **IN5** requires the energy of +13.53 kcal/mol, the σ-bond metathesis *via* **IN9** and transition state **TS4** is facile. The C-H bond is formed and the benzene is eliminated as a product. The T-shape nickel complex $[Ni^{II}(SIPr)(OPh)(H)]^0$ with the hydride *trans* to the empty site (**IN10**) is obtained. The benzene elimination to form **IN10** is more favorable than the phenol elimination to form **IN8** by -17.36 kcal/mol, corresponding to the fact that the benzene C-H bond is stronger than the phenol O-H bond.[27]

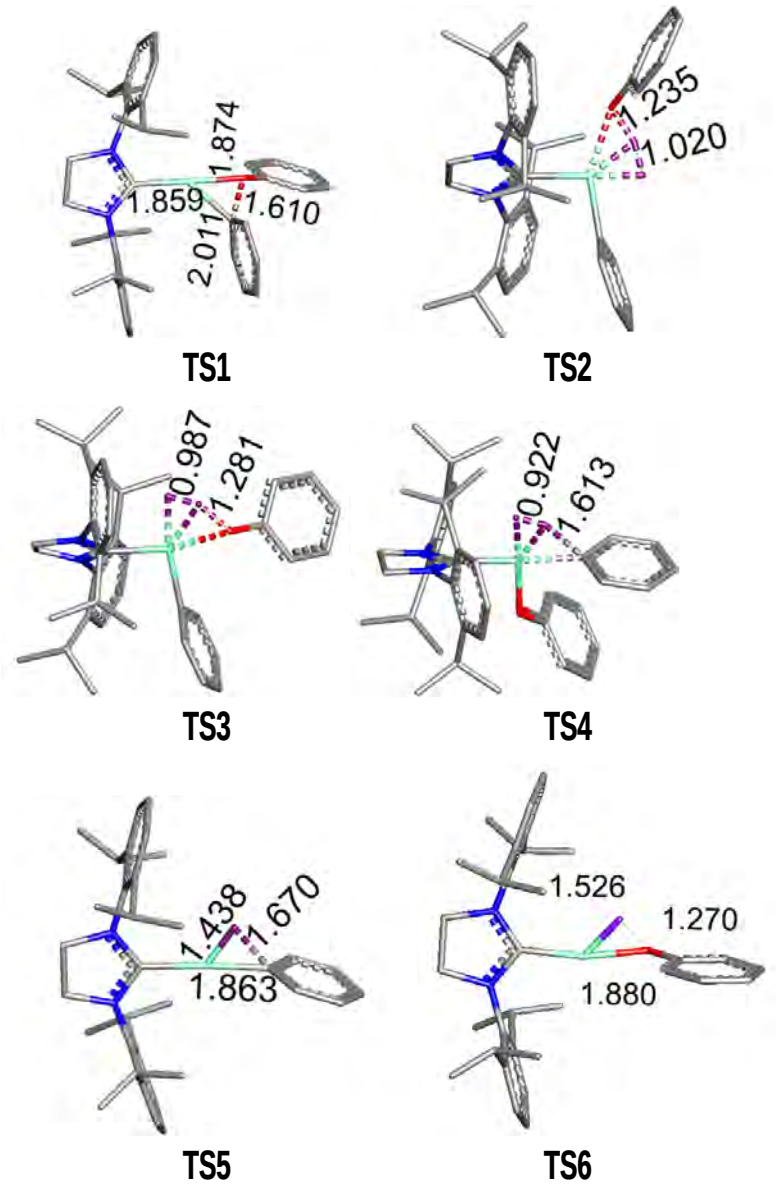

Figure 4. Selected optimized structures for hydrogenolysis C-O bond activation. Calculated bond distances are shown in Å.

c) The Reductive Elimination

The **IN8** can reductively eliminate the benzene *via* three-centered transition state **TS5**, which easily forms C-H bond and binds diphenyl ether to regenerate Ni(SIPr)(□^{2}-PhOPh) (Figure 3). On the other hand, the reductive elimination of the phenol from **IN10** *via* **TS6** requires a high energy barrier of +19.37 kcal/mol. Corresponding to the energy barriers, the structure of **TS5** represents the early transition state while the **TS6**

represents the later transition state; the C-H bond is formed with the distance of 1.67 Å in **TS5** and the O-H bond is formed with the distance of 1.26 Å in **TS6** (Figure 4).

d) The Overall Mechanism

The Ni(SIPr)(η^2-PhOPh) undergoes oxidative addition to form [Ni(SIPr)(Ph)(OPh)]^0 with the energy barrier of +24.01 kcal/mol. The three-coordinate complex with the phenyl *trans* to the vacant site (**IN3**) is obtained. The **IN3** bind H_2, proceed to σ-bond metathesis to form phenol, and reductively eliminate benzene with the highest energy barrier at the σ-bond metathesis step (+21.19 kcal/mol). Alternatively, the **IN3** can rearrange to **IN5**, the [Ni(SIPr)(Ph)(OPh)]^0 with the phenolate *trans* to the vacant site. The **IN5** binds H_2, proceed to σ-bond metathesis to form benzene, and reductively eliminate phenol with the highest energy barrier at the reductive elimination step (+19.37 kcal/mol). The overall energy barriers for both pathways *via* **IN3** and **IN5** are thus comparable. Note that, for both pathways, the O-H bond formation needs to overcome a high energy barrier (19-21 kcal/mol) while the C-H bond formation is facile. Considered the overall catalytic reaction, the oxidative addition of diphenyl ether via **TS1** is the rate determining step (Figure 2).

C. The Oxidative Addition of Diaryl Ether with Trifluoromethyl Substituent

We also calculated the oxidative addition of diaryl ethers with electron withdrawing trifluoromethyl group. According to the free energy barriers, the C-O bond activation preferably occurs at the carbon near aryl ring with electron withdrawing group (*via* **TS1-Fa**) (Figure 5), in agreement with the products from the experiment.[6b] The free energy barrier for the oxidative addition of Ni(SIPr)(η^2-PhOC$_6$H$_4$CF$_3$) via **TS1-Fa** is also lower than that of Ni(SIPr)(η^2-PhOPh) via **TS1**; Sergeev et al. showed that the reaction of diaryl ether with trifluoromethyl substituent can proceed at lower temperature than that of diphenyl ether.

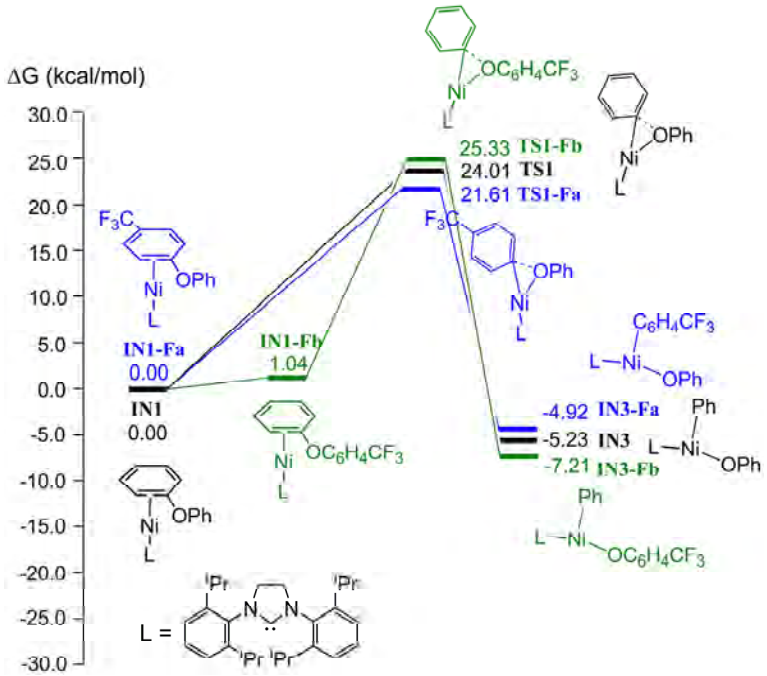

Figure 5. Free energy profiles for the oxidative addition of C-O bond of diaryl ether. Solvent corrected relative free energies in *m*-xylene are given in kcal/mol.

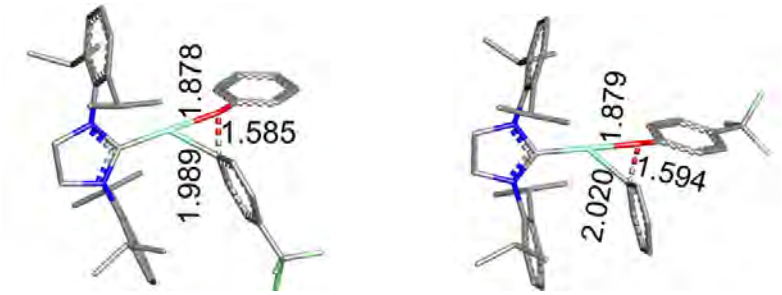

TS1-Fa **TS1-Fb**

Figure 6. Selected optimized structures for the oxidative addition of C-O bond of diaryl ether with trifluoromethyl electron withdrawing group.

D. Hydrogenation of Benzene

The benzene, which is the product of the hydrogenolysis C-O bond activation of methyl phenyl ether, can bind to the nickel to form Ni(SIPr)(η^6-C_6H_6) and Ni(SIPr)(η^2-C_6H_6). Unlike heterogenous Ni catalyst, the hydrogenation products, e.g., cyclohexadiene, cyclohexane, are not observed for Ni-SIPr.[6b] Thus, we explored further for the hydrogenation of Ni(SIPr)(η^2-C_6H_6).

The H_2 binding leads to the [Ni^0(SIPr)(H_2)(η^2-C_6H_6)] (**INH3**), which is +8.42 kcal/mol less favorable than Ni(SIPr)(η^2-C_6H_6) (Figure 7). Then, the H on the Ni center of [Ni^0(SIPr)(H_2)(η^2-C_6H_6)] transfers to the *ipso*-carbon of the benzene in *via* **TSH2** with the energy barrier of +26.98 kcal/mol. The ipso C-H bond distance in the transition state **TSH2** is shortened by -0.92Å from that of **INH3** (Figure 8). The **INH4** is formed, in isoenergetic (< 1 kcal/mol) with **TSH2**.

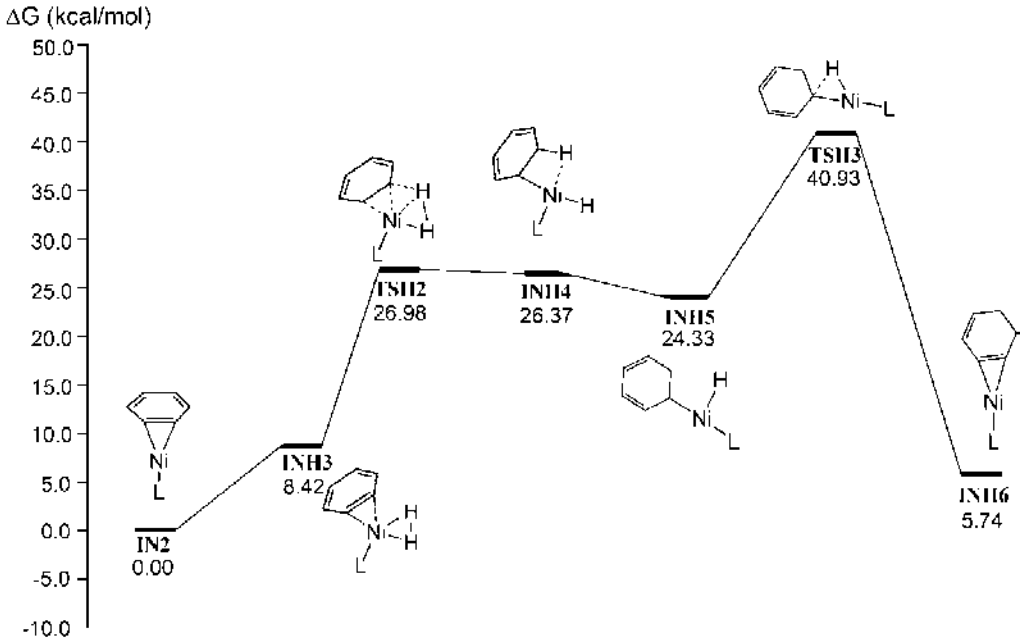

Figure 7. Free energy profiles for the hydrogenation of benzene. Solvent corrected relative free energies in *m*-xylene are given in kcal/mol.

The **INH4** can isomerize to **INH5** (Figure 7), which is more stable by -2.04 kcal/mol. Then, the second H on the Ni of **INH5** transfers to the *ipso*-carbon in the transition state **TSH3** with the energy barrier of +16.60 kcal/mol, relative **to INH5** to generate the [Ni^0(SIPr)(η^2-C_6H_8)] (**INH6**). The overall reaction is endergonic by +5.74 kcal/mol and it needs to overcome the overall energy barrier of +40.93 kcal/mol. Thus, the hydrogenation of benzene on Ni-SIPr to form cyclohexadiene requires a rather high energy; it is unlikely to occur. This is in corresponding to the experiment where only benzene and phenol were obtained as the products.

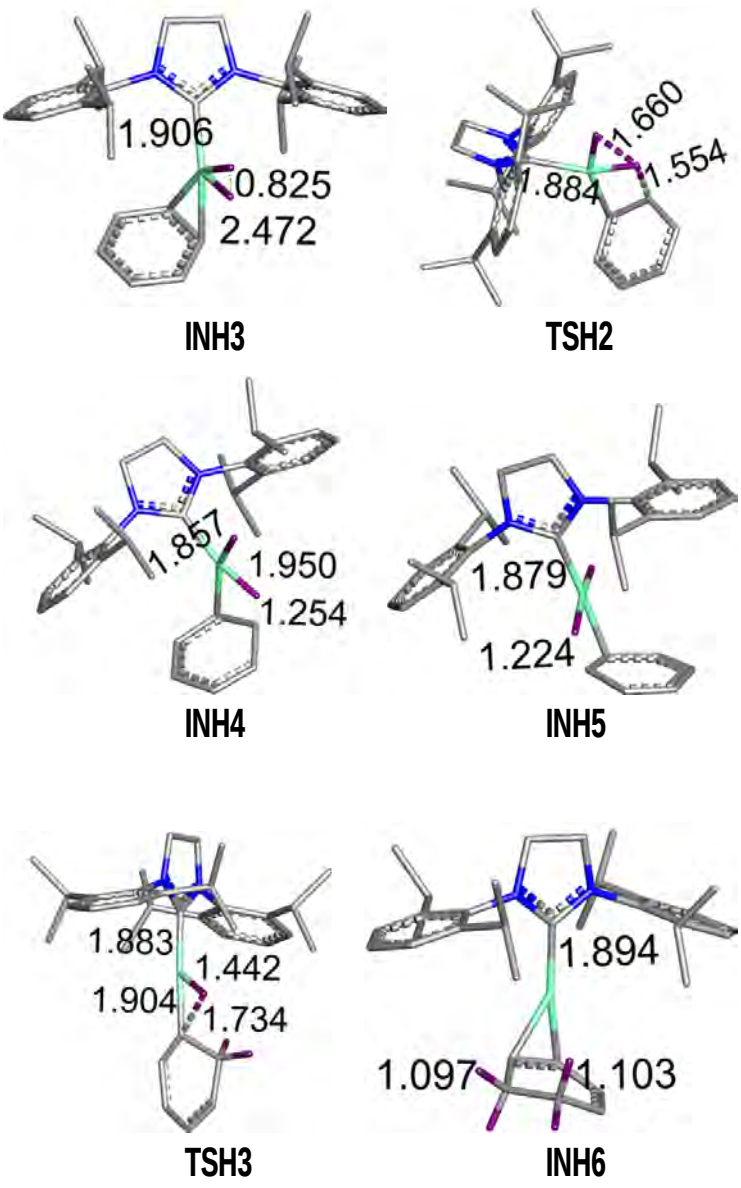

Figure 8. Selected optimized structures for the hydrogenation of benzene on Ni-SIPr. Calculated bond distances are shown in Å.

SUMMARY (สรุปผลการทดลอง)

We investigated the mechanisms for the hydrogenolysis C-O bond activation of diphenyl ether by the nickel complex with *N*-heterocyclic carbene (SIPr) to obtain benzene and phenol as products. According to the calculation, the $Ni(COD)_2$ precursor undergoes SIPr ligand substitution to form Ni(SIPr)(η^6-PhOPh), which can easily rearrange to Ni(SIPr)(η^2-PhOPh), the active species for C-O bond activation. The catalytic reaction includes three basic steps: (i) oxidative addition of Ni(SIPr)(η^2-PhOPh) to form $[Ni(SIPr)(OPh)(Ph)]^0$, (ii) σ-bond metathesis, in which H_2 binds to the nickel to form $[Ni(SIPr)(OPh)(Ph)(H_2)]^0$, then the phenol (or benzene) is eliminated, and (iii) reductive elimination of the benzene (or phenol) and binding of PhOPh to regenerate Ni(SIPr)(η^2-PhOPh).

Diphenyl ether is not only a substrate but also serves as ligand to stabilize Ni-SIPr complex. The rate determining step is found at the oxidative addition (+24 kcal/mol), in agreement with the experiment that the substrate with electron withdrawing substituent on the aryl ring can undergo the catalytic reaction faster than unsubstituted aryl ether. We also showed that the hydrogenation of benzene via Ni(SIPr)(η^2-C_6H_6) requires high energy barrier (+40 kcal/mol), in corresponding to the experiment that the hydrogenation products, e.g., cyclohexane, cyclohexadiene, were not observed.

SUGGESTIONS (ข้อเสนอแนะ)

From the experiment by Sergeev et al.,[6b] high loading of nickel precursor and SIPr ligand (10-20%) need to be used to complete the reaction at 100-120 ^{o}C. Our calculation suggested that high loading of the catalyst can be due to the formation and accumulation of rather stable Ni(SIPr)$_2$ complex which cannot undergo C-O bond activation. Although, the active species, Ni(SIPr)(η^2-PhOPh) is less stable than Ni(SIPr)$_2$, the formation of Ni(SIPr)(η^2-PhOPh) is feasible (~14 kcal/mol, Figure 1). This is not efficient for the catalytic reaction. Therefore, if we can avoid the formation of Ni(SIPr)$_2$, for example, by using Ni(SIPr)(η^6-Benzene) as a starting catalyst, we may generate more active species and require lower catalyst loading.

REFERENCES (บรรณานุกรม)

1. Shafiee, S.; Topal, E., When will fossil fuel reserves be diminished? *Energy Policy* **2009,** *37* (1), 181-189.

2. Himmel, M. E.; Ding, S.-Y.; Johnson, D. K.; Adney, W. S.; Nimlos, M. R.; Brady, J. W.; Foust, T. D., Biomass Recalcitrance: Engineering Plants and Enzymes for Biofuels Production. *Science* **2007,** *315* (5813), 804-807.

3. Quinlan, R. J.; Sweeney, M. D.; Lo Leggio, L.; Otten, H.; Poulsen, J.-C. N.; Johansen, K. S.; Krogh, K. B. R. M.; Jorgensen, C. I.; Tovborg, M.; Anthonsen, A.; Tryfona, T.; Walter, C. P.; Dupree, P.; Xu, F.; Davies, G. J.; Walton, P. H., Insights into the oxidative degradation of cellulose by a copper metalloenzyme that exploits biomass components. *Proc. Natl. Acad. Sci.* **2011,** *108* (37), 15079-15084.

4. Hatakka, A., Biodegradation of Lignin. *Biopolymers: Lignin, Humic Substances and Coal* **2004,** *1*, 129.

5. Brunow, G., Methods to Reveal the Structure of Lignin. *Biopolymers: Lignin, Humic Substances and Coal* **2004,** *1*, 89.

6. (a) Zakzeski, J.; Bruijnincx, P. C. A.; Jongerius, A. L.; Weckhuysen, B. M., The Catalytic Valorization of Lignin for the Production of Renewable Chemicals. *Chemical Reviews* **2010,** *110* (6), 3552-3599; (b) Sergeev, A. G.; Hartwig, J. F., Selective, Nickel-Catalyzed Hydrogenolysis of Aryl Ethers. *Science* **2011,** *332* (6028), 439-443.

7. Wenkert, E.; Michelotti, E. L.; Swindell, C. S., Nickel-induced conversion of carbon-oxygen into carbon-carbon bonds. One-step transformations of enol ethers into olefins and aryl ethers into biaryls. *Journal of the American Chemical Society* **1979,** *101* (8), 2246-2247.

8. (a) Li, B.-J.; Xu, L.; Wu, Z.-H.; Guan, B.-T.; Sun, C.-L.; Wang, B.-Q.; Shi, Z.-J., Cross-Coupling of Alkenyl/Aryl Carboxylates with Grignard Reagent via Fe-Catalyzed C-O Bond Activation. *Journal of the American Chemical Society* **2009,** *131* (41), 14656-14657; (b) Guan, B.-T.; Xiang, S.-K.; Wang, B.-Q.; Sun, Z.-P.; Wang, Y.; Zhao, K.-Q.; Shi, Z.-J., Direct Benzylic Alkylation via Ni-Catalyzed Selective Benzylic sp3 C-O Activation. *Journal of the American Chemical Society* **2008,** *130* (11), 3268-3269.

9. Li, B.-J.; Li, Y.-Z.; Lu, X.-Y.; Liu, J.; Guan, B.-T.; Shi, Z.-J., Cross-Coupling of Aryl/Alkenyl Pivalates with Organozinc Reagents through Nickel-Catalyzed C-O Bond Activation under Mild Reaction Conditions. *Angewandte Chemie International Edition* **2008,** *47* (52), 10124-10127.

10. (a) Guan, B.-T.; Wang, Y.; Li, B.-J.; Yu, D.-G.; Shi, Z.-J., Biaryl Construction via Ni-Catalyzed C-O Activation of Phenolic Carboxylates. *Journal of the American Chemical Society* **2008,** *130* (44), 14468-14470; (b) Tobisu, M.; Shimasaki, T.; Chatani, N., Nickel-Catalyzed Cross-Coupling of Aryl Methyl Ethers with Aryl Boronic Esters. *Angewandte Chemie International Edition* **2008,** *47* (26), 4866-4869; (c) Molander, G. A.; Beaumard, F., Nickel-Catalyzed C-O Activation of Phenol Derivatives with Potassium Heteroaryltrifluoroborates. *Organic Letters* **2010,** *12* (18), 4022-4025.

11. He, J.; Zhao, C.; Lercher, J. A., Ni-Catalyzed Cleavage of Aryl Ethers in the Aqueous Phase. *Journal of the American Chemical Society* **2012,** *134* (51), 20768-20775.

12. (a) Choi, J.; Choliy, Y.; Zhang, X.; Emge, T. J.; Krogh-Jespersen, K.; Goldman, A. S., Cleavage of sp3 C-O bonds via oxidative addition of C-H bonds. *Journal of the American Chemical Society* **2009,** *131* (43), 15627-9; (b) Li, Z.; Jiang, Y. Y.; Fu, Y., Theoretical study on the mechanism of Ni-catalyzed alkyl-alkyl Suzuki cross-coupling. *Chemistry* **2012,** *18* (14), 4345-57.

13. Li, Z.; Zhang, S.-L.; Fu, Y.; Guo, Q.-X.; Liu, L., Mechanism of Ni-Catalyzed Selective C-O Bond Activation in Cross-Coupling of Aryl Esters. *Journal of the American Chemical Society* **2009,** *131* (25), 8815-8823.

14. M. J. Frisch, G. W. T., H. B. Schlegel, G. E. Scuseria,; M. A. Robb, J. R. C., G. Scalmani, V. Barone, B. Mennucci,; G. A. Petersson, H. N., M. Caricato, X. Li, H. P. Hratchian,; A. F. Izmaylov, J. B., G. Zheng, J. L. Sonnenberg, M. Hada,; M. Ehara, K. T., R. Fukuda, J. Hasegawa, M. Ishida, T. Nakajima,; Y. Honda, O. K., H. Nakai, T. Vreven, J. A. Montgomery, Jr.,; J. E. Peralta, F. O., M. Bearpark, J. J. Heyd, E. Brothers,; K. N. Kudin, V. N. S., T. Keith, R. Kobayashi, J. Normand,; K. Raghavachari, A. R., J. C. Burant, S. S. Iyengar, J. Tomasi,; M. Cossi, N. R., J. M. Millam, M. Klene, J. E. Knox, J. B. Cross,; V. Bakken, C. A., J. Jaramillo, R. Gomperts, R. E. Stratmann,; O. Yazyev, A. J. A., R. Cammi, C. Pomelli, J. W. Ochterski,; R. L. Martin, K. M., V. G. Zakrzewski, G. A. Voth,; P. Salvador, J. J. D., S. Dapprich, A. D. Daniels,; O. Farkas, J. B. F., J. V. Ortiz, J. Cioslowski, D. J. Fox, *Gaussian 09, Revision C.01, Gaussian, Inc., Wallingford CT* **2010**.

15. (a) Becke, A. D., Density-functional thermochemistry. III. The role of exact exchange. *J. Chem. Phys.* **1993,** *98*, 5648; (b) Lee, C.; Yang, W.; Parr, R. G., Development of the Colle-Salvetti correlation-energy formula into a functional of the electron density. *Phys. Rev. B* **1988,** *37*, 785; (c) Stephens, P. J.; Devlin, F. J.; Chabalowski, C. F.; Frisch, M. J., Ab Initio Calculation of Vibrational Absorption and Circular Dichroism Spectra Using Density Functional Force Fields. *J. Phys. Chem.* **1994,** *98*, 11623.

16. Bergner, A.; Dolg, M.; Kuumlchle, W.; Stoll, H.; Preuszlig, H., Ab initio energy-adjusted pseudopotentials for elements of groups 13-17. *Mol. Phys.* **1993,** *80*, 1431.

17. (a) Hariharan, P. C.; Pople, J. A., *Theor. Chim. Acta* **1973,** *28*, 213-222; (b) Petersson, G. A.; Al-Laham, M. A., *J. Chem. Phys.* **1991** *94*, 6081-6090; (c) Petersson, G. A.; Bennett, A.; Tensfeldt, T. G.; Al-Laham, M. A.; Shirley, W. A.; Mantzaris, J., *J. Chem. Phys.* **1988,** *89*, 2193-2218.

18. Zhao, Y.; Truhlar, D. G., The M06 suite of density functionals for main group thermochemistry, thermochemical kinetics, noncovalent interactions, excited states, and transition elements: two new functionals and systematic testing of four M06-class functionals and 12 other functionals. *Theor. Chem. Acc.* **2008,** *120*, 215.

19. Cornella, J.; Gómez-Bengoa, E.; Martin, R., Combined Experimental and Theoretical Study on the Reductive Cleavage of Inert C-O Bonds with Silanes: Ruling out a Classical Ni(0)/Ni(II) Catalytic Couple and Evidence for Ni(I) Intermediates. *Journal of the American Chemical Society* **2013,** *135* (5), 1997–2009.

20. (a) Barone, V.; Cossi, M., *J. Phys. Chem. A* **1998,** *102*, 1995; (b) Cossi, M.; Rega, N.; Scalmani, G.; Barone, V., *J. Comp. Chem.* **2003,** *24*, 669-681.

21. Danopoulos, A. A.; Pugh, D., A method for the synthesis of nickel(0) bis(carbene) complexes. *Dalton Transactions* **2008,** (1), 30-31.

22. Böhm, V. P. W.; Gstöttmayr, C. W. K.; Weskamp, T.; Herrmann, W. A., Catalytic C–C Bond Formation through Selective Activation of C–F Bonds. *Angewandte Chemie International Edition* **2001,** *40* (18), 3387-3389.

23. Surawatanawong, P.; Fan, Y.; Hall, M. B., Density functional study of the complete pathway for the Heck reaction with palladium diphosphines. *J. Organomet. Chem.* **2008,** *693*, 1552-1563.

24. Hoshimoto, Y.; Hayashi, Y.; Suzuki, H.; Ohashi, M.; Ogoshi, S., One-Pot, Single-Step, and Gram-Scale Synthesis of Mononuclear [(η6-arene)Ni(N-heterocyclic carbene)] Complexes: Useful Precursors of the Ni0–NHC Unit. *Organometallics* **2014,** *33* (5), 1276-1282.

25. (a) Devarajan, D.; Ess, D. H., Metal-mediated dihydrogen activation. What determines the transition-state geometry? *Inorganic chemistry* **2012,** *51* (11), 6367-75; (b) Kubas, G. J., Fundamentals of H2 Binding and Reactivity on Transition Metals Underlying Hydrogenase Function and H2 Production and Storage. *Chemical Reviews* **2007,** *107* (10), 4152-4205; (c) Tye, J. W.; Darensbourg, M. Y.; Hall, M. B., The Activation of Dihydrogen. In *Activation of Small Molecules*, Wiley-VCH Verlag GmbH & Co. KGaA: 2006; pp 121-158.

26. Došlić, N.; Gomzi, V.; Mališ, M.; Matanović, I.; Eckert, J., Fluxionality of Hydrogen Ligands in Fe(H)2(H2)(PEtPh2)3. *Inorganic Chemistry* **2011,** *50* (21), 10740-10747.

27. Luo, Y. R., *Comprehensive Handbook of Chemical Bond Energies*. CRC Press: Boca Raton, FL, 2007.

CHAPTER 2

Proton-Coupled Electron Transfer for C4a-Hydroperoxyflavin Formation and Stabilization in a Flavoenzyme

INTRODUCTION (บทนำ)

Flavoenzymes not only have indispensible roles in cellular metabolism[1], but are also useful as biocatalysts for chemical synthesis reactions and as bioelectrocatalysts for biofuel cell applications.[2,3] Baeyer-Villiger monooxygenase has been used widely in pharmaceutical industries to synthesize drugs.[4] Recently, flavin derivatives were successfully used for catalytic water oxidation in a photochemical water splitting process.[3] Therefore, understanding how flavoenzymes function is crucial to improving their applications and to developing biomimetic flavin derivatives for use as efficient biocatalysts, and biosensors, and in biofuel cells.[5]

The physical and chemical basis underlying the reactions of reduced flavin and dioxygen in flavoenzymes is one of the most fascinating issues in flavoenzymology.[6] The same reduced flavin (FAD or FMN) when bound to different proteins reacts differently with dioxygen (i.e. to form H_2O_2 in oxidases, to form C4a-(hydro)peroxyflavin in monooxygenases, or to have sluggish reactivity toward dioxygen in dehydrogenases in order to transfer electrons to other acceptors). The different reaction outcomes due to the different active site environments of these proteins allow nature to use the same set of chemical reactants to perform a variety of flavoenzyme functions, including use of the abundant oxygen in aerobic systems as an electron acceptor (oxidase), to incorporate an oxygen atom into an organic substrate (monooxygenase), or to mediate electron transfer in complex protein systems (dehydrogenase). Most of our current understanding of flavin chemistry in flavoenzymes is based on work performed in the 1970s-1980s by Bruice et al.[7,8] and Massey et al.[9] and the current view of the reaction of reduced flavin with oxygen in oxidases and oxygenases can be summarized as depicted in Scheme 1 (path a and b).

In chemical synthesis, catalytic oxidative reactions and oxygen insertions with high selectivity generally require multiple steps and often require heavy metals. Flavin is among a few organic cofactors that can use molecular oxygen for oxygenation reactions.[5] The mechanism for the control of this reaction should be well coordinated so that leakage of hazardous reactive oxygen species during enzyme turnover is minimized and the

oxygenases can most efficiently catalyze oxygenation. Many research groups in the past recent years have investigated the role of active site residues that are important for dioxygen activation.[10-17] One of the recurrent features found in these systems is the presence of a positively charged residue that is located near the flavin N5. Previous work suggested that this positive charge provides a pre-organized environment that stabilizes the superoxide anion species[10-14,16] that forms after the first step of electron transfer (path a and b in Scheme 1).[8] However, the electronic structures and energies of key intermediates in the dioxygen activation mechanisms have not been studied in detail.

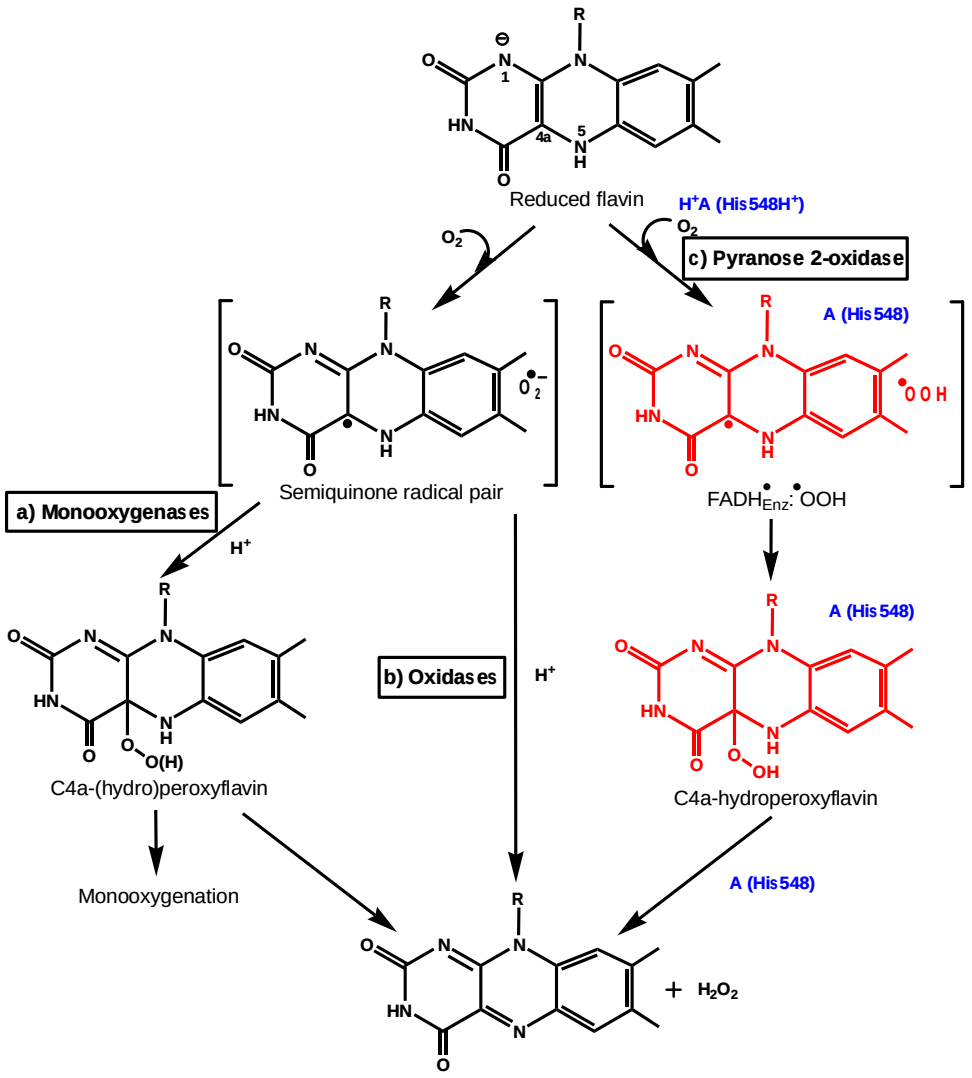

Scheme 1. Flavin reaction mechanisms with dioxygen. Path (a) and path (b) are conventional pathways for the reactions with O_2 in monooxygenases and oxidases, respectively. Path (c) is the alternative pathway for the reactions with O_2 in pyranose 2-oxidase, according to the findings of the current study.

Pyranose 2-oxidase (P2O) is a suitable flavoenzyme for exploring dioxygen activation and C4a-hydroperoxyflavin stabilization. P2O catalyzes the oxidation of pyranose sugars to form 2-keto-sugars and H_2O_2 (Scheme S1). The enzyme has been applied in the synthesis of rare sugars.[2] Thus far, it has been the only flavoenzyme oxidase, in which C4a-hydroperoxyflavin has been detected as an intermediate under natural turnover conditions.[18,19] The reaction of P2O could be viewed as a missing-link in evolution connecting flavin-dependent monooxygenases in which formation of C4a(hydro)peroxyflavin is mandatory and flavoenzyme oxidases in which formation of C4a-hydroperoxyflavin is possibly just one of the means of generating H_2O_2 (Scheme 1). As no X-ray structure of enzyme-bound C4a-hydroperoxyflavin is available, it remains elusive how the intermediate is stabilized in flavoenzymes. It has been proposed that a cavity that is commonly found above the flavin C4a atom of monooxygenases may serve as an entrance for oxygen diffusion and accommodate the peroxide adduct.[6]

Theoretical calculations have been used to study electronic structures and energies in enzymatic reactions.[20-23] Reaction mechanisms have been theoretically investigated for a few flavoenzymes, e.g., a Baeyer-Villiger monooxygenase (oxygen insertion[24]), *p*-hydroxybenzoate hydroxylase and phenol hydroxylase (aromatic hydroxylation[25,26]), 2-methyl-3-hydroxypyridine-5-carboxylate monooxygenase (ring-cleavage reaction[27,28]), BluB (cleavage of riboflavin[29]), glucose 1-oxidase and aryl alcohol oxidase (oxidation of alcohol moiety[30,31]). The mechanisms of H_2O_2 elimination from a free C4a-hydroperoxyflavin species was recently investigated by Bach and Mattevi.[32] In combination with experimental data, computational studies can provide greater insights on the enzyme mechanisms.[20]

In this report, the reaction of reduced flavin and dioxygen catalyzed by P2O was explored using density functional theory (DFT). The calculated activation energies were compared to the experimental activation enthalpies determined from the Eyring plot based on transient kinetic studies at various temperatures. The calculations agreed well with the results from kinetic isotope effect (KIE) and site-directed mutagenesis studies. DFT analysis gave the following new insights into this reaction: (i) the protonated His548 does not stabilize the superoxide anion via electrostatic interactions—rather, it acts as a general acid by providing a proton for the proton-coupled electron transfer in dioxygen activation (path c in Scheme 1) and (ii) the –OOH moiety of C4a-hydroperoxyflavin is in the "face-on" configuration and stabilized by a hydrogen bonding network from His548, Asn593 and Thr169.

METHODOLOGY (วิธีการทดลอง)

Computational Details.

All calculations were performed with the Gaussian 09 program.[33] B3LYP[34-36] density functional theory has been shown to be suitable for the study of enzymatic reactions.[29,37,38] Thus, B3LYP was used for all geometry optimizations and frequency calculations in this study. The 6-31++G(d,p)[39-41] basis set was used for the H that forms H_2O_2 and 6-31G(d) was used for all other atoms.[39-41] The single point energy and solvation free energy corrections were calculated by B3LYP/6-311+G(d,p) on the geometries based on the gas-phase optimizations using the conductor-like polarizable continuum model (CPCM)[42] with UAKS[43] atomic radii and a dielectric constant of 4.0 to represent the protein environment. The energy barrier based on the electronic energy with solvation correction obtained from B3LYP/6-311+G(d,p) calculations is lower than the electronic energy obtained from B3LYP/6-31G(d) calculations, especially for the H_2O_2 elimination step (Table S1). Open-shell systems were treated using spin unrestricted B3LYP (UB3LYP).

The active site model was taken from the crystal structure of P2O(WT) in the closed conformation (1.80 Å; PDB code: 1TT0).[44] The model consists of 118 atoms, which includes $FADH^-$ (the isoalloxazine part) and the residues within about a 5 Å radius from the N5 atom of the $FADH^-$ (Trp168, Thr169, and Cys170) and the key conserved residues[45] (His167, His548, and Asn593) of the enzyme (Figure 1). To minimize the computational power for the relevant protein environment, only the side chains were allowed to be flexible during the geometry optimization. Thus, the atoms on the backbone were constrained at the initial positions in the crystal structure to maintain a reasonable geometry of the active site while all other atoms were optimized (Figure 1). For transition states, frequencies were calculated to ensure that there was one imaginary frequency corresponding to the reaction coordinate. Note that since some atoms in the model are constrained during optimization, the intermediate and transition state structures are not strictly stationary points. Thus, the zero-point vibrational energy corrections and thermal effects are not well defined and are not considered in this study.

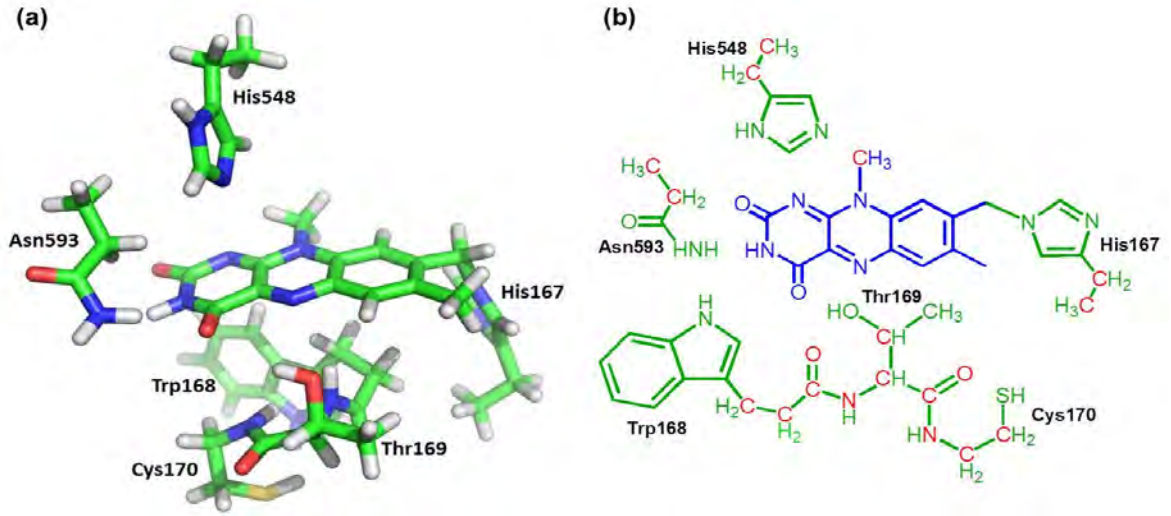

Figure 1. Active site model of P2O(WT) in the closed conformation. (a) X-ray structure of the active site model. (b) Schematic representation of the active site model. The isoalloxazine ring of FAD is shown in blue, flexible residues in green, and constrained atoms in red.

To critically evaluate the extent of spin contamination in open-shell species, the expectation value for the total spin angular momentum, $\langle S^2 \rangle$, of all diradical species in this study were calculated and are shown in Table S2. The data indicate that, for the triplet species, there is no significant problem with the spin contamination as all of the $\langle S^2 \rangle^{triplet}$ values are close to 2. For the open-shell singlet species, the $\langle S^2 \rangle^{singlet}$ values are close to 1 and largely differ from zero. This may be because the use of the broken symmetry approach to calculate the open-shell singlet species can result in spin contamination from higher spin states. As the spin projection (SP) technique was successfully employed in the calculation of diradical energies in previous works[29,46], we used this method to estimate the energy of the spin-unrestricted open-shell singlet species (Equation 1-2).[46] E^X is the electronic energy and $\langle S^2 \rangle^X$ is the expectation value for the total spin angular momentum of the spin state X (X = singlet or triplet).[46]

$$E_{SP}^{\text{singlet}} = E^{\text{singlet}} + C_{SC}\left[E^{\text{singlet}} - E^{\text{triplet}}\right] \qquad \text{Equation 1}$$

$$C_{SC} = \frac{\left\langle S^2 \right\rangle^{\text{singlet}}}{\left\langle S^2 \right\rangle^{\text{triplet}} - \left\langle S^2 \right\rangle^{\text{singlet}}} \qquad \text{Equation 2}$$

Temperature dependence studies.

The measurements were performed using a TgK Scientific Model SF-61DX stopped-flow spectrophotometer in single-mixing mode. The optical path-length of the observation cell was 1 cm. The experimental protocols used were similar to those in a previous report.[18,47,48] In brief, the stopped-flow apparatus was made anaerobic by flushing the flow system with an anaerobic buffer containing 10 mM sodium dithionite in 50 mM sodium phosphate buffer, pH 7.0. The buffer was made anaerobic by equilibrating with oxygen-free nitrogen (ultra high purity) that had been passed through an Oxyclear oxygen removal column (Labclear). The anaerobic buffer was allowed to stand in the flow system overnight. The flow unit was then rinsed with the anaerobic buffer before experiments. For studying the oxidative half-reaction, an anaerobic enzyme solution was equilibrated in an anaerobic glove box (Belle Technology). The enzyme was then reduced with a solution of 10 mM D-glucose in 100 mM sodium phosphate buffer pH 7.0. While adding the solution of D-glucose, enzyme spectra were recorded using a spectrophotometer inside the glove box to ensure complete reduction. The reduced enzyme solution was placed in a glass tonometer and loaded onto the stopped-flow spectrophotometer.

Reduced P2O(WT) (53 μM) was mixed with buffers containing 1.22 mM O_2 (concentrations before mixing) at various temperatures (5, 10, 15, 20, 25, and 30 °C) in a stopped-flow spectrophotometer. Large amplitude changes were detected at 395 and 458 nm. The reaction showed two kinetic phases. For example, at 5 °C, the first phase (0.002-0.04 s, increase of absorbance at 395 nm) indicates the formation of a C4a-hydroperoxyflavin intermediate that subsequently decays in the second phase (0.04-1 s) to yield H_2O_2 and the oxidized enzyme. The second phase occurred simultaneously with an absorbance increase at 458 nm (Figure 5).[18,49,50] Apparent rate constants (k_{obs}) were calculated from the kinetic traces using exponential fits and the software packages Kinetic Studio (TgK Scientific, Bradford-on-Avon, UK) or Program A (developed by R. Chang, C.-J. Chiu, J. Dinverno, and D. P. Ballou, at University of Michigan, Ann Arbor, MI). Simulations were performed by numerical methods with Runge-Kutta algorithms implemented in Berkeley Madonna 8.3 with a time step of 10^{-3} s. Rate constants associated with Scheme 2 can be analyzed according to Equation 3 and 4.[18] Analysis yielded a bimolecular rate constant for the formation of C4a-hydroperoxyflavin (k_1), a reverse rate constant (k_2), and a rate constant for H_2O_2 elimination (k_3). A summary of

the rate constants is provided in Table S4. The rate constants (k_1, k_2, and k_3) were plotted against the temperature used (Figure S5).

$$FADH^-_{Enz} + O_2 \underset{k_{-1}}{\overset{k_1}{\rightleftharpoons}} C4a\text{-}OOH \xrightarrow{k_2} FAD_{Enz} + H_2O_2$$

Scheme 2. Reaction mechanism of the oxidative half-reaction of P2O(WT).

$$k_{obs1} = k_1[O_2] + k_{-1} + k_2 - \frac{k_1 k_2 [O_2]}{k_1[O_2] + k_{-1} + k_2} \qquad \text{Equation 3}$$

$$k_{obs2} = \frac{k_1 k_2 [O_2]}{k_1[O_2] + k_{-1} + k_2} \qquad \text{Equation 4}$$

The Eyring equation was used for determining the enthalpy of activation ($\Delta H^{\ddagger}$) in this reaction (Equation 5, where k is a rate constant, T is absolute temperature, $\Delta H^{\ddagger}$ is enthalpy of activation, R is the gas constant (1.987 cal mol^{-1} K^{-1}), k_B is the Boltzmann constant (1.381×10^{-23} J K^{-1}), h is Planck's constant (6.626×10^{-34} J s), and $\Delta S^{\ddagger}$ is the entropy of activation).[51,52] The linear form of the Eyring plot is shown in equation 6. The plot of ln(k/T) versus 1/T gives a straight line with a slope of $-\Delta H^{\ddagger}/R$ from which the value of the enthalpy of activation can be derived.

$$k = \left(\frac{k_B T}{h}\right) \exp\left(\frac{\Delta S^{\ddagger}}{\mathrm{R}}\right) \exp\left(-\frac{\Delta H^{\ddagger}}{RT}\right) \qquad \text{Equation 5}$$

$$\ln\frac{k}{T} = -\frac{\Delta H^{\ddagger}}{R}\frac{1}{T} + \ln\frac{k_B}{h} + \frac{\Delta S^{\ddagger}}{R} \qquad \text{Equation 6}$$

Reaction of variant P2O with O_2.

The previous study indicated that the H548A, H548C, H548S, and H548N variant enzymes contained mixed populations of covalently linked and non-covalent flavins.[53] Therefore, in order to investigate the role of His548 in flavin oxidation, double mutations containing both His548 and H167A (a mutation in which the covalent histidyl-FAD linkage was removed) in addition to single mutations were constructed. We have shown previously that the H167A variant enzyme reacts with molecular oxygen to form C4a-hydroperoxyflavin with similar rate constants as those found for the wild-type enzyme, indicating that the covalent linkage is not an important factor for formation of the intermediate.[49] The effects of removal of a covalent histidyl-FAD linkage are mainly on

the reductive half-reaction.[49] Therefore, the absence of the covalent histidyl-FAD linkage in P2O variants in this study should not introduce any confounding artifacts to the kinetic analysis.

For studying the oxidative half-reaction of N593H and H167A/H548 variant enzymes, an anaerobic enzyme solution was equilibrated in an anaerobic glove box (as described above). The enzyme was then reduced with a solution of 10 mM D-glucose in 100 mM sodium phosphate buffer pH 7.0 for the N593H variant enzyme. For H167A/H548A, H167A/H548C, H167A/H548S, and H167A/H548N variants which are catalytically inactive for the reductive half-reaction, the enzymes were reduced with a solution of 10 mM sodium dithionite. The oxidation of reduced variant enzyme by O_2 was monitored at various wavelengths (300 to 500 nm) using a stopped-flow spectrophotometer. Buffer solutions with various concentrations of O_2 were made by bubbling certified O_2/N_2 gas mixtures of 20%, 50%, 100% and 100% on ice through syringes for 8 minutes. After mixing, this procedure resulted in O_2 concentrations of 0.13 mM, 0.31 mM, 0.61 mM and 0.96 mM, respectively. Equilibration of a buffer on ice with a 100% O_2/N_2 gas mixture results in a buffer solution that contains 1.92 mM O_2 before mixing. Apparent rate constants (k_{obs}) from kinetic traces were calculated as described above.

Imidazole rescue experiment.

The imidazole rescue experiment on H167A/H548 variants were investigated over a pH range from 6.0 to 8.0 using 100 mM sodium phosphate for pH 6.0 and 7.0, and 100 mM Tris-HCl for pH 8.0. The enzyme solution was mixed with 100 μM imidazole and exchanged into each pH buffer. The resulting solution was equilibrated at that pH for 14-16 h (overnight). Sodium dithionite solutions which were used for reducing the enzyme were prepared by dissolving solid sodium dithionite powder into each pH buffer. A reduced variant enzyme solution was prepared as previously described and the experiments were done at various pH values. Experimental protocols were similar to those described above.

RESULTS (ผลการทดลอง)

A. QM analysis of the reaction of reduced P2O with oxygen (oxidative half-reaction).

The density functional calculations described in Methodology were used to analyze the physical parameters associated with the individual steps and transition states of the reaction of the P2O-bound $FADH^-$ ($FADH^-_{Enz}$) (truncated at only the isoalloxazine ring) and dioxygen.

The starting flavin species was assigned as an anionic form in which the N1 position is deprotonated (Species 1 in Scheme 3). The relevance of this form in the P2O reaction is supported by the fact that the oxidized enzyme can react with sulfite to form the flavin N(5)-sulfite adduct in which the flavin N1 is in the anionic form.[54] In general, the anionic form of the reduced flavin is the form that is bound to flavoenzyme oxidases.[55] Based on the active site structure of P2O,[45] residues approximately 5 Å away from the N5 atom of the $FADH^-$ (Trp168, Thr169, and Cys170) and the key conserved residues (His167, His548, and Asn593) were included in the QM model (Figure 1).

Among these residues, His548 is the most likely to be in the protonated state. According to previous studies of P2O, upon completion of the reductive half-reaction, the oxidized flavin is reduced by D-glucose, and His548 is expected to be in the protonated state.[53] Furthermore, the results of pH-dependence studies of the oxidative half-reaction at various pH values suggest that one of the active site residues should be protonated to allow the reaction to proceed via formation of C4a-hydroperoxyflavin.[50] On the basis of these findings, the calculation model was started with His548 in the protonated state (Species 1 in Scheme 3).

Transient kinetics studies of the P2O oxidative half-reaction indicated that the reaction proceeds via two stages, involving C4a-hydroperoxyflavin formation and decay (H_2O_2 elimination).[18,50,56] Results from the density functional calculations give insights into the electronic structures, spin states, and energies of the transition states and intermediates involved (Figure 2-4), and point to a 5-step process (Scheme 3).

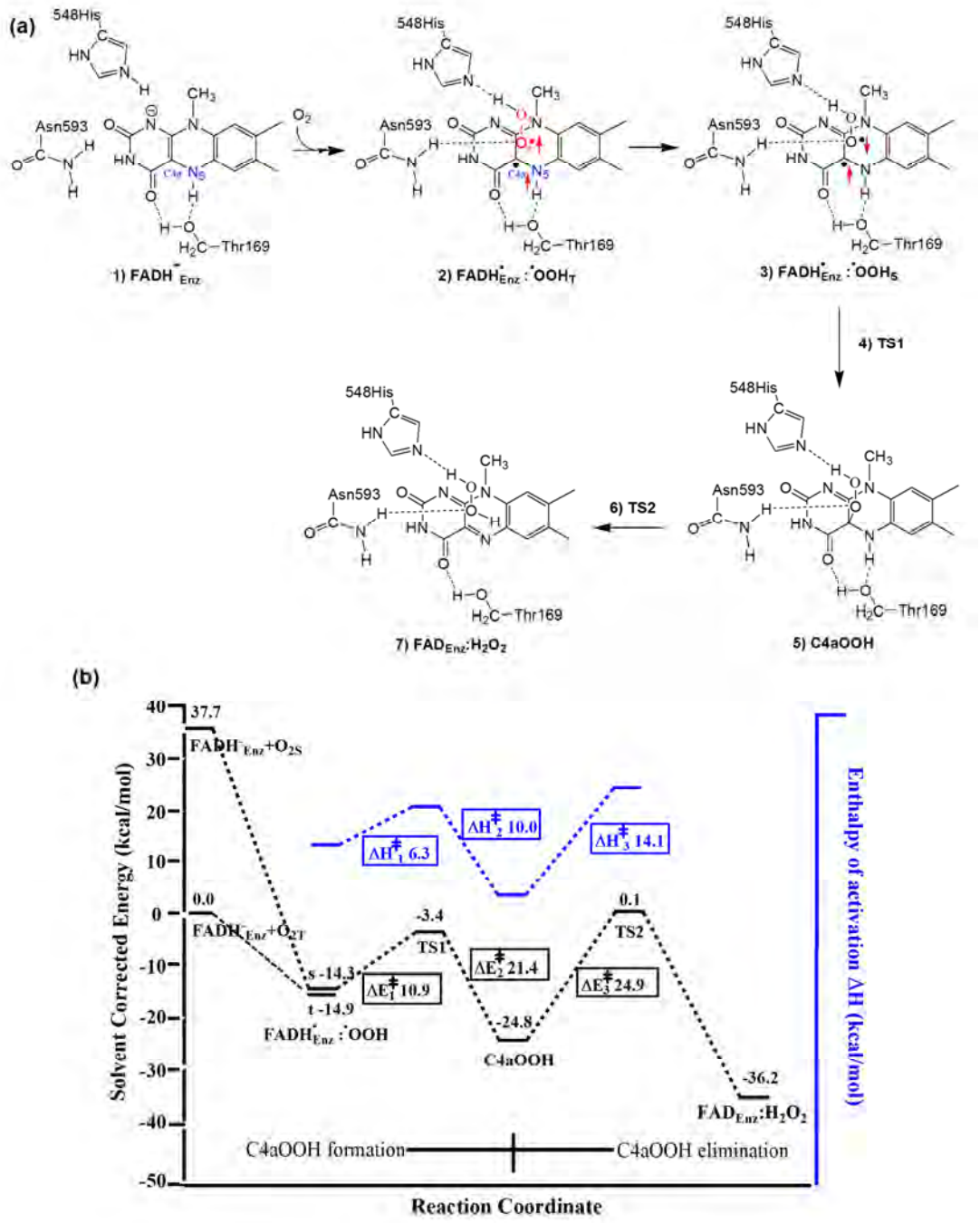

Scheme 3. The reaction of P2O-bound reduced FAD ($FADH^-_{Enz}$) with oxygen. (a) Proposed mechanisms for the reaction of $FADH^-_{Enz}$ with oxygen. Stage 1 is C4a-hydroperoxyflavin formation (1-5) while Stage 2 is H_2O_2 elimination and oxidized flavin generation (5-7). (b) Calculated energy profiles along the proposed reaction pathway. The enthalpy of activation obtained from the transient kinetics results in Figure 5 is overlaid in blue.

Step 1: *Proton-coupled electron transfer to triplet dioxygen (Species 1 to Species 2).*

The energy of the first species, $FADH^-_{Enz}+O_{2T}$ (or $FADH^-_{Enz}+O_{2S}$), is a combination of the electronic energy with solvation correction from the optimized structure of $FADH^-_{Enz}$ (Species 1) and that of O_{2T} (or O_{2S}). The stabilized complex of reduced flavin ($FADH^-_{Enz}$) and dioxygen was found to be improbable through calculations. After several attempts, when the O_2 was placed in the vicinity above the C4a position and upon geometry optimization, the proton from the protonated His548 was immediately transferred to the dioxygen. This was concomitant with the first electron transfer from the reduced flavin to the dioxygen to generate the flavin semiquinone:$^\bullet$OOH radical pair in the triplet state ($FADH^\bullet_{Enz}$:$^\bullet OOH_T$) (Figure 2). It should be mentioned that when this reaction step was calculated using other functionals such as TPSS, the concomitant proton and electron transfer was similar to the results obtained using B3LYP.

Mulliken charge populations on the two oxygen atoms of the $FADH^\bullet_{Enz}$:$^\bullet OOH_T$ (-0.480) are relatively more negative than that of the triplet dioxygen (0.000); this indicates that an electron is transferred to $^\bullet$OOH. As the charge population on the overall OOH fragment is -0.081, the concomitant electron and proton transfer neutralizes the negative charge of the superoxide species and increases the ability of dioxygen to accept an electron from $FADH^-_{Enz}$. Mulliken spin populations on the $^\bullet$OOH (+1.004) and the flavin (+0.991) fragments reveal the identity of Species 2 as the triplet $FADH^\bullet_{Enz}$:$^\bullet OOH_T$ (Table in Figure 2), with a single unpaired electron located on each of the OOH and the flavin fragments.

Note that the proton-coupled electron transfer process for the reaction of reduced flavin and dioxygen presented here is different from the current view[7,9] that describes the first step as an electron transfer to generate a radical pair of flavinsemiquinone and superoxide anion before the subsequent proton transfer occurs (path a and b in Scheme 1).

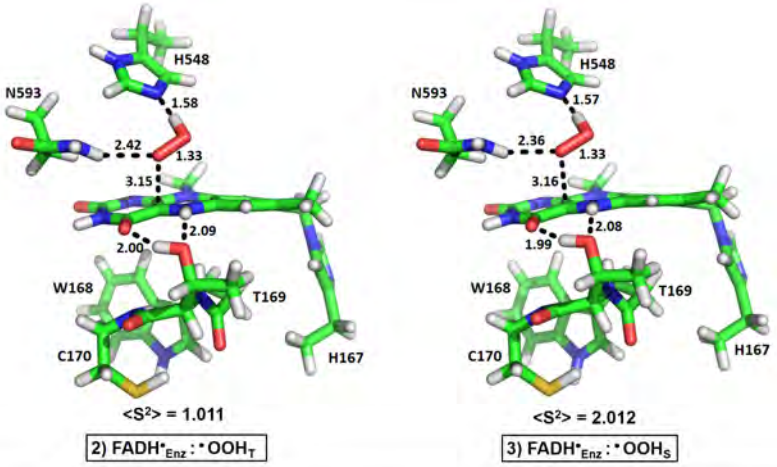

	FADH•Enz: •OOHT	FADH•Enz: •OOHS	FADH•Free: •OOHT	FADH•Free: •OOHS	FADH⁻Free:O2T	FADH⁻Free:O2S	O2T	O2S
ΔE_{S-T} (kcal/mol)	0.6		0.0		7.3		37.7	
q_{O-O}	-0.480	-0.469	-0.424	-0.423	-0.249	-0.273	0.000	0.000
q_{OOH}	-0.081	-0.080	-0.028	-0.028	-	-	-	-
ρ_{O-O}	+1.013	-1.011	+1.017	+1.019	+1.702	+0.007	+2.000	0.000
ρ_{OOH}	+1.004	-1.002	+1.007	+1.010	-	-	-	-
ρ_{Flavin}	+0.991	+0.990	+1.015	-1.010	+0.304	-0.005	-	-
d_{Op-Od}(Å)	1.33	1.33	1.32	1.32	1.25	1.25	1.21	1.21

Figure 2. Optimized structures of FADH•Enz:•OOH complexes. The subscripts T and S represent triplet state and singlet state, respectively. ΔE_{S-T} represents the energy difference between the spin-unrestricted open-shell singlet state and the triplet state. Mulliken charge populations (q) on the two oxygen atoms (q_{O-O}) of the •OOH fragment and on the •OOH fragment (q_{OOH}) are shown. Mulliken spin populations (ρ) on the O_2 (ρ_{O-O}), •OOH (ρ_{OOH}), and flavin (ρ_{Flavin}) fragments are shown. Distances between the two oxygen atoms on the •OOH fragment (d_{Op-Od}) are shown in Å.

Step 2: Triplet (FADH•Enz:•OOHT) to singlet (FADH•Enz:•OOHS) spin transition (Species 2 to Species 3).

The triplet (FADH•Enz:•OOHT) can undergo a spin transition with a small energy requirement (+0.6 kcal/mol, Scheme 3, Table in Figure 2) to become an open-shell singlet diradical (FADH•Enz:•OOHS), in which the spin populations on the •OOH fragment change from +1.004 to -1.002, but remain the same on the flavin fragment at about +0.99 (Table in Figure 2, Figure S3). Overall, the structural geometries of the triplet FADH•Enz:•OOHT and the open-shell singlet diradical FADH•Enz:•OOHS complexes are

similar (Table in Figure 2). The O_p-O_d bond distance in both $FADH^{\bullet}_{Enz}$:$^{\bullet}OOH_T$ and $FADH^{\bullet}_{Enz}$:$^{\bullet}OOH_S$ (1.33 Å) is significantly longer than that in the $O2_T$ (1.21 Å), corresponding to the addition of one electron into the anti-bonding orbital of the dioxygen.

To identify the active site residues involved in the P2O dioxygen activation process, we studied this process in the absence of all residues. Thus, the electronic structures and energies in both triplet and open-shell singlet states for the dioxygen (O_2), the $FADH^{-}_{Free}$:O_2 complex, and the $FADH^{\bullet}_{Free}$:$^{\bullet}OOH$ complex were investigated in order to compare them with those for the $FADH^{\bullet}_{Enz}$:$^{\bullet}OOH$. For dioxygen (O_2) in the absence of a flavin cofactor, the spin transition process from the triplet O_{2T} ($\rho_{O\text{-}O}$ = +2.000) to the singlet O_{2S} ($\rho_{O\text{-}O}$ = 0.000) requires a large energy input of 37.7 kcal/mol (Table in Figure 2). The O_p-O_d bond distances in both spin states are similar (1.21 Å) (Table in Figure 2).

To explore the effects of a flavin cofactor, the $FADH^{-}_{Free}$:O_2 model was investigated (Figure S1). The spin transition proceeding from the triplet $FADH^{-}_{Free}$:O_{2T} to the open-shell singlet $FADH^{-}_{Free}$:O_{2S} requires 7.3 kcal/mol of energy, which is significantly lower than that of the dioxygen (37.7 kcal/mol) (Table in Figure 2). The spin population on the O_2 fragment (+1.702) of the triplet $FADH^{-}_{Free}$:O_{2T} (Table in Figure 2, Figure S1) is slightly less than that on the free triplet O_{2T} (+2.000). The charge population on the dioxygen fragment is -0.249, and the O_p-O_d bond becomes slightly weaker (1.25 Å) than that found in the free triplet O_{2T} (1.21 Å). These findings imply that the presence of a flavin cofactor causes some charge transfer to the dioxygen, which also results in a decrease in the energy gap between the singlet and the triplet states. The C_{4a}-O_p distance is shorter in the open-shell singlet $FADH^{-}_{Free}$:O_{2S} (3.10 Å) complex when compared that of the triplet $FADH^{-}_{Free}$:O_{2T} (3.23 Å) complex (Table S3). Altogether, our data indicate that the flavin cofactor partly assists with the electron transfer and spin transition process.

To evaluate the importance of protonation in the dioxygen activation process, an additional proton was included into the triplet $FADH^{-}_{Free}$:O_{2T} and the open-shell singlet $FADH^{-}_{Free}$:O_{2S} models giving the triplet $FADH^{\bullet}_{Free}$:$^{\bullet}OOH_T$ and the open-shell singlet $FADH^{\bullet}_{Free}$:$^{\bullet}OOH_S$, respectively (Figure S2). Interestingly, with an additional proton, the energy difference between the $FADH^{\bullet}_{Free}$:$^{\bullet}OOH_T$ and the $FADH^{\bullet}_{Free}$:$^{\bullet}OOH_S$ complexes became insignificant (0.01 kcal/mol) (Table in Figure 2). Unlike the triplet $FADH^{-}_{Free}$:$O_{2T,}$ in which only partial charge is transferred from the flavin to the dioxygen, the electronic structure of the triplet $FADH^{\bullet}_{Free}$:$^{\bullet}OOH_T$ implies that one electron is

transferred from the flavin to the OOH fragment; the $FADH^{\bullet}_{Free}$:$^{\bullet}OOH_T$ complex contains similar spin populations on the OOH (+1.007) and the flavin (+1.015) fragments. The O_p-O_d bond distance in the $FADH^{\bullet}_{Free}$:$^{\bullet}OOH_T$ (1.32 Å) complex is also weaker than that found in the $FADH^{-}_{Free}$:O_{2T} complex (1.25 Å) (Table in Figure 2).

The open-shell singlet $FADH^{\bullet}_{Free}$:$^{\bullet}OOH_S$ complex was identified as the open-shell singlet diradical species with a spin population on the OOH fragment of +1.010 and on the flavin fragment of -1.010 (Table in Figure 2, Figure S2). The structural geometries of the triplet $FADH^{\bullet}_{Free}$:$^{\bullet}OOH_T$ and the open-shell singlet diradical $FADH^{\bullet}_{Free}$:$^{\bullet}OOH_S$ complexes are similar; the C_{4a}-O_p distances of both spin states are about the same (3.75 Å) (Table S3). Altogether, the data indicate that the additional proton facilitates the spin transition, as the energy required for this process is reduced.

This result highlights the importance of the proton-coupled electron transfer process as a driving factor that facilitates the formation of the open-shell singlet diradical species ($FADH^{\bullet}_{Free}$:$^{\bullet}OOH_S$). In P2O, the protonated His548 plays an important role in the supply of a proton to the dioxygen during the first electron transfer process to mediate the formation of $FADH^{\bullet}_{Enz}$:$^{\bullet}OOH_S$.

Step 3: *C4a-hydroperoxyflavin formation and TS1 (Species 3 to Species 5).*

In the open-shell singlet diradical $FADH^{\bullet}_{Enz}$:$^{\bullet}OOH_S$ complex, the opposite spins on the $^{\bullet}OOH$ (-1.002) and the flavin (+0.990) fragments facilitate bond formation between the proximal oxygen (O_p) of $^{\bullet}OOH$ and the C4a of the isoalloxazine ring (Figure 2) to form the C4aOOH via TS1 (Figure 3). Two hydrogen bond interactions from the N^{ε} of His548 (1.57 Å) and the $N^{\delta}H$ of Asn593 (2.36 Å) to the $^{\bullet}OOH$ fragment (Figure2) play a role in the positioning the O_p atom of the $^{\bullet}OOH$ fragment; the O_p is located directly above the flavin C4a position. In $FADH^{\bullet}_{Enz}$:$^{\bullet}OOH_S$, the C4a-O_p distance is 3.16 Å and the O_p-O_d distance is 1.33 Å (Figure 2, Table in Figure 3). In TS1, the C4a-O_p distance is shortened to 2.35 Å and the O_p-O_d distance is lengthened to 1.37 Å. The activation energy for this step is 10.9 kcal/mol. Once TS1 transforms to the C4aOOH, the C4a-O_p bond is completely formed (1.44 Å) and the O_p-O_d bond distance has a single bond character (1.45 Å) (calculated O-O bond distance in H_2O_2 is 1.46 Å) (Table in Figure 3).

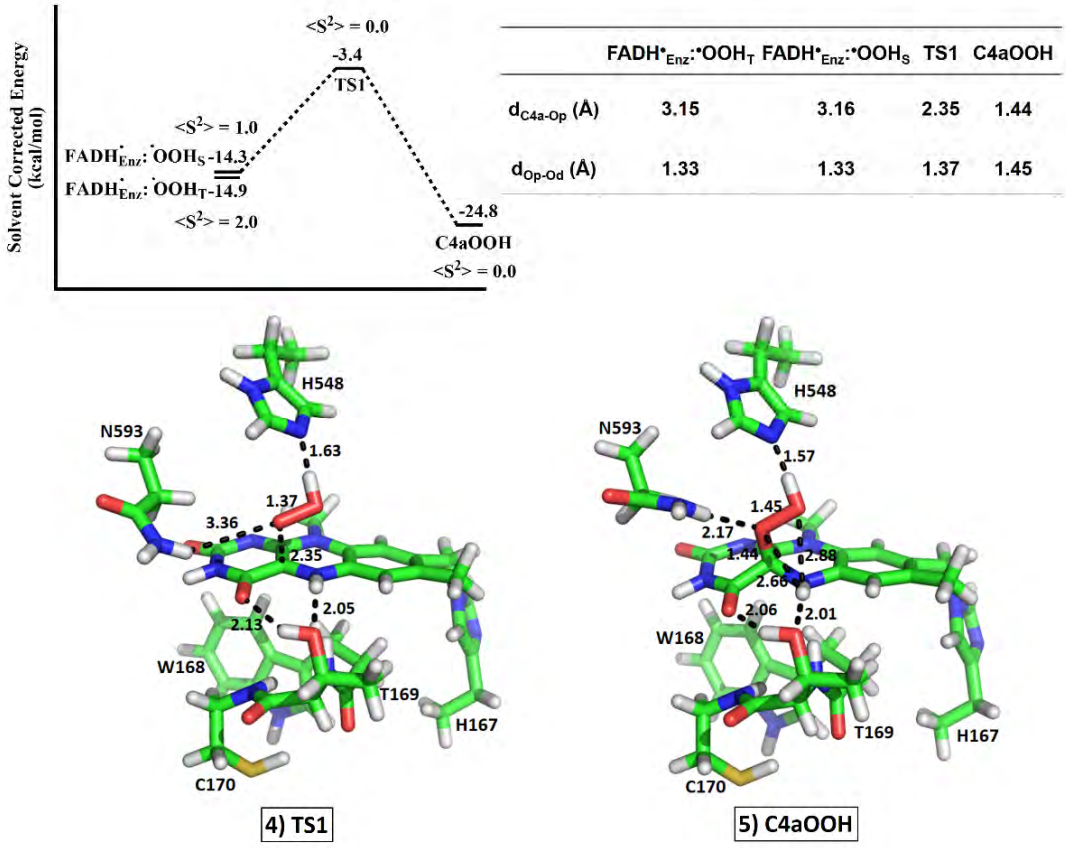

Figure 3. Relative energy profiles for the formation of C4a-hydroperoxyflavin intermediate (C4aOOH, Species 5 in Scheme 3). The optimized structures of transition state 1 (TS1) and the C4aOOH intermediate are shown. The C4a-O_p distance ($d_{C4a\text{-}Op}$) and the O_p-O_d distance ($d_{Op\text{-}Od}$) are shown in the table.

The position of the –OOH moiety of the C4aOOH intermediate above the flavin ring is consistent with the conventional assignment of being *re*-side and compatible with a "face-on" configuration (Figure 3). As most flavoenzymes that form C4aOOH only have space available on the *re*-side to accommodate the –OOH moiety, we explored the P2O preference for C4aOOH formation on the *re*-side versus the *si*-side.

In the absence of the active site residues of P2O, we calculated the energy of H_2O_2 elimination from the C4aOOH intermediate for the free flavin model, where the -OOH moiety is located above (*re*-side) and below (*si*-side) the C4a position of the isoalloxazine ring (Figure S4). The reaction on both sides of the ring essentially required the same amount of energy (29.7 kcal/mol). Thus, the preference for the *re*-side reaction in P2O (and other flavoenzymes) is not attributed to the differences in the electronic effect above and below the isoalloxazine ring.

In the P2O active site, the *si*-side of the isoalloxazine ring is, in fact, crowded with bulky active site residues (Trp168 and Cys170), while the *re*-side has an empty cavity for accommodating O_2 and the resulting -OOH moiety. Therefore, the preference for the *re*-side reaction in P2O is mainly due to the steric hindrance effects on the *si*-side. Trp168 and Cys170 are thus important for directing the formation of the C4aOOH on the *re*-side in P2O.

Step 4 and 5: *H_2O_2 elimination from C4a-hydroperoxyflavin and TS2 (Species 5 to Species 7).*

There are four hydrogen bond interactions to the –OOH moiety and the isoalloxazine ring of the C4aOOH intermediate: (1) the $N^{\varepsilon}$of His548 accepts a hydrogen bond from the -OOH moiety (1.57 Å), (2) the $N^{\delta}H$ of Asn593 donates a hydrogen bond to the O_p of OOH moiety (2.17 Å), (3) the O^{γ} of Thr169 accepts a hydrogen bond from the N5H of the isoalloxazine (2.01 Å), and (4) the -$O^{\gamma}H$ of Thr169 donates a hydrogen bond to the O4 of the isoalloxazine (2.06 Å) (Figure 3). Among these hydrogen bonds, the one from Asn593 in the C4aOOH intermediate (Species 5) is significantly stronger (2.17 Å) than the corresponding one in Species 2-4 (>2.36 Å). Thus, Asn593 is not only positioning the O_p atom of the $^{\bullet}$OOH to be directly above the flavin C4a position to form the C4aOOH intermediate, it also stabilizes the C4aOOH intermediate by tightening the hydrogen bond interaction.

For H_2O_2 elimination, a direct proton transfer from the flavin N5-H to the O_p of a peroxide leaving group can occur with a calculated activation energy (from C4aOOH to TS2) of 24.9 kcal/mol (Figure 4), making it the rate-limiting step in the oxidative half-reaction of P2O. The C4aOOH has a C4a-O_p distance of 1.44 Å and an O_p-H(N5) distance of 2.66 Å. (Figure 3, Table in Figure 4). In TS2, the C4a-O_p distance is lengthened to 2.55 Å and the O_p-H(N5) distance is shortened to 1.54 Å. As the O_d-H(N5) distance is also shortened from 2.88 Å in C4a-OOH to 2.04 Å in TS2, the proton transfer from N5 to O_p of a peroxide leaving group is mediated through the N5 and O_d interaction.

The bond distance between the O^{γ} of Thr169 and the N5H of the isoalloxazine in TS2 (2.60 Å) is relatively weaker than that found in C4aOOH (2.01 Å). Thus, the hydrogen bonds from Thr169 appear to be flexible i.e. changing from a tight interaction which stabilizes C4aOOH to a more relaxed interaction in the H_2O_2 elimination process.

The loosening of the hydrogen bond interaction between O^{γ} of Thr169 and the N5H of the isoalloxazine in TS2 is also consistent with experimental observation. Variants of Thr169, in which the interaction at the flavin N5H is absent, do not stabilize the C4aOOH intermediate.[48]

The intramolecular proton transfer step to eliminate H_2O_2 via TS2 is consistent with previous experimental data showing that H_2O_2 elimination from the C4aOOH intermediate is controlled by a single proton transfer from the flavin N5 to an O_p of a peroxide leaving group.[56] Stopped-flow experiments showed that mutation of His548, Asn593 (see results in Figure 6 and Figure S6-S8) and Thr169[48] resulted in the abolishment of C4a-hydroperoxyflavin formation. This is consistent with our calculations that reveal the importance of protonated His548 for proton-coupled electron transfer to activate dioxygen to form the C4aOOH intermediate and the role of hydrogen bonds from Asn593, His548 and Thr169 in stabilizing the C4aOOH intermediate.

Once the proton is transferred from the flavin N5 to a peroxide leaving group to form the FAD_{Enz}:H_2O_2 complex (Species 7), the C4a-O_p distance is lengthened to 3.27 Å, confirming cleavage of the C4a-O_p bond. Overall, the process of H_2O_2 elimination results in a release of energy of -36.2 kcal/mol. The reverse reaction via TS2 needs to overcome an energy barrier of +36.3 kcal/mol. Thus, formation of H_2O_2 tends to be irreversible and H_2O_2 departure from the active site is presumably facilitated by conformational changes of the P2O enzyme.[45,57]

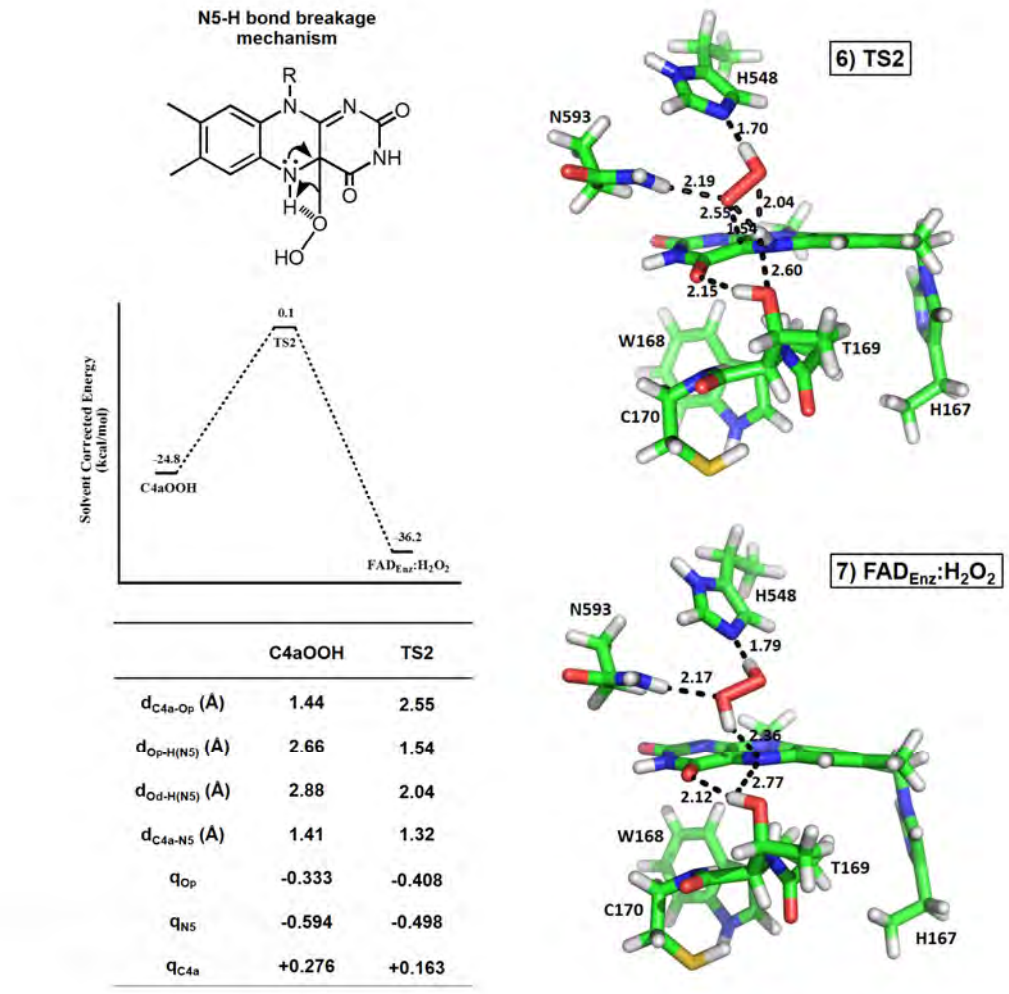

	C4aOOH	TS2
d_{C4a-Op} (Å)	1.44	2.55
$d_{Op-H(N5)}$ (Å)	2.66	1.54
$d_{Od-H(N5)}$ (Å)	2.88	2.04
d_{C4a-N5} (Å)	1.41	1.32
q_{Op}	-0.333	-0.408
q_{N5}	-0.594	-0.498
q_{C4a}	+0.276	+0.163

Figure 4. Relative energy profiles of H_2O_2 elimination from C4a-hydroperoxyflavin, the optimized structures of TS2, and the final product FAD_{Enz}:H_2O_2 complex. Values for the C4a-O_p distance (d_{C4a-Op}), O_p-H(N5) distance ($d_{Op-H(N5)}$), O_d-H(N5) distance ($d_{Od-H(N5)}$), and C4a-N5 distance (d_{C4a-N5}) are shown in the table. Mulliken charge populations on the O_p (q_{Op}), the N5 (q_{N5}), and the C4a (q_{C4a}) are also shown.

B. Activation energy of the reaction of reduced P2O with oxygen analyzed by the Eyring equation.

To complement our density functional calculations, reactions of reduced P2O with dioxygen at various temperatures (5-30 °C) were carried out using stopped-flow spectrophotometry to determine the enthalpy of activation ($\Delta H^{\ddagger}$) for C4aOOH formation from the reaction of $FADH^{-}_{Enz}$ and O_2 in both forward and reverse directions, and for

H_2O_2 elimination (Experimental Procedures). As determined by analysis of the Eyring plot, the transient kinetics data (Figure 5, Table S4 and Figure S5) show that the enthalpy of activation for C4aOOH formation from the reaction of $FADH^-_{Enz}$ and O_2 in the forward direction ($\Delta H_1^{\ddagger}$) is 6.3 kcal/mol and in the reverse reaction ($\Delta H_2^{\ddagger}$) is 10.0 kcal/mol. The enthalpy for H_2O_2 elimination ($\Delta H_3^{\ddagger}$) is 14.1 kcal/mol. The calculated energy barrier is in agreement with the experimental enthalpy barrier in that the energy barrier for C4aOOH formation is lower than that for its reverse reaction ($\Delta E_1^{\ddagger}$ and $\Delta E_2^{\ddagger}$ vs $\Delta H_1^{\ddagger}$ and $\Delta H_2^{\ddagger}$) (Scheme 3, Table in Figure 5). Proton abstraction from N5H was determined as the rate-determining step as the energy barrier for H_2O_2 elimination is the highest ($\Delta E_3^{\ddagger}$ and $\Delta H_3^{\ddagger}$).

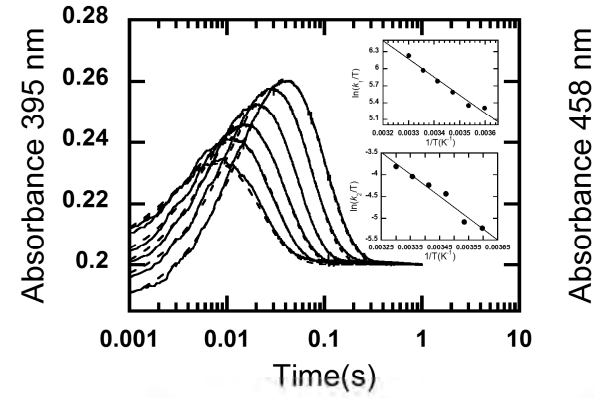

$FADH^- + O_2 \underset{\Delta H_2^{\ddagger}}{\overset{\Delta H_1^{\ddagger}}{\rightleftharpoons}}$ C4a-OOH $\xrightarrow{\Delta H_3^{\ddagger}}$ $FAD + H_2O_2$

Eyring plot (kcal/mol)		QM calculation (kcal/mol)	
$\Delta H_1^{\ddagger}$	6.3	$\Delta E_1^{\ddagger}$ ($FADH^{\bullet}_{Enz}$:$^{\bullet}OOH_S \rightarrow$TS1)	10.9
$\Delta H_2^{\ddagger}$	10.0	$\Delta E_2^{\ddagger}$ (C4aOOH$\rightarrow$TS1)	21.4
$\Delta H_3^{\ddagger}$	14.1	$\Delta E_3^{\ddagger}$ (C4aOOH$\rightarrow$TS2)	24.9

Figure 5. The oxidative half-reaction of P2O at various temperatures and Eyring plots. The transient kinetics of the oxidative half-reaction of P2O was investigated at various temperatures (5, 10, 15, 20, 25, and 30 °C) using stopped-flow spectrophotometry. Kinetic simulations with a two-step consecutive model (dotted line traces) according to the method described in[18] were used for analysis of rate constants. Insets show the Eyring plots of rate constants for formation (k_1), decay of C4a-OOH (k_2), and H_2O_2 elimination (k_3). The enthalpy of activation from the Eyring plots and the activation energies from QM calculations are summarized in Table and the values were plotted in Scheme 3.

Since only the active site as a part of the enzyme was considered in the model studied for computational feasibility and the corrections for zero-point vibrational energy and thermal effects cannot be included in the calculation, we expect some discrepancies between the calculated energy and the experimental enthalpy to exist. A similar level of discrepancy between experimental and calculation results was also present in other works.[58] Overall, the results show that the relative activation energy ($\Delta E^{\ddagger}$) displays the same trend as the relative enthalpy of activation ($\Delta H^{\ddagger}$) derived experimentally from the Eyring plots. Specifically, this implies that the energy change for O_2 activation by P2O mainly derives from the change of electronic structures of the intermediates and transition states that involved.

C. Transient kinetics of reactions of reduced H548 and N593 variants with oxygen.

Transient kinetic experiments for Asn593 variant (N593H), and His548 variants (H167A/H548A, H167A/H548C, H167A/H548S, and H167A/H548N) were performed to confirm the involvement of these two conserved residues in stabilization of C4a-hydroperoxyflavin. For the oxidative half-reactions of P2O(WT) and H167A variant enzymes,[18,49] the reaction shows biphasic kinetics, indicating formation of a C4a-hydroperoxyflavin intermediate (Figure 5). For His548 and Asn593 variants, the results showed only one kinetic phase, indicating that only flavin oxidation was observed (Figure 6, Figure S6-S8). These data indicate that a C4a-hydroperoxyflavin intermediate does not form in these variants (Figure 6, Figure S6-S8), confirming the findings from QM calculations that His548 and Asn593 are important for stabilization of C4a-hydroperoxyflavin. Moreover, when the imidazole rescue experiment for His548 variants at various pHs was performed, the results were similar to those in the absence of imidazole in which no C4a-hydroperoxyflavin was detected (Table S5). These results indicate that not only is a proton required, but proper geometry of the protonated His548 in the active site of the P2O enzyme is mandatory for formation of the C4a-hydroperoxyflavin intermediate.

Our previously published results for T169A, T169S, T169N, and T169G variants indicated that all of these variants also void formation of C4a-hydroperoxyflavin.[48] Therefore, the QM analysis results in which Thr169, His548 and Asn593 were identified as residues important for the stabilization of TS1 and C4a-hydroperoxyflavin are supported well by stopped-flow studies of the variant enzymes.

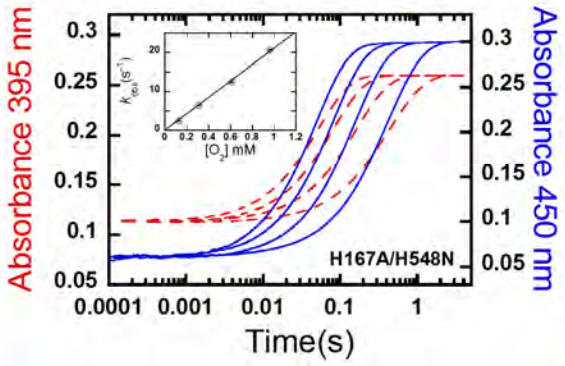

Variants	Bimolecular rate constant ($M^{-1}s^{-1}$)
H167A/H548A	58 ± 2
H167A/H548C	233 ± 3
H167A/H548S	359 ± 2
H167A/H548N	21,000 ± 8
N593H	529 ± 6

Figure 6. Kinetics of the reactions of reduced H167A/H548N variant with O_2. The data show monophasic kinetics, indicating that flavin is oxidized without forming C4a-hydroperoxyflavin. The inset shows the observed rate constants which are linearly dependent on O_2 concentrations. Summary of bimolecular rate constants of the oxidative half-reactions of N593H and H167A/H548 variants are shown in Table.

DISCUSSION (วิจารณ์ผลการทดลอง)

Our findings based on QM analysis and transient kinetic studies have identified the physical factors underlying the reaction of reduced flavin and dioxygen catalyzed by P2O. The data provide mechanistic insight that is different from the general model currently used for explaining the reaction of reduced flavin and oxygen.[6,9,55] The initial protonation of dioxygen by His548 of P2O that occurs in a concerted manner with an electron transfer is key for the oxygen activation process. The data obtained from QM analysis and transient kinetics indicate that the –OOH moiety of the C4a-hydroperoxyflavin is stabilized via a "face-on" configuration. The C4a-hydroperoxyflavin is stabilized by the hydrogen bond interactions from His548, Asn593 and Thr169. H_2O_2 elimination occurs via a direct proton transfer from the flavin N5-H. The trends observed for the energy profiles based on the QM results also correlated well with the enthalpy of activation profiles obtained from the Eyring plots.

The data in Figure 2 suggest that the first step of the P2O reaction is a single electron transfer that is coupled with a proton transfer. The relative timing of proton transfer in Figure 2 is different from the current views toward the reaction of reduced flavin and oxygen in flavoenzymes which propose that a single electron is first transferred to form the flavin semiquinone and superoxide radical pair (path a and b in Scheme 1[6,7,9]). A new model based on our results can be summarized as in Scheme 1 path C. Results from DFT calculations agree well with the experimental data because they suggest that no net proton transfer is involved in the TS1 transformation to the C4a-hydroperoxyflavin intermediate (Figure 3), which is consistent with the previous experiments indicating that no solvent kinetic isotope effect (SKIE) was detected for the C4a-hydroperoxyflavin formation.[56] However, with a similar calculation method, different results were obtained for the QM analysis of flavindestructase (BluB) because the first step of the BluB-catalyzed reaction is a single electron transfer from reduced flavin to dioxygen to generate the flavin semiquinone and superoxide radical pair before it collapses to form a negatively charged C4a-flavin peroxide intermediate. This intermediate is stabilized by two hydrogen bonds from the backbone amide of Gly61 and the O2 hydroxyl group of reduced FMN.[29] As the next step of BluB reaction is a cleavage of the isoalloxazine ring, it can thus be seen that protonation is not necessary for C4a-flavin peroxide in BluB catalysis. Therefore, different active site environments can influence the relative timing of electron and proton transfers differently.

The DFT analysis and transient kinetics indicate that the conserved His548 in P2O provides an internal proton for oxygen activation. This protonation process makes oxygen a better electron acceptor as the Mulliken charge of dioxygen atoms on the •OOH molecule in the active site model (-0.480) is more negative than in the free flavin model (-0.249)—the model that describes the unprotonated His548 condition (Figure 2). The His548 and Asn593 help in aligning a •OOH radical such that it is properly oriented for the next step in C4a-hydroperoxyflavin formation. The DFT results agree well with the experimental data because the reaction at lower pH is much faster than that at higher pH and formation of C4a-hydroperoxyflavin can only be detected at pH values lower than 8.0.[50] Moreover, results from studies of the reductive half-reaction of P2O indicate that the conserved His548, which acts as a general base during the reductive half-reaction likely exists in the protonated form at the initial stage of the oxidative half-reaction.[53] Therefore, the functional role of His548 in P2O can be viewed as that of a general base in the reductive half-reaction and a general acid in the oxidative half-reaction (path c in Scheme 1).

In addition to P2O, many studies of other flavoenzyme oxidases have shown that positive charges near the flavin N5 are important for the oxygen activation process. For glucose oxidase, the protonated His516 is required because the pH-rate profiles showed that the $k_{cat}/K_{m(O2)}$ is 2,600 fold higher at lower pH than at higher pH.[59,60] In contrast, for choline oxidase, oxygen activation is thought to be caused by the positive charge of the substrate.[16] For monomeric sarcosine oxidase, *N*-methyltryptophan oxidase and fructosamine oxidase, mutation of Lys 256 to a neutral amino acid results in a 550-9000 fold decrease in oxygen reactivity.[13-15] More moderate effects were observed for similar mutations in polyamine oxidase and dihydroorotate dehydrogenase.[15,17] In most of these studies, the role of the positively charged residues was proposed to be to provide electrostatic interactions to stabilize the formation of a negatively charge superoxide radical. Our current findings suggest that quantum mechanical calculations for these enzymes should be useful for analyzing whether these positively charged residues can act as proton donors similar to what is observed in the P2O reaction.

The DFT optimized structure of C4a-hydroperoxyflavin (Figure 3) offers a molecular view of the physical and chemical interactions required for stabilization of the intermediate in a flavoenzyme. The data show that the intermediate is closely interacting with the side chains of Thr169, His548 and Asn593. Experimental evidence also confirms that these interactions are important because mutation of His548, Asn593 (Figure 6,

Figure S6-S8) and Thr169 variants[48] failed to stabilize the C4a-hydroperoxyflavin intermediate. Moreover, the imidazole rescue experiment for the His548 variants could not restore the formation of C4a-hydroperoxyflavin (Table S5), implying that the geometry of the general acid (His548) in relation to the flavin position is very important for stabilization of TS1 or C4a-hydroperoxyflavin. It is interesting to note that the –OOH moiety in Figure 3 is configured in a "face-on" configuration. In most of X-ray structures of enzymes that can form C4a-hydroperoxyflavin, a cavity above the *re*-face of the flavin C4a atom is common.[6] Therefore, the "face-on" configuration can fit in active sites and may be prevalent in many enzymes.

Data in Figure 4 also confirm that the C4a-hydroperoxyflavin can undergo a unimolecular reaction to generate H_2O_2 and the relaxed H-bond interaction between the Oγ of Thr169 and the N5H of the isoalloxazine in TS2 (bond length of 2.60 Å) could be a key feature that enables this process. In previous studies, when the reduced enzyme which was specifically labeled with a single deuterium atom to give flavin N5-D reacted with dioxygen, a KIE of ~ 3 for the H_2O_2 elimination was observed. The KIE is the same as that observed when the reaction was carried out in D_2O.[56] These experimental results agree well with the formation of species 5, TS2 and species 7. They also provide evidence supporting a unimolecular mechanism of H_2O_2 elimination consisting of a single proton transfer from N5-H to a peroxide leaving group.

The importance of H-bond interactions at the flavin N5 in stabilization of the C4a-hydroperoxyflavin has been observed in many systems. For Thr169 variants of P2O in which a H-bond interaction at the flavin N5 is absent, the C4a-hydroperoxyflavin intermediate could not be detected.[48] In the oxygenase component of *p*-hydroxylphenylacetate hydroxylase, upon removal of the residue (Ser171) that forms hydrogen bonds with the flavin N5, the rate of H_2O_2 elimination increased by ~1400-fold.[61]

For a Baeyer–Villiger monooxygenase, the interaction between the flavin N5 and a bound $NADP^+$ is necessary in order to stabilize the C4a-hydroperoxyflavin.[62] A recent DFT calculation by Bach and Mattevi[32] suggests that in the absence of protein environment, the H_2O_2 elimination from C4a-hydroperoxyflavin is not feasible. When H_2O or CH_3OH (to model Thr or Ser) was included to serve as a proton shuttle path, the energy barrier for H_2O_2 elimination significantly decreased. Interaction of amine or amide residues with the N5 locus of C4a-hydroperoxyflavin also markedly reduces the energy barrier for H_2O_2 elimination. The interaction of Thr169 and flavin N5-locus shown in TS2

(Figure 4) may be similar to those found in the Bach and Mattevi study[32]. Based on our data in Figure 3-4, we propose that a more relaxed H-bond interaction to the flavin N5-H in TS2 when compared to a tighter H-bond interaction in C4a-OOH (bond length of 2.01 Å) is important for allowing H_2O_2 elimination to occur.

SUMMARY (สรุปผลการทดลอง)

In summary, the combined usage of QM analysis and transient kinetics provides the theoretical basis underlying oxygen activation and the C4a-hydroperoxyflavin stabilization in P2O. Results in this report represent the chemical reaction in a flavoenzyme oxidase that uniquely stabilizes C4a-hydroperoxyflavin. It should be interesting to explore in future studies whether a similar basis holds for monooxygenases in which C4a-hydroperoxyflavin is utilized as a reactive intermediate.

SUPPLEMENTARY TABLES AND FIGURES (ตารางและรูปเพิ่มเติม)

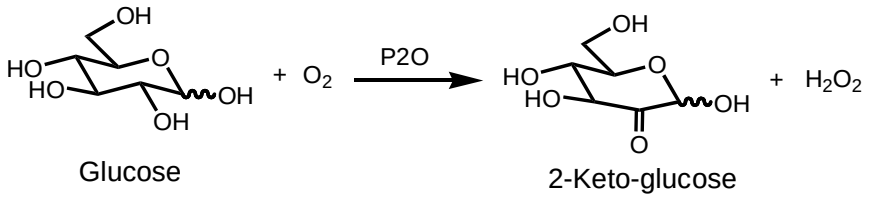

Scheme S1 Reaction catalyzed by P2O.

Table S1. Summary of the relative electronic energies obtained from B3LYP/6-31G(d) calculation and the relative electronic energies with solvation correction obtained from B3LYP/6-311+G(d,p) calculation. All geometries were optimized by B3LYP/6-31G(d).

Reaction	ΔE (kcal/mol)	
	6-31G(d)	6-311+G(d,p)
$FADH^-_{Enz}+O_{2S} \rightarrow FADH^{\bullet}_{Enz}:{}^{\bullet}OOH_S$	-44.8	-52.0
$FADH^-_{Enz}+O_{2T} \rightarrow FADH^{\bullet}_{Enz}:{}^{\bullet}OOH_T$	-11.0	-14.9
$FADH^{\bullet}_{Enz}:{}^{\bullet}OOH_T \rightarrow FADH^{\bullet}_{Enz}:{}^{\bullet}OOH_S$	0.1	0.6
$FADH^{\bullet}_{Enz}:{}^{\bullet}OOH_S \rightarrow$ TS1	15.0	10.9
TS1 $\rightarrow$ C4aOOH	-33.9	-21.4
C4aOOH $\rightarrow$ TS2	37.5	24.9
TS2 $\rightarrow FAD_{Enz}:H_2O_2$	-35.5	-36.3

Table S2. The expectation values for the total spin angular momentum, $\langle S^2 \rangle$, of the triplet and the open-shell singlet species in this study.

Optimized structure	$\langle S^2 \rangle^{singlet}$	$\langle S^2 \rangle^{triplet}$	$E^{singlet}_{SP}$
$FADH^{-}_{Free}:O_{2T}$	-	2.0083	-
$FADH^{-}_{Free}:O_{2S}$	0.9626	-	-1023.48012988
$FADH^{\bullet}_{Free}:{}^{\bullet}OOH_{T}$	-	2.0110	-
$FADH^{\bullet}_{Free}:{}^{\bullet}OOH_{S}$	1.0105	-	-1023.97116988
$FADH^{\bullet}_{Enz}:{}^{\bullet}OOH_{T}$	-	2.0121	-
$FADH^{\bullet}_{Enz}:{}^{\bullet}OOH_{S}$	1.0110	-	-3331.50620665

Table S3. Summary of the distance between the C4a atom of the flavin and the O_p atom of the OOH molecule ($d_{C4a\text{-}Op}$) in O_2, $FADH^-_{Free}$:O_2, $FADH^{\bullet}_{Free}$: $^{\bullet}OOH$, and $FADH^{\bullet}_{Enz}$: $^{\bullet}OOH$.

	$d_{C4a\text{-}Op}$ (Å)
O_{2T}	-
O_{2S}	-
$FADH^-_{Free}$:O_{2T}	3.23
$FADH^-_{Free}$:O_{2S}	3.10
$FADH^{\bullet}_{Free}$: $^{\bullet}OOH_T$	3.75
$FADH^{\bullet}_{Free}$: $^{\bullet}OOH_S$	3.75
$FADH^{\bullet}_{Enz}$: $^{\bullet}OOH_T$	3.15
$FADH^{\bullet}_{Enz}$: $^{\bullet}OOH_S$	3.16

Table S4. Summary of rate constants associated with Scheme S3 at various temperatures

	k_1 ($M^{-1}s^{-1}$)	k_2 (s^{-1})	k_3 (s^{-1})
5 °C	5.6×10^4	**1.5**	**19**
10 °C	6.0×10^4	**1.7**	**36**
15 °C	7.7×10^4	**3.4**	**44**
20 °C	9.5×10^4	**4.2**	**74**
25 °C	1.2×10^5	**5.2**	**113**
30 °C	1.5×10^5	**6.7**	**188**

Table S5. Summary of bimolecular rate constants for the imidazole rescue experiments in the oxidative half-reaction of H167A/H548 variants.

Variants	Bimolecular rate constant ($M^{-1}s^{-1}$)	Bimolecular rate constant in the presence of imidazole ($M^{-1}s^{-1}$)		
		pH 6.0	pH 7.0	pH 8.0
H167A/H548A	58 ± 2	62	63	56
H167A/H548C	233 ± 3	219	176	227
H167A/H548S	359 ± 2	346	392	355
H167A/H548N	21,000 ± 4	23,600	20,970	22,480

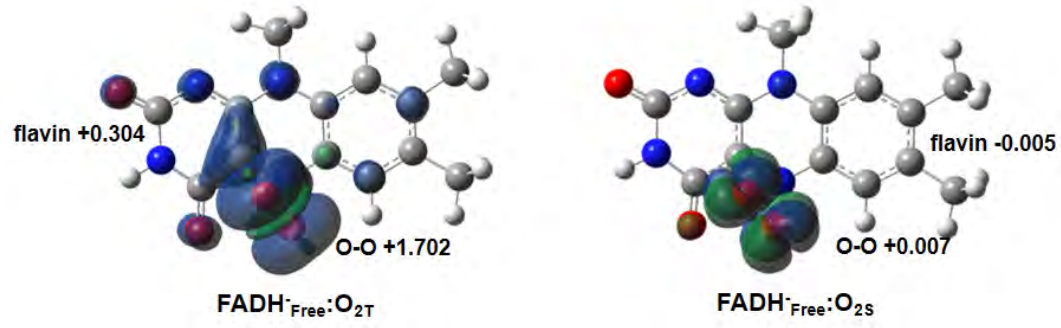

Figure S1. Spin densities of the $FADH^{-}_{Free}$:O_2 complex in the triplet state ($FADH^{-}_{Free}$:O_{2T}) and the spin-unrestricted open-shell singlet state ($FADH^{-}_{Free}$:O_{2S}).

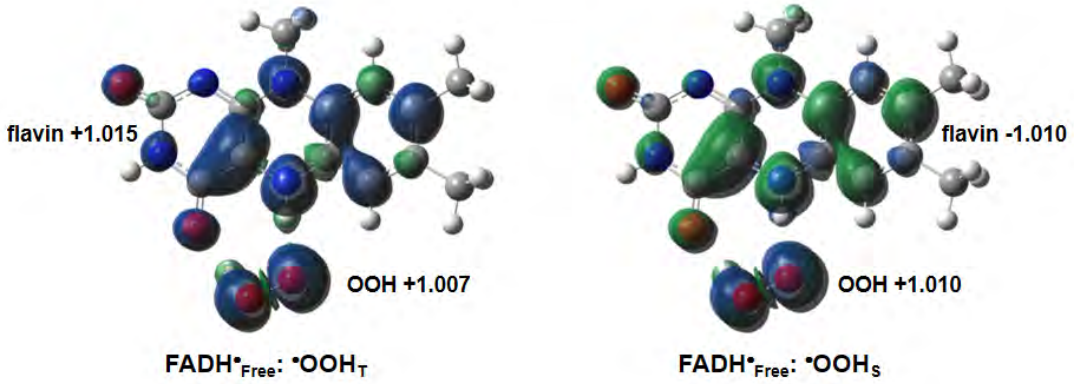

Figure S2. Spin densities of the $FADH^{\bullet}_{Free}$:$^{\bullet}OOH$ complex in the triplet state ($FADH^{\bullet}_{Free}$:$^{\bullet}OOH_T$) and the unrestricted open-shell singlet state ($FADH^{\bullet}_{Free}$:$^{\bullet}OOH_S$).

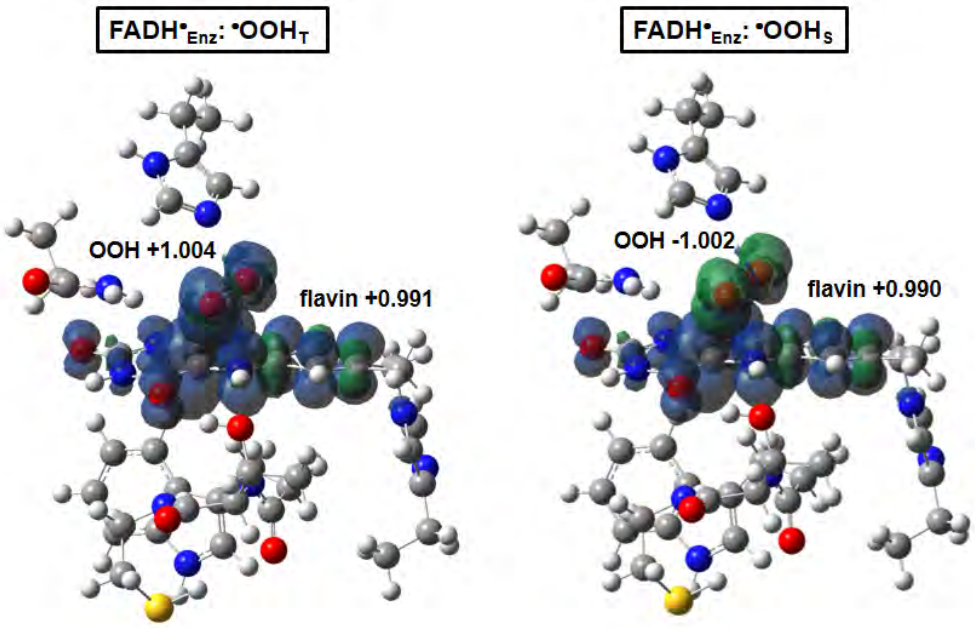

Figure S3. Spin densities of the $FADH^{\bullet}_{Enz}$: $^{\bullet}OOH$ complex in the triplet state ($FADH^{\bullet}_{Enz}$: $^{\bullet}OOH_T$) and the unrestricted open-shell singlet state ($FADH^{\bullet}_{Enz}$: $^{\bullet}OOH_S$).

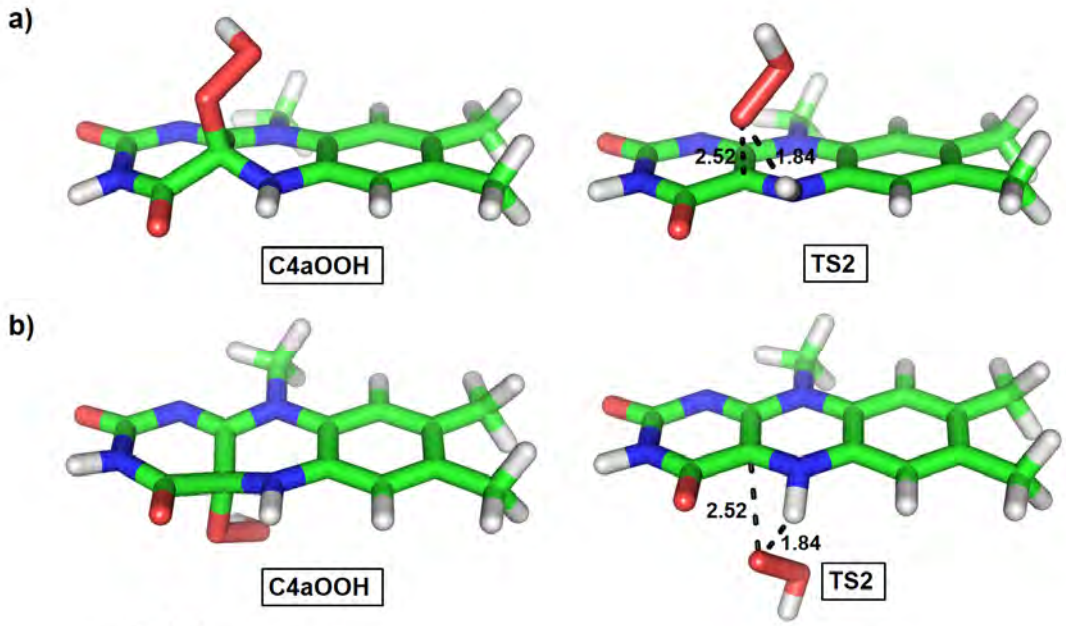

Table

	re-face		si-face	
	C4aOOH	TS2	C4aOOH	TS2
$\Delta E_{TS2\text{-}C4aOOH}$ (kcal/mol)	29.7		29.7	
$d_{Op\text{-}Od}$ (Å)	1.45	1.40	1.45	1.40
$d_{C4a\text{-}Op}$ (Å)	1.46	2.52	1.46	2.52
$d_{Op\text{-}H(N5)}$ (Å)	2.78	1.84	2.78	1.84
$d_{C4a\text{-}N5}$ (Å)	1.41	1.33	1.41	1.33

Figure S4. Optimized structures and reaction energies for the H_2O_2 elimination from the C4aOOH in the (a) re-face, and (b) si-face.

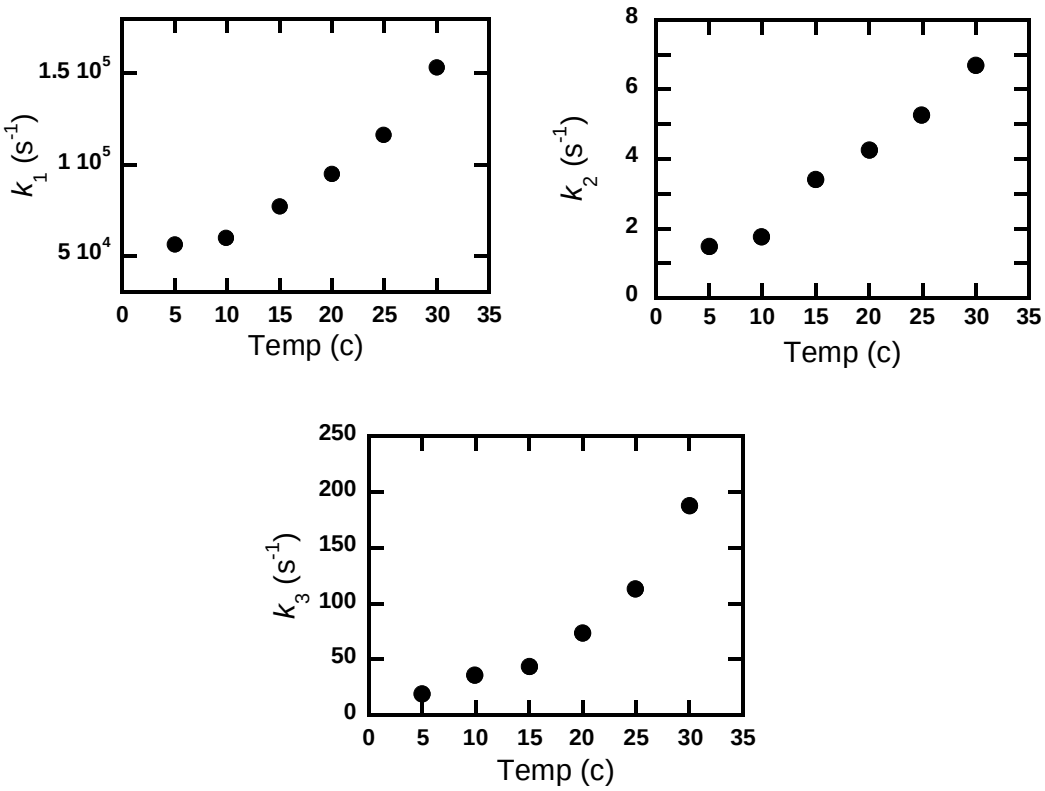

Figure S5. Effect of temperature on the oxidative half-reaction of P2O(WT). Individual rate constants were plotted against the temperature (5-30 °C).

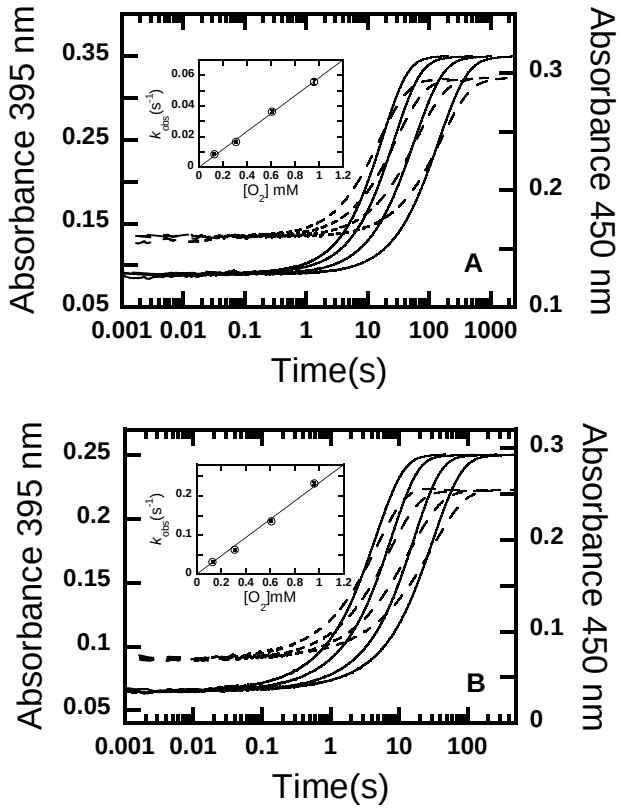

Figure S6. Kinetics of the reactions of reduced H167A/H548 variants with O_2. **(A)** A solution of reduced **H167A/H548A** (30 μM) in 100 mM sodium phosphate buffer pH 7.0 was mixed with the same buffer containing various O_2 concentrations (0.13 mM, 0.31 mM, 0.61 mM and 0.96 mM; right to left traces) in a stopped-flow spectrophotometer at 4 °C. The concentrations given are those after mixing. The reactions were monitored by measuring the absorbance changes at 395 nm (dotted lines) and 450 nm (solid lines). The data show monophasic kinetics, indicating that the flavin is oxidized without forming C4a-hydroperoxyflavin. The observed rate constants according to low to high O_2 concentrations are $8.7 \pm 0.8 \times 10^{-3}$, $1.67 \pm 0.08 \times 10^{-2}$, $3.6 \pm 0.1 \times 10^{-2}$, and $5.6 \pm 0.2 \times 10^{-2}$ s^{-1}, respectively. **Inset A** shows the observed rate constants which are linearly dependent on O_2 concentrations with a bimolecular rate constant of 58 $M^{-1}s^{-1}$. The reaction of **H167A/H548C (B)** was carried out in a similar fashion as that of the H167A/H548A mutant in panel A. The data also show monophasic kinetics. The observed rate constants according to low to high O_2 concentrations are $3.1 \pm 0.2 \times 10^{-2}$, $6.2 \pm 0.3 \times 10^{-2}$, 0.13 ± 0.01, and 0.23 ± 0.01 s^{-1}, respectively. I**nset B** shows the observed rate constants which are linearly dependent on O_2 concentrations with a bimolecular rate constant of 233 $M^{-1}s^{-1}$.

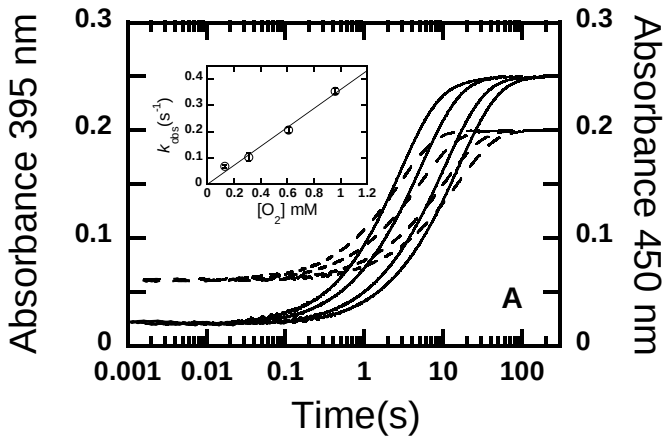

Figure S7. Kinetics of the reactions of reduced H167A/H548S variant with O_2. A solution of reduced **H167A/H548S** (30 µM) in 100 mM sodium phosphate buffer pH 7.0 was mixed with the same buffer containing various O_2 concentrations (0.13 mM, 0.31 mM, 0.61 mM and 0.96 mM; right to left traces) in a stopped-flow spectrophotometer at 4 °C. The concentrations given are those after mixing. The reactions were monitored by measuring absorbance changes at 395 nm (dotted lines) and 450 nm (solid lines). The data show monophasic kinetics, indicating that flavin is oxidized without forming C4a-hydroperoxyflavin. The observed rate constants according to low to high O_2 concentrations are $6.9 \pm 0.6 \times 10^{-2}$, 0.11 ± 0.02, 0.21 ± 0.01, and 0.35 ± 0.01 s^{-1}, respectively. The inset shows the observe rate constants which are linearly dependent on O_2 concentrations with a bimolecular rate constant of 359 $M^{-1}s^{-1}$.

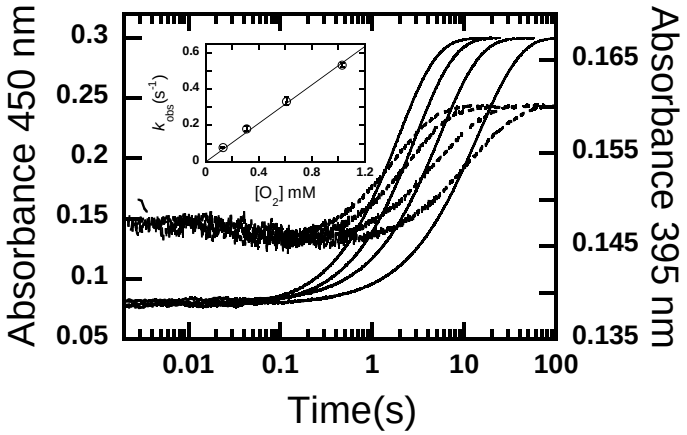

Figure S8. Kinetics of the reactions of reduced N593H variant with O_2. A solution of reduced **N593H** (30 µM) in 100 mM sodium phosphate buffer pH 7.0 was mixed with the same buffer containing various O_2 concentrations (0.13 mM, 0.31 mM, 0.61 mM and 0.96 mM; right to left traces) in the stopped-flow spectrophotometer at 4 °C. The concentrations given are those after mixing. The reactions were monitored by measuring the absorbance changes at 395 nm (dotted lines) and 450 nm (solid lines). The data show monophasic kinetics, indicating that flavin is oxidized without forming C4a-hydroperoxyflavin. The observed rate constants according to low to high O_2 concentrations are $8.1 \pm 0.3 \times 10^{-2}$, 0.18 ± 0.01, 0.33 ± 0.02, and 0.53 ± 0.01 s^{-1}, respectively. The inset shows the observed rate constants which are linearly dependent on O_2 concentrations with a bimolecular rate constant of 529 $M^{-1}s^{-1}$.

REFERENCES (บรรณานุกรม)

(1) Fagan, R. L.; Palfey, B. A. In *Comprehensive Natural Products II: Chemistry and Biology*; Mander, L., Lui, H.-W., Eds.; Elsevier: Oxford, 2010; Vol. 7, pp 37-113.

(2) Monti, D.; Ottolina, G.; Carrea, G.; Riva, S. *Chem Rev.* **2011,** *111*, 4111-4140.

(3) Mirzakulova, E.; Khatmullin, R.; Walpita, J.; Corrigan, T.; Vargas-Barbosa, N. M.; Vyas, S.; Oottikkal, S.; Manzer, S. F.; Hadad, C. M.; Glusac, K. D. *Nat Chem* **2012,** *4*, 794-801.

(4) Leisch, H.; Morley, K.; Lau, P. C. *Chem Rev.* **2011**, *111*, 4165-4222.

(5) Fraaije, M. W.; Berkel, W. J. H. v., Flavin-Containing Oxidative Biocatalysts. In *Biocatalysis in the Pharmaceutical and Biotechnology Industries*, Patel, R. N., Ed. CRC Press, Taylor & Francis Group: Boca Raton, FL, 2006; p 181.

(6) Chaiyen, P.; Fraaije, M. W. Mattevi, A. *Trends. Biochem. Sci.* **2012,** *37,* 373-380.

(7) Bruice, T. C. *Isr. J. Chem.* **1984,** *24,* 54-61.

(8) Eberlein, G.; Bruice, T. C. *J. Am. Chem. Soc.* **1983,** *105,* 6685-6697.

(9) Massey, V. *J. Biol. Chem.* **1994,** *269,* 22459-22462.

(10) Klinman, J. P. *Acc. Chem. Res.* **2007,** *40,* 325-333.

(11) Kommoju, P. R.; Chen, Z. W.; Bruckner, R. C.; Mathews, F. S.; Jorns, M. S. *Biochemistry* **2011,** *50,* 5521-5534.

(12) Jorns, M. S.; Chen, Z. W.; Mathews, F. S. *Biochemistry* **2010,** *49,* 3631-3639.

(13) Zhao, G.; Bruckner, R. C.; Jorns, M. S. *Biochemistry* **2008,** *47,* 9124-9135.

(14) Bruckner, R. C.; Winans, J.; Jorns, M. S. *Biochemistry* **2011,** *50,* 4949-4962.

(15) McDonald, C. A.; Fagan, R. L.; Collard, F.; Monnier, V. M.; Palfey, B. A. *J. Am. Chem. Soc.* **2011,** *133,* 16809-16811.

(16) Gadda, G. *Biochemistry* **2012,** *51,* 2662-2669.

(17) Henderson Pozzi, M.; Fitzpatrick, P. F. *Arch. Biochem. Biophys.* **2010,** *498,* 83-88.

(18) Sucharitakul, J.; Prongjit, M.; Haltrich, D.; Chaiyen, P. *Biochemistry* **2008,** *47,* 8485-8490.

(19) Wongnate, T.; Chaiyen, P. *FEBS J.* **2013,** *280,* 3009-3027.

(20) van der Kamp, M. W.; Mulholland, A. J. *Biochemistry* **2013,** *52,* 2708-2728.

(21) Groenhof, G. *Methods Mol. Biol.* **2013,** *924,* 43-66.

(22) Siegbahn, P. E.; Himo, F. *J. Biol. Inorg. Chem.* **2009,** *14,* 643-651.

(23) Senn, H. M.; Thiel, W. *Angew. Chem. Int. Ed. Engl.* **2009,** *48,* 1198-1229.

(24) Polyak, I.; Reetz, M. T.; Thiel, W. *J. Am. Chem. Soc.* **2012,** *134,* 2732-2741.

(25) Mata, R. A.; Werner, H. J.; Thiel, S.; Thiel, W. *J. Chem. Phys.* **2008,** *128,* 025104.

(26) Ridder, L.; Mulholland, A. J.; Rietjens, I. M.; Vervoort, J. *J. Mol. Graph. Model.* **1999,** *17,* 163-175, 214.

(27) Tian, B.; Strid, A.; Eriksson, L. A. *J. Phys. Chem. B.* **2011,** *115,* 1918-1926.

(28) Tian, B.; Tu, Y.; Strid, A.; Eriksson, L. A. *Chemistry* **2010,** *16,* 2557-2566.

(29) Wang, X. L.; Quan, J. M. *J. Am. Chem. Soc.* **2011,** *133,* 4079-4091.

(30) Prabhakar, R.; Siegbahn, P. E.; Minaev, B. F. *Biochim. Biophys. Acta.* **2003,** *1647,* 173-178.

(31) Hernández-Ortega, A.; Lucas, F.; Ferreira, P.; Medina, M.; Guallar, V.; Martínez, A. T. *Biochemistry* **2012,** *51,* 6595-6608.

(32) Bach, R. D.; Mattevi, A. *J. Org. Chem.* **2013,** *78,* 8585-8593.

(33) Frisch, M. J.; Trucks, G. W.; Schlegel, H. B.; Scuseria, G. E.; Robb, M. A.; Cheeseman, J. R.; Scalmani, G.; Barone, V.; Mennucci, B.; Petersson, G. A.; Nakatsuji, H.; Caricato, M.; Li, X.; Hratchian, H. P.; Izmaylov, A. F.; Bloino, J.; Zheng, G.; Sonnenberg, J. L.; Hada, M.; Ehara, M.; Toyota, K.; Fukuda, R.; Hasegawa, J.; Ishida, M.; Nakajima, T.; Honda, Y.; Kitao, O.; Nakai, H.; Vreven, T.; Montgomery, J. A.; Peralta, J. E.; Ogliaro, F.; Bearpark, M.; Heyd, J. J.; Brothers, E.; Kudin, K. N.; Staroverov, V. N.; Keith, T.; Kobayashi, R.; Normand, J.; Raghavachari, K.; Rendell, A.; Burant, J. C.; Iyengar, S. S.; Tomasi, J.; Cossi, M.; Rega, N.; Millam, J. M.; Klene, M.; Knox, J. E.; Cross, J. B.; Bakken, V.; Adamo, C.; Jaramillo, J.; Gomperts, R.; Stratmann, R. E.; Yazyev, O.; Austin, A. J.; Cammi, R.; Pomelli, C.; Ochterski, J. W.; Martin, R. L.; Morokuma, K.; Zakrzewski, V. G.; Voth, G. A.; Salvador, P.; Dannenberg, J. J.; Dapprich, S.; Daniels, A. D.; Farkas, O.; Foresman, J. B.; Ortiz, J. V.; Cioslowski, J.; Fox D. J. 2010, Gaussian 09, Revision C.01. *Gaussian, Inc.* Wallingford CT.

(34) Becke, A. D. *J. Chem. Phys.* **1993,** *98,* 5648-5652.

(35) Lee, C.; Yang, W.; Parr, R. G. *Phys. Rev. B.* **1988,** *37,* 785-789.

(36) Stephens, P. J.; Devlin, F. J.; Chabalowski, C. F.; Frisch, M. J. *J. Phys. Chem.* **1994,** *98,* 11623-11627.

(37) Siegbahn, P. E.; Borowski, T. *Acc. Chem. Res.* **2006,** *39,* 729-738.

(38) Bauschlicher, C. W. Jr.; Ricca, A.; Partridge, H.; Langhoff, S. R. In *Recent Advances in Density Functional Methods, Part II*, Chong DP, Ed., World Scientific Publishing Co. Singapore, 1997, Vol. 1, pp 165─ 228.

(39) Hariharan, P. C.; Pople, J. A. *Theor. Chim. Acta* **1973**, *28*, 213–222.

(40) Petersson, G. A.; Al-Laham, M. A. *J. Chem. Phys.* **1991**, *94*, 6081.

(41) Petersson, G. A.; Bennett, A.; Tensfeldt, T. G.; Al-Laham, M. A.; Shirley, W. A.; Mantzaris, J. *J. Chem. Phys.* **1988**, *89*, 2193.

(42) Barone, V.; Cossi, M. *J. Phys. Chem. A.* **1998,** *102,* 1995-2001.

(43) Adamo, C.; Barone, V. *J. Chem. Phys.* **1999,** *110,* 6158-6170.

(44) Hallberg, B. M.; Leitner, C.; Haltrich, D.; Divne, C. *J. Mol. Biol.* **2004,** *341,* 781-796.

(45) Kujawa, M.; Ebner, H.; Leitner, C.; Hallberg, B. M.; Prongjit, M.; Sucharitakul, J.; Ludwig, R.; Rudsander, U.; Peterbauer, C.; Chaiyen, P.; Haltrich, D.; Divne, C. *J. Biol. Chem.* **2006,** *281,* 35104-35115.

(46) Isobe, H.; Yamanaka, S.; Kuramitsu, S.; Yamaguchi, K. *J. Am. Chem. Soc.* **2008,** *130,* 132-149.

(47) Prongjit, M.; Sucharitakul, J.; Wongnate, T.; Haltrich, D.; Chaiyen, P. *Biochemistry* **2009,** *48,* 4170-4180.

(48) Pitsawong, W.; Sucharitakul, J.; Prongjit, M.; Tan, T. C.; Spadiut, O.; Haltrich, D.; Divne, C.; Chaiyen, P. *J. Biol. Chem.* **2010,** *285,* 9697-9705.

(49) Sucharitakul, J.; Wongnate, T.; Chaiyen, P. *Biochemistry* **2010,** *49,* 3753-3765.

(50) Prongjit, M.; Sucharitakul, J.; Palfey, B. A.; Chaiyen, P. *Biochemistry* **2013,** *52,* 1437-1445.

(51) Eyring, H. *J. Chem. Phys.* **1935,** *3,* 107.

(52) Winzor, D. J.; Jackson, C. M. *J. Mol. Recognit.* **2006,** *19,* 389–407.

(53) Wongnate, T.; Sucharitakul, J.; Chaiyen, P. *ChemBioChem* **2011,** *12,* 2577-2586.

(54) Tan, T. C.; Pitsawong, W.; Wongnate, T.; Spadiut, O.; Haltrich, D.; Chaiyen, P.; Divne, C. *J. Mol. Biol.* **2010,** *402,* 578-594.

(55) Mattevi, A. *Trends Biochem. Sci.* **2006,** *31,* 276-283.

(56) Sucharitakul, J.; Wongnate, T.; Chaiyen, P. *J. Biol. Chem.* **2011,** *286,* 16900-16909.

(57) Tan, T. C.; Haltrich, D.; Divne, C. *J. Mol. Biol.* **2011,** *409,* 588-600.

(58) Tian, B.; Strid, A.; Eriksson, L. A. *J. Phys. Chem. B.* **2011,** *115*, 1918-1926.

(59) Su, Q.; Klinman, J. P. *Biochemistry* **1999,** *38,* 8572-8581.

(60) Roth, J. P.; Klinman, J. P. *Proc. Natl. Acad. Sci.* **2003,** *100,* 62-67.

(61) Thotsaporn, K.; Chenprakhon, P.; Sucharitakul, J.; Mattevi, A.; Chaiyen, P. *J. Biol. Chem.* **2011,** *286,* 28170–28180.

(62) Orru, R.; Pazmiño, D. E.; Fraaije, M. W.; Mattevi. A. *J. Biol. Chem.* **2010,** *285,* 35021-35028.

OUTPUT จากโครงการวิจัยที่ได้รับทุนจาก สกว.

1. ผลงานตีพิมพ์ 2 ฉบับ

(1) Wongnate†, T.; **Surawatanawong†, P.**; Visitsatthawong, S.; Sucharitakul, J.; Scrutton, N. S.; Chaiyen, P. "Proton-Coupled Electron Transfer and Adduct Configuration are Important for C4a-Hydroperoxyflavin Formation and Stabilization in a Flavoenzyme" *J. Am. Chem. Soc.*, **2014**, *136*, 241. **(†These authors contribute equally.)**

(2) Prachyawarakorn, V.; Sangpetsiripan, S.; **Surawatanawong, P.**; Mahidol, C.; Ruchirawat, S.; Kittakoop, P. "Flavans from *Desmos Cochinchinensis* as Potent Aromatase Inhibitors" *Med. Chem. Comm.,* **2013**, *4*, 1590.

2. การนำผลงานวิจัยไปใช้ประโยชน์เชิงวิชาการ

มีการพัฒนาการเรียนการสอน นักศึกษาระดับปริญญาตรีในการทำงานวิจัยเป็นโครงงานสำหรับจบการศึกษาจำนวน 3 คน

(1) นางสาวบุศรินทร์ สวัสดิ์ล้น (Boodsarin Sawatlon, B.Sc. May 2013)
(2) นายทวีชัย วิทิตสุวรรณกุล (Taveechai Wititsuwannakul, B.Sc. May 2014)
(3) นายสุรวิช วิสิษฐ์สัทธาวงศ์ (Surawit Visitsatthawong, B.Sc. May 2014)

3. การเสนอผลงานในที่ประชุมวิชาการ

(1) Poster presentation at the 8th Conference on Science and Technology for Youths, March 21-23, 2013, Bitec, Bangna “Mechanistic study of nickel-catalyzed C-O bond activation in hydrogenolysis of diphenyl ether by density functional theory” Boodsarin Sawatlon and Panida Surawatanawong

(2) Poster presentation at the 14th Science Project Exhibition, March 13, 2013, Faculty of Science, Mahidol University, “Mechanistic study of nickel-catalyzed C-O bond activation in hydrogenolysis of diphenyl ether by density functional theory” Boodsarin Sawatlon and Panida Surawatanawong

(3) Poster presentation at the 15th Science Project Exhibition, March 17, 2014, Faculty of Science, Mahidol University, “Mechanistic study of nickel-catalyzed C-O bond activation in hydrogenolysis of diphenyl ether by density functional theory” Taveechai Wititsuwannakul and Panida Surawatanawong

(4) Poster presentation at Interface between experimental and theoretical approaches to energy-related enzyme catalysis, June 4-6, 2014, University College London, United Kingdom, “Proton-Coupled Electron Transfer for C4a-Hydroperoxyflavin Formation and Stabilization in a Flavoenzyme” Panida Surawatanawong, Thanyaporn Wongnate, Surawit Visitsatthawong, Jeerus Sucharitakul, Nigel S. Scrutton, and Pimchai Chaiyen

APPENDIX (ภาคผนวก)

ผลงานตีพิมพ์ 2 ฉบับ

(1) Wongnate†, T.; **Surawatanawong†, P.**; Visitsatthawong, S.; Sucharitakul, J.; Scrutton, N. S.; Chaiyen, P. "Proton-Coupled Electron Transfer and Adduct Configuration are Important for C4a-Hydroperoxyflavin Formation and Stabilization in a Flavoenzyme" *J. Am. Chem. Soc.*, **2014**, *136*, 241. **(†These authors contribute equally.)**

(2) Prachyawarakorn, V.; Sangpetsiripan, S.; **Surawatanawong, P.**; Mahidol, C.; Ruchirawat, S.; Kittakoop, P. "Flavans from *Desmos Cochinchinensis* as Potent Aromatase Inhibitors" *Med. Chem. Comm.,* **2013**, *4*, 1590.

JACS
JOURNAL OF THE AMERICAN CHEMICAL SOCIETY
Article
pubs.acs.org/JACS

Proton-Coupled Electron Transfer and Adduct Configuration Are Important for C4a-Hydroperoxyflavin Formation and Stabilization in a Flavoenzyme

Thanyaporn Wongnate,[†,‡] Panida Surawatanawong,[§,‡] Surawit Visitsatthawong,[§] Jeerus Sucharitakul,[∥] Nigel S. Scrutton,[⊥] and Pimchai Chaiyen*[,†]

[†]Department of Biochemistry and Center of Excellence in Protein Structure and Function, Faculty of Science, Mahidol University, Bangkok, 10400 Thailand

[§]Department of Chemistry and Center of Excellence for Innovation in Chemistry, Mahidol University, Bangkok 10400 Thailand

[∥]Department of Biochemistry, Faculty of Dentistry, Chulalongkorn University, Henri-Dunant Road, Patumwan, Bangkok, 10300 Thailand

[⊥]Manchester Institute of Biotechnology and Faculty of Life Sciences, The University of Manchester, Manchester M1 7DN United Kingdom

S *Supporting Information*

ABSTRACT: Determination of the mechanism of dioxygen activation by flavoenzymes remains one of the most challenging problems in flavoenzymology for which the underlying theoretical basis is not well understood. Here, the reaction of reduced flavin and dioxygen catalyzed by pyranose 2-oxidase (P2O), a flavoenzyme oxidase that is unique in its formation of C4a-hydroperoxyflavin, was investigated by density functional calculations, transient kinetics, and site-directed mutagenesis. Based on work from the 1970s−1980s, the current understanding of the dioxygen activation process in flavoenzymes is believed to involve electron transfer from flavin to dioxygen and subsequent proton transfer to form C4a-hydroperoxyflavin. Our findings suggest that the first step of the P2O reaction is a single electron transfer coupled with a proton transfer from the conserved residue, His548. In fact, proton transfer enhances the electron acceptor ability of dioxygen. The resulting ·OOH of the open-shell diradical pair is placed in an optimal position for the formation of C4a-hydroperoxyflavin. Furthermore, the C4a-hydroperoxyflavin is stabilized by the side chains of Thr169, His548, and Asn593 in a "face-on" configuration where it can undergo a unimolecular reaction to generate H_2O_2 and oxidized flavin. The computational results are consistent with kinetic studies of variant forms of P2O altered at residues Thr169, His548, and Asn593, and kinetic isotope effects and pH-dependence studies of the wild-type enzyme. In addition, the calculated energy barrier is in agreement with the experimental enthalpy barrier obtained from Eyring plots. This work revealed new insights into the reaction of reduced flavin with dioxygen, demonstrating that the positively charged residue (His548) plays a significant role in catalysis by providing a proton for a proton-coupled electron transfer in dioxygen activation. The interaction around the N5-position of the C4a-hydroperoxyflavin is important for dictating the stability of the intermediate.

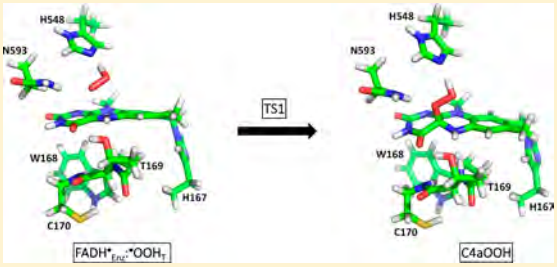

INTRODUCTION

Flavoenzymes not only have indispensible roles in cellular metabolism[1] but also are useful as biocatalysts for chemical synthesis reactions and as bioelectrocatalysts for biofuel cell applications.[2,3] Baeyer−Villiger monooxygenase has been used widely in pharmaceutical industries to synthesize drugs.[4] Recently, flavin derivatives were successfully used for catalytic water oxidation in a photochemical water splitting process.[3] Therefore, understanding how flavoenzymes function is crucial to improving their applications and to developing biomimetic flavin derivatives for use as efficient biocatalysts and biosensors and in biofuel cells.[5]

The physical and chemical basis underlying the reactions of reduced flavin and dioxygen in flavoenzymes is one of the most fascinating issues in flavoenzymology.[6] The same reduced flavin (FAD or FMN) when bound to different proteins reacts differently with dioxygen (i.e., to form H_2O_2 in oxidases, to form C4a-(hydro)peroxyflavin in monooxygenases, or to have sluggish reactivity toward dioxygen in dehydrogenases in order to transfer electrons to other acceptors). The different reaction outcomes due to the different active site environments of these proteins allow nature to use the same set of chemical reactants to perform a variety of flavoenzyme functions, including use of the abundant oxygen in aerobic systems as an electron acceptor (oxidase), to incorporate an oxygen atom into an organic

Received: August 30, 2013
Published: December 16, 2013

   dx.doi.org/10.1021/ja4088055 | *J. Am. Chem. Soc.* 2014, 136, 241−253

Scheme 1. Flavin Reaction Mechanisms with Dioxygen[a]

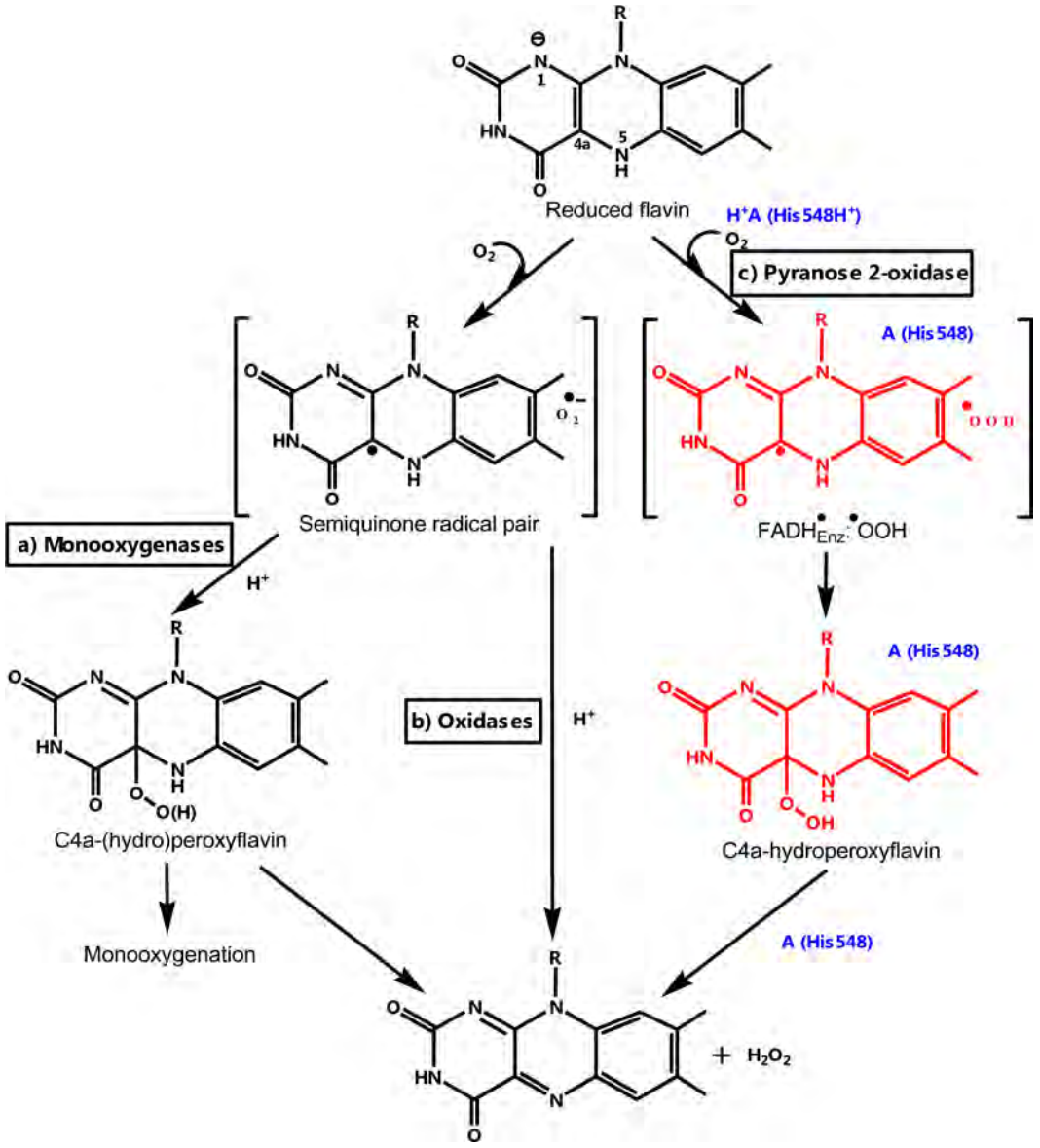

[a]Paths (a) and path (b) are conventional pathways for the reactions with O_2 in monooxygenases and oxidases, respectively. Path (c) is the alternative pathway for the reactions with O_2 in pyranose 2-oxidase, according to the findings of the current study.

substrate (monooxygenase), or to mediate electron transfer in complex protein systems (dehydrogenase). Most of our current understanding of flavin chemistry in flavoenzymes is based on work performed in the 1970s−1980s by Bruice et al.[7,8] and Massey et al.,[9] and the current view of the reaction of reduced flavin with oxygen in oxidases and oxygenases can be summarized as depicted in Scheme 1 (paths a and b).

In chemical synthesis, catalytic oxidative reactions and oxygen insertions with high selectivity generally require multiple steps and often require heavy metals. Flavin is among a few organic cofactors that can use molecular oxygen for oxygenation reactions.[5] The mechanism for the control of this reaction should be well coordinated so that leakage of hazardous reactive oxygen species during enzyme turnover is minimized and the oxygenases can most efficiently catalyze oxygenation. Many research groups in the past recent years have investigated the role of active site residues that are important for dioxygen activation.[10−17] One of the recurrent features found in these systems is the presence of a positively charged residue that is located near the flavin N5. Previous work suggested that this positive charge provides a preorganized environment that stabilizes the superoxide anion species[10−14,16] that forms after the first step of electron transfer (path a and b in Scheme 1).[8] However, the electronic structures and energies of key intermediates in the dioxygen activation mechanisms have not been studied in detail.

Pyranose 2-oxidase (P2O) is a suitable flavoenzyme for exploring dioxygen activation and C4a-hydroperoxyflavin stabilization. P2O catalyzes the oxidation of pyranose sugars to form 2-keto-sugars and H_2O_2 (Scheme S1, Supporting Information [SI]). The enzyme has been applied in the synthesis of rare sugars.[2] Thus far, it has been the only flavoenzyme oxidase, in which C4a-hydroperoxyflavin has been detected as an intermediate under natural turnover conditions.[18,19] The reaction of P2O could be viewed as a missing link in evolution connecting flavin-dependent monooxygenases

dx.doi.org/10.1021/ja4088055 | J. Am. Chem. Soc. 2014, 136, 241−253

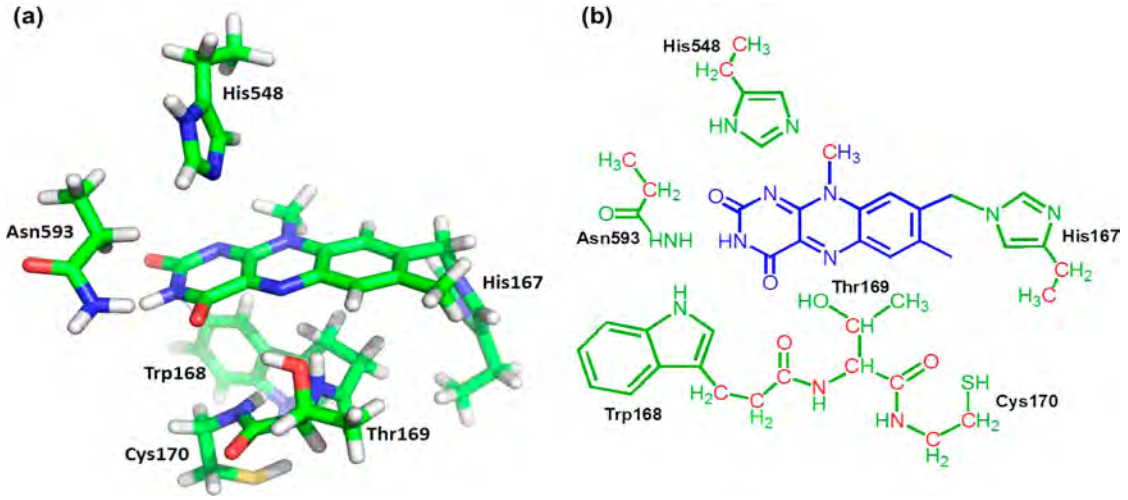

Figure 1. Active site model of P2O(WT) in the closed conformation. (a) X-ray structure of the active site model. (b) Schematic representation of the active site model. The isoalloxazine ring of FAD is shown in blue, flexible residues in green, and constrained atoms in red.

in which formation of C4a(hydro)peroxyflavin is mandatory and flavoenzyme oxidases in which formation of C4a-hydroperoxyflavin is possibly just one of the means of generating H_2O_2 (Scheme 1). As no X-ray structure of enzyme-bound C4a-hydroperoxyflavin is available, it remains elusive how the intermediate is stabilized in flavoenzymes. It has been proposed that a cavity that is commonly found above the flavin C4a atom of monooxygenases may serve as an entrance for oxygen diffusion and accommodate the peroxide adduct.[6]

Theoretical calculations have been used to study electronic structures and energies in enzymatic reactions.[20−23] Reaction mechanisms have been theoretically investigated for a few flavoenzymes, e.g., a Baeyer−Villiger monooxygenase (oxygen insertion[24]), *p*-hydroxybenzoate hydroxylase and phenol hydroxylase (aromatic hydroxylation[25,26]), 2-methyl-3-hydroxypyridine-5-carboxylate monooxygenase (ring-cleavage reaction[27,28]), BluB (cleavage of riboflavin[29]), glucose 1-oxidase and aryl alcohol oxidase (oxidation of alcohol moiety[30,31]). The mechanisms of H_2O_2 elimination from a free C4a-hydroperoxyflavin species was recently investigated by Bach and Mattevi.[32] In combination with experimental data, computational studies can provide greater insights on the enzyme mechanisms.[20]

In this report, the reaction of reduced flavin and dioxygen catalyzed by P2O was explored using density functional theory (DFT). The calculated activation energies were compared to the experimental activation enthalpies determined from the Eyring plot based on transient kinetic studies at various temperatures. The calculations agreed well with the results from kinetic isotope effect (KIE) and site-directed mutagenesis studies. DFT analysis gave the following new insights into this reaction: (i) the protonated His548 does not stabilize the superoxide anion via electrostatic interactions; rather, it acts as a general acid by providing a proton for the proton-coupled electron transfer in dioxygen activation (path c in Scheme 1) and (ii) the −OOH moiety of C4a-hydroperoxyflavin is in the "face-on" configuration and stabilized by a hydrogen-bonding network from His548, Asn593, and Thr169.

EXPERIMENTAL PROCEDURES

Computational Details. All calculations were performed with the *Gaussian 09* program.[33] B3LYP[34−36] functional has been shown to be suitable for the study of enzymatic reactions.[29,37,38] Thus, B3LYP was used for all geometry optimizations and frequency calculations in this study. The 6-31++G(d,p)[39−41] basis set was used for the H that forms H_2O_2 and 6-31G(d) was used for all other atoms.[39−41] The single-point energy and solvation free energy corrections were calculated by B3LYP/6-311+G(d,p) on the geometries based on the gas-phase optimizations using the conductor-like polarizable continuum model (CPCM)[42] with UAKS[43] atomic radii and a dielectric constant of 4.0 to represent the protein environment. The energy barrier based on the electronic energy with solvation correction obtained from B3LYP/6-311+G(d,p) calculations is lower than the electronic energy obtained from B3LYP/6-31G(d) calculations, especially for the H_2O_2 elimination step (Table S1, SI). Open-shell systems were treated using spin unrestricted B3LYP (UB3LYP).

The active site model was taken from the crystal structure of P2O(WT) in the closed conformation (1.80 Å; PDB code: 1TT0).[44] The model consists of 118 atoms, which includes $FADH^-$ (the isoalloxazine part) and the residues within ∼5 Å radius from the N5 atom of the $FADH^-$ (Trp168, Thr169, and Cys170) and the key conserved residues[45] (His167, His548, and Asn593) of the enzyme (Figure 1). To minimize the computational power for the relevant protein environment, only the side chains were allowed to be flexible during the geometry optimization. Thus, the atoms on the backbone were constrained at the initial positions in the crystal structure to maintain a reasonable geometry of the active site while all other atoms were optimized (Figure 1). For transition states, frequencies were calculated to ensure that there was one imaginary frequency corresponding to the reaction coordinate. Note that, since some atoms in the model are constrained during optimization, the intermediate and transition state structures are not strictly stationary points. Thus, the zero-point vibrational energy corrections and thermal effects are not well-defined and are not considered in this study.

To critically evaluate the extent of spin contamination in open-shell species, the expectation value for the total spin angular momentum, $\langle S^2 \rangle$, of all diradical species in this study were calculated and are shown in Table S2 in SI. The data indicate that, for the triplet species, there is no significant problem with the spin contamination as all of the $\langle S^2 \rangle^{\text{triplet}}$ values are close to 2. For the open-shell singlet species, the $\langle S^2 \rangle^{\text{singlet}}$ values are close to 1 and largely differ from zero. This may be because the use of the broken symmetry approach to calculate the open-shell singlet species can result in spin contamination from higher spin states. As the spin projection (SP) technique was successfully employed in the calculation of diradical energies in previous works,[29,46] we used this method to estimate the energy of the spin-

dx.doi.org/10.1021/ja4088055 | J. Am. Chem. Soc. 2014, 136, 241−253

unrestricted open-shell singlet species (eqs 1, 2).[46] E^X is the electronic energy, and $\langle S^2\rangle^X$ is the expectation value for the total spin angular momentum of the spin state X (X = singlet or triplet).[46]

$$E_{SP}^{\text{singlet}} = E^{\text{singlet}} + C_{SC}[E^{\text{singlet}} - E^{\text{triplet}}] \quad (1)$$

$$C_{SC} = \frac{\langle S^2\rangle^{\text{singlet}}}{\langle S^2\rangle^{\text{triplet}} - \langle S^2\rangle^{\text{singlet}}} \quad (2)$$

Temperature Dependence Studies. The measurements were performed using a TgK Scientific model SF-61DX stopped-flow spectrophotometer in single-mixing mode. The optical path length of the observation cell was 1 cm. The experimental protocols used were similar to those in a previous report.[18,47,48] In brief, the stopped-flow apparatus was made anaerobic by flushing the flow system with an anaerobic buffer containing 10 mM sodium dithionite in 50 mM sodium phosphate buffer, pH 7.0. The buffer was made anaerobic by equilibrating with oxygen-free nitrogen (ultrahigh purity) that had been passed through an Oxyclear oxygen removal column (Labclear). The anaerobic buffer was allowed to stand in the flow system overnight. The flow unit was then rinsed with the anaerobic buffer before experiments. For studying the oxidative half-reaction, an anaerobic enzyme solution was equilibrated in an anaerobic glovebox (Belle Technology). The enzyme was then reduced with a solution of 10 mM D-glucose in 100 mM sodium phosphate buffer pH 7.0. While adding the solution of D-glucose, enzyme spectra were recorded using a spectrophotometer inside the glovebox to ensure complete reduction. The reduced enzyme solution was placed in a glass tonometer and loaded onto the stopped-flow spectrophotometer.

Reduced P2O(WT) (53 μM) was mixed with buffers containing 1.22 mM O_2 (concentrations before mixing) at various temperatures (5, 10, 15, 20, 25, and 30 °C) in a stopped-flow spectrophotometer. Large amplitude changes were detected at 395 and 458 nm. The reaction showed two kinetic phases. For example, at 5 °C, the first phase (0.002−0.04 s, increase of absorbance at 395 nm) indicates the formation of a C4a-hydroperoxyflavin intermediate that subsequently decays in the second phase (0.04−1 s) to yield H_2O_2 and the oxidized enzyme. The second phase occurred simultaneously with an absorbance increase at 458 nm (Figure 5).[18,49,50] Apparent rate constants (k_{obs}) were calculated from the kinetic traces using exponential fits and the software packages Kinetic Studio (TgK Scientific, Bradford-on-Avon, UK) or Program A (developed by R. Chang, C.-J. Chiu, J. Dinverno, and D. P. Ballou, at University of Michigan, Ann Arbor, MI). Simulations were performed by numerical methods with Runge−Kutta algorithms implemented in Berkeley Madonna 8.3 with a time step of 10^{-3} s. Rate constants associated with Scheme 2 can be analyzed according to eqs 3 and 4.[18] Analysis yielded

Scheme 2. Reaction Mechanism of the Oxidative Half-Reaction of P2O(WT)

$$\text{FADH}^-_{\text{Enz}} + O_2 \underset{k_2}{\overset{k_1}{\rightleftharpoons}} \text{C4a-OOH} \xrightarrow{k_3} \text{FAD}_{\text{Enz}} + H_2O_2$$

a bimolecular rate constant for the formation of C4a-hydroperoxyflavin (k_1), a reverse rate constant (k_2), and a rate constant for H_2O_2 elimination (k_3). A summary of the rate constants is provided in Table S4 in SI. The rate constants (k_1, k_2, and k_3) were plotted against the temperature used (see Figure S5, SI).

$$k_{obs1} = k_1[O_2] + k_2 + k_3 - \frac{k_1k_3[O_2]}{k_1[O_2] + k_2 + k_3} \quad (3)$$

$$k_{obs2} = \frac{k_1k_3[O_2]}{k_1[O_2] + k_2 + k_3} \quad (4)$$

The Eyring equation was used for determining the enthalpy of activation ($\Delta H^{\ddagger}$) in this reaction (eq 5, where k is a rate constant, T is absolute temperature, $\Delta H^{\ddagger}$ is enthalpy of activation, R is the gas constant (1.987 cal mol^{-1} K^{-1}), k_B is the Boltzmann constant (1.381×10^{-23} J K^{-1}), h is Planck's constant (6.626×10^{-34} J s), and $\Delta S^{\ddagger}$ is the entropy of activation).[51,52] The linear form of the Eyring plot is shown in eq 6. The plot of $\ln(k/T)$ versus $1/T$ gives a straight line with a slope of $-\Delta H^{\ddagger}/R$ from which the value of the enthalpy of activation can be derived.

$$k = \left(\frac{k_BT}{h}\right)\exp\left(\frac{\Delta S^{\ddagger}}{R}\right)\exp\left(-\frac{\Delta H^{\ddagger}}{RT}\right) \quad (5)$$

$$\ln\frac{k}{T} = -\frac{\Delta H^{\ddagger}}{R}\frac{1}{T} + \ln\frac{k_B}{h} + \frac{\Delta S^{\ddagger}}{R} \quad (6)$$

Reaction of Variant P2O with O_2. The previous study indicated that the H548A, H548C, H548S, and H548N variant enzymes contained mixed populations of covalently linked and noncovalent flavins.[53] Therefore, in order to investigate the role of His548 in flavin oxidation, double mutations containing both His548 and H167A (a mutation in which the covalent histidyl-FAD linkage was removed) in addition to single mutations were constructed. We have shown previously that the H167A variant enzyme reacts with molecular oxygen to form C4a-hydroperoxyflavin with rate constants similar to those found for the wild-type enzyme, indicating that the covalent linkage is not an important factor for formation of the intermediate.[49] The effects of removal of a covalent histidyl-FAD linkage are mainly on the reductive half-reaction.[49] Therefore, the absence of the covalent histidyl-FAD linkage in P2O variants in this study should not introduce any confounding artifacts to the kinetic analysis.

For studying the oxidative half-reaction of N593H and H167A/H548 variant enzymes, an anaerobic enzyme solution was equilibrated in an anaerobic glovebox (as described above). The enzyme was then reduced with a solution of 10 mM D-glucose in 100 mM sodium phosphate buffer pH 7.0 for the N593H variant enzyme. For H167A/H548A, H167A/H548C, H167A/H548S, and H167A/H548N variants which are catalytically inactive for the reductive half-reaction, the enzymes were reduced with a solution of 10 mM sodium dithionite. The oxidation of reduced variant enzyme by O_2 was monitored at various wavelengths (300−500 nm) using a stopped-flow spectrophotometer. Buffer solutions with various concentrations of O_2 were made by bubbling certified O_2/N_2 gas mixtures of 20%, 50%, 100%, and 100% on ice through syringes for 8 min. After mixing, this procedure resulted in O_2 concentrations of 0.13 mM, 0.31 mM, 0.61 mM, and 0.96 mM, respectively. Equilibration of a buffer on ice with a 100% O_2/N_2 gas mixture results in a buffer solution that contains 1.92 mM O_2 before mixing. Apparent rate constants (k_{obs}) from kinetic traces were calculated as described above.

Imidazole Rescue Experiment. The imidazole rescue experiments on H167A/H548 variants were investigated over a pH range from 6.0 to 8.0 using 100 mM sodium phosphate for pH 6.0 and 7.0, and 100 mM Tris-HCl for pH 8.0. The enzyme solution was mixed with 100 μM imidazole and exchanged into each pH buffer. The resulting solution was equilibrated at that pH for 14−16 h (overnight). Sodium dithionite solutions which were used for reducing the enzyme were prepared by dissolving solid sodium dithionite powder into each pH buffer. A reduced variant enzyme solution was prepared as previously described, and the experiments were done at various pH values. Experimental protocols were similar to those described above.

RESULTS

QM Analysis of the Reaction of Reduced P2O with Oxygen (oxidative half-reaction). The density functional calculations described in Experimental Procedures were used to analyze the physical parameters associated with the individual steps and transition states of the reaction of the P2O-bound $FADH^-$ ($FADH^-_{Enz}$) (truncated at only the isoalloxazine ring) and dioxygen.

The starting flavin species was assigned as an anionic form in which the N1 position is deprotonated (species 1 in Scheme 3).

dx.doi.org/10.1021/ja4088055 | J. Am. Chem. Soc. 2014, 136, 241−253

Scheme 3. Reaction of P2O-Bound Reduced FAD ($FADH^-_{Enz}$) with Oxygen[a]

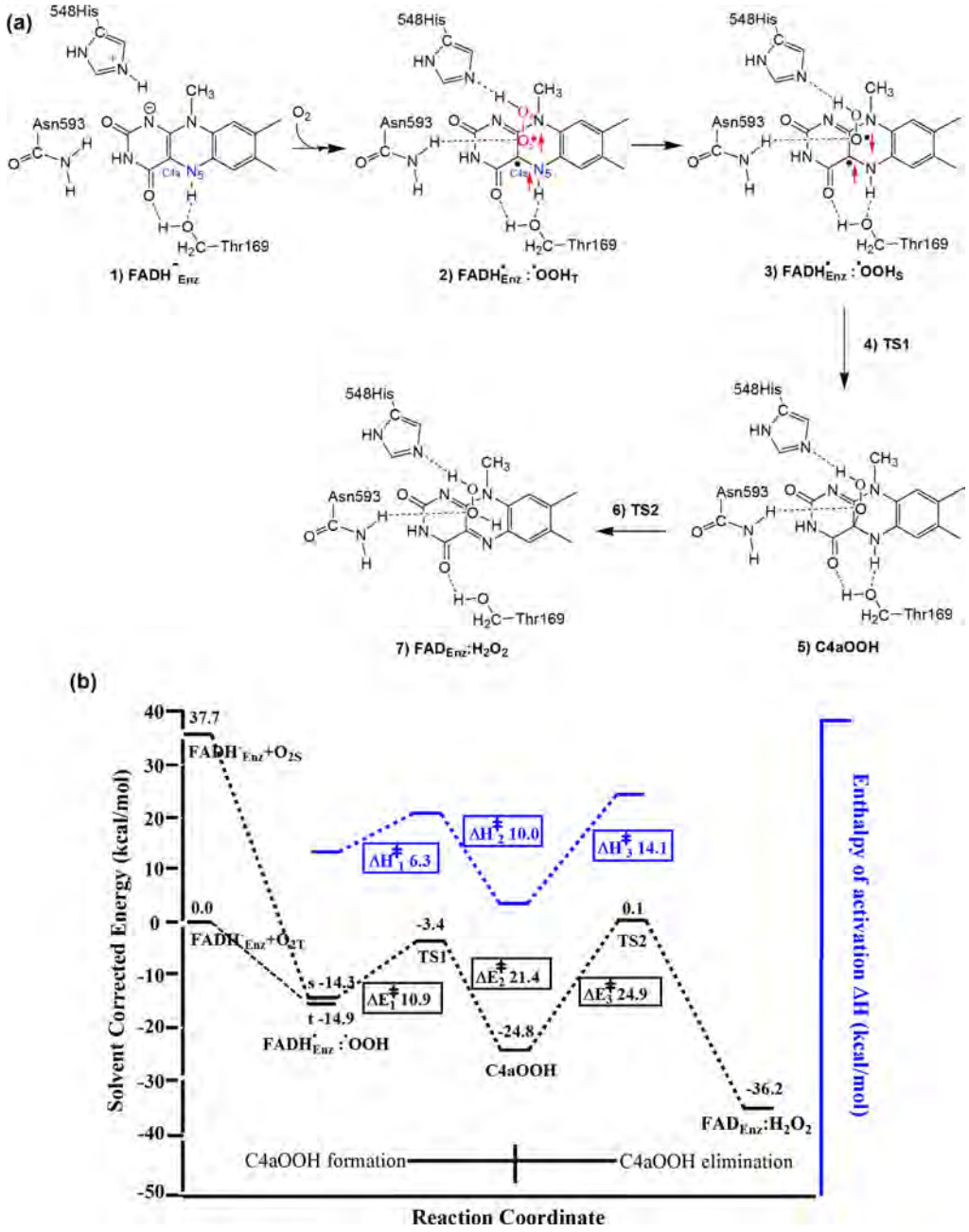

[a](a) Proposed mechanisms for the reaction of $FADH^-_{Enz}$ with oxygen. Stage 1 is C4a-hydroperoxyflavin formation (**1**–**5**) while Stage 2 is H_2O_2 elimination and oxidized flavin generation (**5**–**7**). (b) Calculated energy profiles along the proposed reaction pathway. The enthalpy of activation obtained from the transient kinetics results in Figure 5 is overlaid in blue.

The relevance of this form in the P2O reaction is supported by the fact that the oxidized enzyme can react with sulfite to form the flavin N(5)-sulfite adduct in which the flavin N1 is in the anionic form.[54] In general, the anionic form of the reduced flavin is the form that is bound to flavoenzyme oxidases.[55] Based on the active site structure of P2O,[45] residues approximately 5 Å away from the N5 atom of the $FADH^-$ (Trp168, Thr169, and Cys170) and the key conserved residues (His167, His548, and Asn593) were included in the QM model (Figure 1).

Among these residues, His548 is the most likely to be in the protonated state. According to previous studies of P2O, upon completion of the reductive half-reaction, the oxidized flavin is reduced by D-glucose, and His548 is expected to be in the protonated state.[53] Furthermore, the results of pH-dependence studies of the oxidative half-reaction at various pH values suggest that one of the active site residues should be protonated to allow the reaction to proceed via formation of C4a-hydroperoxyflavin.[50] On the basis of these findings, the calculation model was started with His548 in the protonated state (species 1 in Scheme 3).

Transient kinetics studies of the P2O oxidative half-reaction indicated that the reaction proceeds via two stages, involving C4a-hydroperoxyflavin formation and decay (H_2O_2 elimination).[18,50,56] Results from the density functional calculations give insights into the electronic structures, spin states, and

dx.doi.org/10.1021/ja4088055 | J. Am. Chem. Soc. 2014, 136, 241–253

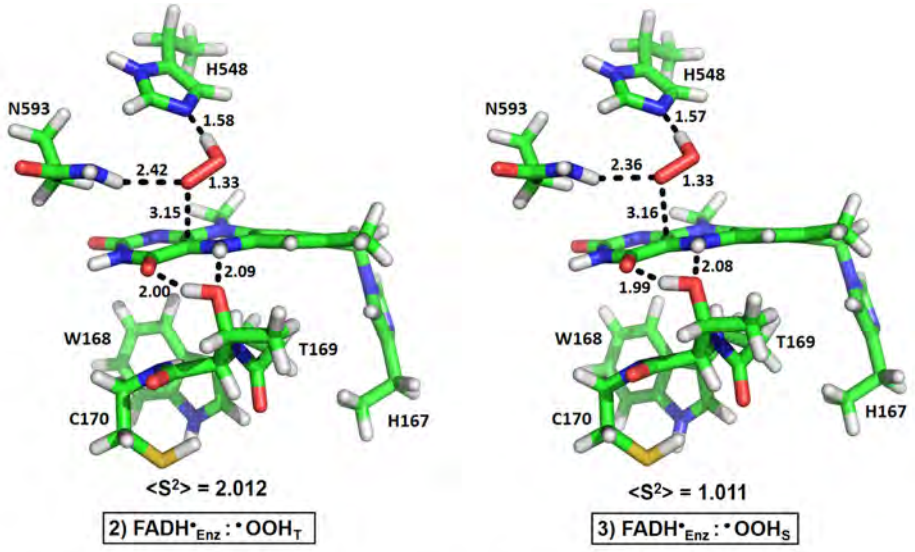

	FADH•Enz: •OOHT	FADH•Enz: •OOHS	FADH•Free: •OOHT	FADH•Free: •OOHS	FADH⁻Free:O2T	FADH⁻Free:O2S	O2T	O2S
$\Delta E_{S\text{-}T}$ (kcal/mol)	0.6		0.0		7.3		37.7	
$q_{O\text{-}O}$	-0.480	-0.469	-0.424	-0.423	-0.249	-0.273	0.000	0.000
q_{OOH}	-0.081	-0.080	-0.028	-0.028	-	-	-	-
$\rho_{O\text{-}O}$	+1.013	-1.011	+1.017	+1.019	+1.702	+0.007	+2.000	0.000
ρ_{OOH}	+1.004	-1.002	+1.007	+1.010	-	-	-	-
ρ_{Flavin}	+0.991	+0.990	+1.015	-1.010	+0.304	-0.005	-	-
$d_{Op\text{-}Od}$(Å)	1.33	1.33	1.32	1.32	1.25	1.25	1.21	1.21

Figure 2. Optimized structures of FADH·$_{Enz}$:·OOH complexes. The subscripts T and S represent triplet state and singlet state, respectively. $\Delta E_{S\text{-}T}$ represents the energy difference between the spin-unrestricted open-shell singlet state and the triplet state. Mulliken charge populations (q) on the two oxygen atoms (q_{O-O}) of the ·OOH fragment and on the ·OOH fragment (q_{OOH}) are shown. Mulliken spin populations (ρ) on the O_2 (ρ_{O-O}), ·OOH (ρ_{OOH}), and flavin (ρ_{Flavin}) fragments are shown. Distances between the two oxygen atoms on the ·OOH fragment ($d_{Op\text{-}Od}$) are shown in Å.

energies of the transition states and intermediates involved (Figure 2−4), and point to a five-step process (Scheme 3).

Step 1: Proton-Coupled Electron Transfer to Triplet Dioxygen (Species 1 to Species 2). The energy of the first species, $FADH^-_{Enz}+O_{2T}$ (or $FADH^-_{Enz}+O_{2S}$), is a combination of the electronic energy with solvation correction from the optimized structure of $FADH^-_{Enz}$ (species 1) and that of O_{2T} (or O_{2S}). The stabilized complex of reduced flavin ($FADH^-_{Enz}$) and dioxygen was found to be improbable through calculations. After several attempts, when the O_2 was placed in the vicinity above the C4a position and upon geometry optimization, the proton from the protonated His548 was immediately transferred to the dioxygen. This was concomitant with the first electron transfer from the reduced flavin to the dioxygen to generate the flavin semiquinone:·OOH radical pair in the triplet state (FADH·$_{Enz}$:·OOH_T) (Figure 2). It should be mentioned that when this reaction step was calculated using other functionals such as TPSS, the concomitant proton and electron transfer was similar to the results obtained using B3LYP.

Mulliken charge populations on the two oxygen atoms of the FADH·$_{Enz}$:·OOH_T (−0.480) are relatively more negative than that of the triplet dioxygen (0.000); this indicates that an electron is transferred to ·OOH. As the charge population on the overall OOH fragment is −0.081, the concomitant electron and proton transfer neutralizes the negative charge of the superoxide species and increases the ability of dioxygen to accept an electron from $FADH^-_{Enz}$. Mulliken spin populations on the OOH (+1.004) and the flavin (+0.991) fragments reveal the identity of species 2 as the triplet FADH·$_{Enz}$:·OOH_T (Table in Figure 2), with a single unpaired electron located on each of the OOH and the flavin fragments.

Note that the proton-coupled electron transfer process for the reaction of reduced flavin and dioxygen presented here is different from the current view[7,9] that describes the first step as an electron transfer to generate a radical pair of flavinsemiquinone and superoxide anion before the subsequent proton transfer occurs (paths a and b in Scheme 1).

Step 2: Triplet (FADH·$_{Enz}$:·OOH_T) to singlet (FADH·$_{Enz}$:·OOH_S) Spin Transition (Species 2 to Species 3). The triplet (FADH·$_{Enz}$:·OOH_T) can undergo a spin transition with a small energy requirement (+0.6 kcal/mol, Scheme 3, Table in Figure 2) to become an open-shell singlet diradical (FADH·$_{Enz}$:·OOH_S), in which the spin populations on the OOH fragment change from +1.004 to −1.002, but remain the same on the flavin fragment at about +0.99 (Table in Figure 2, Figure S3 in SI). Overall, the structural geometries of the triplet FADH·$_{Enz}$:·OOH_T and the open-shell singlet diradical FADH·$_{Enz}$:·OOH_S complexes are similar (Table in Figure 2). The O_p-O_d bond distance in both FADH·$_{Enz}$:·OOH_T and FADH·$_{Enz}$:·OOH_S (1.33 Å) is significantly longer than that in the O_{2T} (1.21 Å),

dx.doi.org/10.1021/ja4088055 | J. Am. Chem. Soc. 2014, 136, 241−253

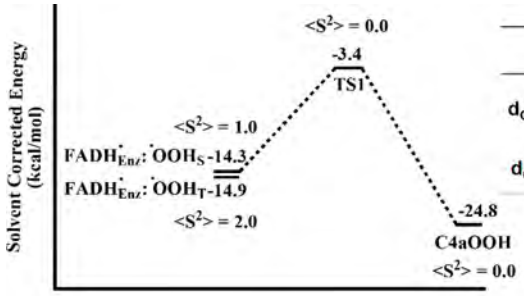

	FADH•Enz:•OOHT	FADH•Enz:•OOHS	TS1	C4aOOH
d_{C4a-Op} (Å)	3.15	3.16	2.35	1.44
d_{Op-Od} (Å)	1.33	1.33	1.37	1.45

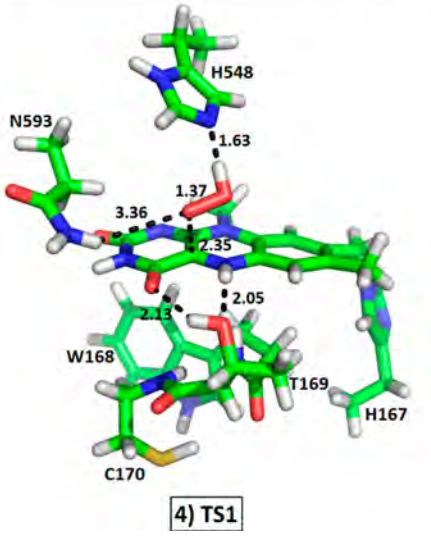

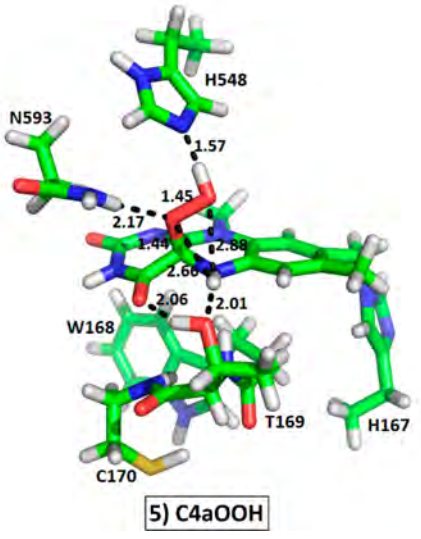

Figure 3. Relative energy profiles for the formation of C4a-hydroperoxyflavin intermediate (C4aOOH, species 5 in Scheme 3). The optimized structures of transition state 1 (TS1) and the C4aOOH intermediate are shown. The C4a−O_p distance (d_{C4a-Op}) and the O_p−O_d distance (d_{Op-Od}) are shown in the table.

corresponding to the addition of one electron into the antibonding orbital of the dioxygen.

To identify the active site residues involved in the P2O dioxygen activation process, we studied this process in the absence of all residues. Thus, the electronic structures and energies in both triplet and open-shell singlet states for the dioxygen (O_2), the $FADH^-_{Free}$:O_2 complex, and the $FADH\cdot_{Free}$:·OOH complex were investigated in order to compare them with those for the $FADH\cdot_{Enz}$:·OOH. For dioxygen (O_2) in the absence of a flavin cofactor, the spin transition process from the triplet O_{2T} (ρ_{O-O} = +2.000) to the singlet O_{2S} (ρ_{O-O} = 0.000) requires a large energy input of 37.7 kcal/mol (Table in Figure 2). The O_p−O_d bond distances in both spin states are similar (1.21 Å) (Table in Figure 2).

To explore the effects of a flavin cofactor, the $FADH^-_{Free}$:O_2 model was investigated (Figure S1, SI). The spin transition proceeding from the triplet $FADH^-_{Free}$:O_{2T} to the open-shell singlet $FADH^-_{Free}$:O_{2S} requires 7.3 kcal/mol of energy, which is significantly lower than that of the dioxygen (37.7 kcal/mol) (Table in Figure 2). The spin population on the O_2 fragment (+1.702) of the triplet $FADH^-_{Free}$:O_{2T} (Table in Figure 2 and Figure S1, SI) is slightly less than that on the free triplet O_{2T} (+2.000). The charge population on the dioxygen fragment is −0.249, and the O_p−O_d bond becomes slightly weaker (1.25 Å) than that found in the free triplet O_{2T} (1.21 Å). These findings imply that the presence of a flavin cofactor causes some charge transfer to the dioxygen, which also results in a decrease in the energy gap between the singlet and the triplet states. The C_{4a}−O_p distance is shorter in the open-shell singlet $FADH^-_{Free}$:O_{2S} (3.10 Å) complex when compared with that of the triplet $FADH^-_{Free}$:O_{2T} (3.23 Å) complex (Table S3, SI). Altogether, our data indicate that the flavin cofactor partly assists with the electron transfer and spin transition process.

To evaluate the importance of protonation in the dioxygen activation process, an additional proton was included into the triplet $FADH^-_{Free}$:O_{2T} and the open-shell singlet $FADH^-_{Free}$:O_{2S} models giving the triplet $FADH\cdot_{Free}$:·OOH_T and the open-shell singlet $FADH\cdot_{Free}$:·OOH_S, respectively (Figure S2, SI). Interestingly, with an additional proton, the energy difference between the $FADH\cdot_{Free}$:·OOH_T and the $FADH\cdot_{Free}$:·OOH_S complexes became insignificant (0.01 kcal/mol) (Table in Figure 2). Unlike the triplet $FADH^-_{Free}$:$O_{2T,}$ in which only partial charge is transferred from the flavin to the dioxygen, the electronic structure of the triplet $FADH\cdot_{Free}$:·OOH_T implies that one electron is transferred from the flavin to the OOH fragment; the $FADH\cdot_{Free}$:·OOH_T complex contains similar spin populations on the OOH (+1.007) and the flavin (+1.015) fragments. The O_p−O_d bond distance in the $FADH\cdot_{Free}$:·OOH_T (1.32 Å) complex is also weaker than that found in the $FADH^-_{Free}$:O_{2T} complex (1.25 Å) (Table in Figure 2).

The open-shell singlet $FADH\cdot_{Free}$:·OOH_S complex was identified as the open-shell singlet diradical species with a spin population on the OOH fragment of +1.010 and on the flavin fragment of −1.010 (Table in Figure 2, Figure S2, SI). The structural geometries of the triplet $FADH\cdot_{Free}$:·OOH_T and the open-shell singlet diradical $FADH\cdot_{Free}$:·OOH_S complexes are similar; the C_{4a}−O_p distances of both spin states are about the same (3.75 Å) (Table S3, SI). Altogether, the data indicate that the additional proton facilitates the spin transition, as the energy required for this process is reduced.

dx.doi.org/10.1021/ja4088055 | J. Am. Chem. Soc. 2014, 136, 241−253

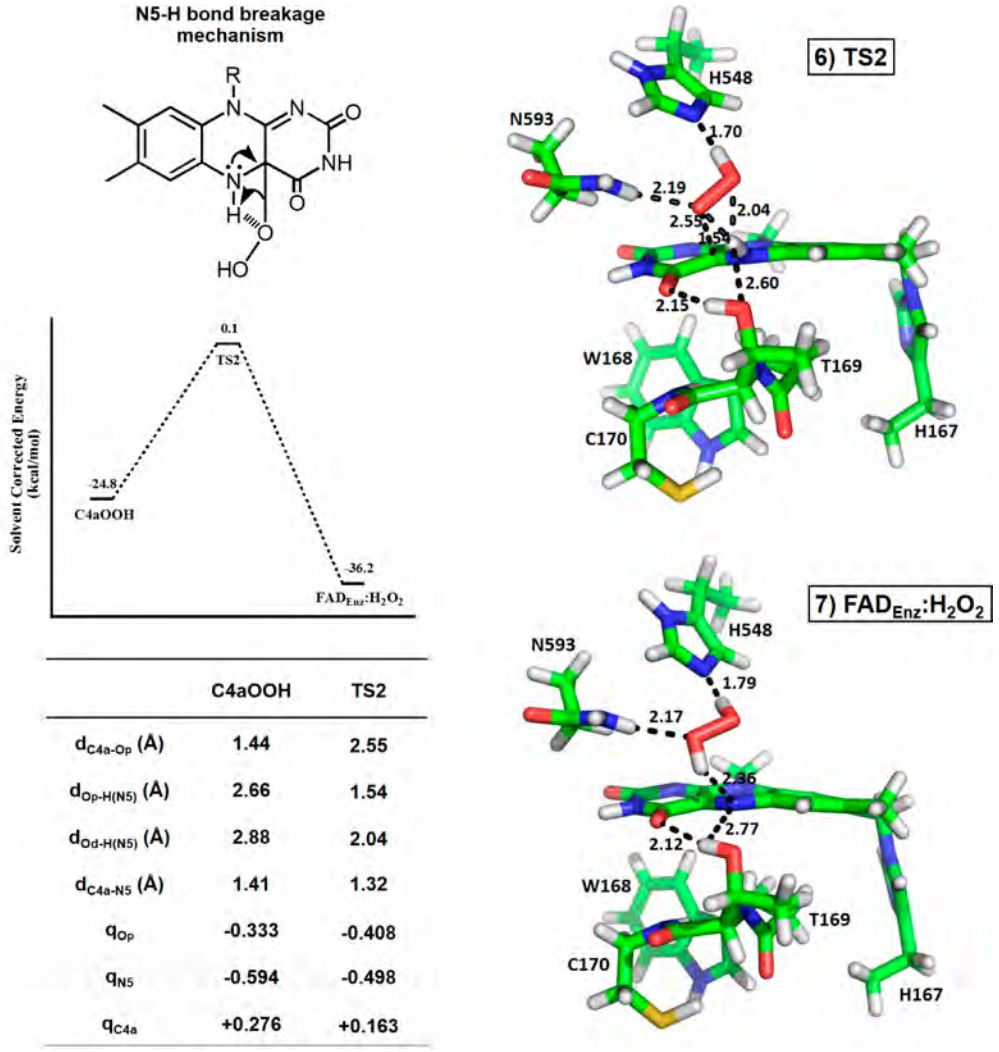

	C4aOOH	TS2
d_{C4a-Op} (Å)	1.44	2.55
$d_{Op-H(N5)}$ (Å)	2.66	1.54
$d_{Od-H(N5)}$ (Å)	2.88	2.04
d_{C4a-N5} (Å)	1.41	1.32
q_{Op}	-0.333	-0.408
q_{N5}	-0.594	-0.498
q_{C4a}	+0.276	+0.163

Figure 4. Relative energy profiles of H_2O_2 elimination from C4a-hydroperoxyflavin, the optimized structures of TS2, and the final product FAD_{Enz}:H_2O_2 complex. Values for the C4a−O_p distance (d_{C4a-Op}), O_p−H(N5) distance ($d_{Op-H(N5)}$), O_d−H(N5) distance ($d_{Od-H(N5)}$), and C4a−N5 distance (d_{C4a-N5}) are shown in the table. Mulliken charge populations on the O_p (q_{Op}), the N5 (q_{N5}), and the C4a (q_{C4a}) are also shown.

This result highlights the importance of the proton-coupled electron transfer process as a driving factor that facilitates the formation of the open-shell singlet diradical species ($FADH\cdot_{Free}$:$\cdot OOH_S$). In P2O, the protonated His548 plays an important role in the supply of a proton to the dioxygen during the first electron transfer process to mediate the formation of $FADH\cdot_{Enz}$:$\cdot OOH_S$.

Step 3: C4a-Hydroperoxyflavin Formation and TS1 (Species 3 to Species 5). In the open-shell singlet diradical $FADH\cdot_{Enz}$:$\cdot OOH_S$ complex, the opposite spins on the ·OOH (−1.002) and the flavin (+0.990) fragments facilitate bond formation between the proximal oxygen (O_p) of ·OOH and the C4a of the isoalloxazine ring (Figure 2) to form the C4aOOH via TS1 (Figure 3). Two hydrogen-bond interactions from the N^{ε} of His548 (1.57 Å) and the $N^{\delta}H$ of Asn593 (2.36 Å) to the ·OOH fragment (Figure2) play a role in positioning the O_p atom of the ·OOH fragment; the O_p is located directly above the flavin C4a position. In $FADH\cdot_{Enz}$:$\cdot OOH_S$, the C4a−O_p distance is 3.16 Å and the O_p−O_d distance is 1.33 Å (Figure 2, Table in Figure 3). In TS1, the C4a−O_p distance is shortened to 2.35 Å and the O_p−O_d distance is lengthened to 1.37 Å. The activation energy for this step is 10.9 kcal/mol. Once TS1 transforms to the C4aOOH, the C4a−O_p bond is completely formed (1.44 Å) and the O_p−O_d bond distance has a single bond character (1.45 Å) (calculated O−O bond distance in H_2O_2 is 1.46 Å) (Table in Figure 3).

The position of the −OOH moiety of the C4aOOH intermediate above the flavin ring is consistent with the conventional assignment of being *re*-side and compatible with a "face-on" configuration (Figure 3). As most flavoenzymes that form C4aOOH only have space available on the *re*-side to accommodate the −OOH moiety, we explored the P2O preference for C4aOOH formation on the *re*-side versus the *si*-side.

In the absence of the active site residues of P2O, we calculated the energy of H_2O_2 elimination from the C4aOOH intermediate for the free flavin model, where the −OOH moiety is located above (*re*-side) and below (*si*-side) the C4a position of the isoalloxazine ring (Figure S4, SI). The reaction on both sides of the ring essentially required the same amount of energy (29.7 kcal/mol). Thus, the preference for the *re*-side reaction in P2O (and other flavoenzymes) is not attributed to the differences in the electronic effect above and below the isoalloxazine ring.

In the P2O active site, the *si*-side of the isoalloxazine ring is, in fact, crowded with bulky active site residues (Trp168 and

dx.doi.org/10.1021/ja4088055 | J. Am. Chem. Soc. 2014, 136, 241−253

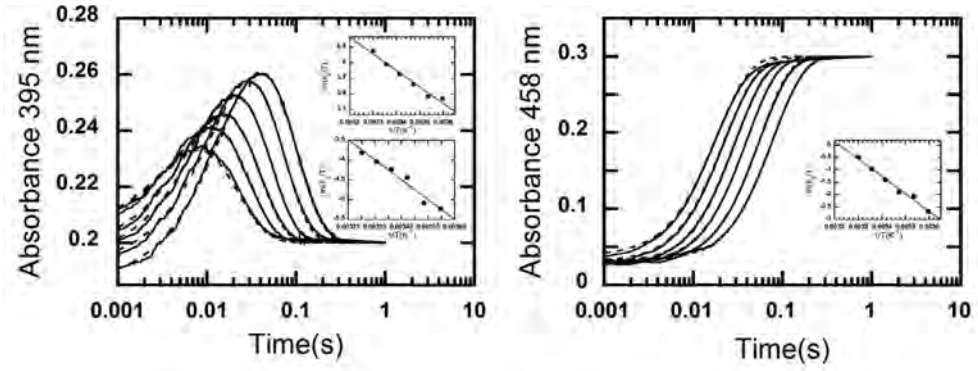

$FADH^- + O_2 \underset{\Delta H_2^{\ddagger}}{\overset{\Delta H_1^{\ddagger}}{\rightleftharpoons}}$ C4a-OOH $\xrightarrow{\Delta H_3^{\ddagger}}$ $FAD + H_2O_2$

Eyring plot (kcal/mol)		QM calculation (kcal/mol)	
$\Delta H_1^{\ddagger}$	6.3	$\Delta E_1^{\ddagger}$ ($FADH^{\bullet}_{Enz}$:$^{\bullet}OOH_S \rightarrow$TS1)	10.9
$\Delta H_2^{\ddagger}$	10.0	$\Delta E_2^{\ddagger}$ (C4aOOH$\rightarrow$TS1)	21.4
$\Delta H_3^{\ddagger}$	14.1	$\Delta E_3^{\ddagger}$ (C4aOOH$\rightarrow$TS2)	24.9

Figure 5. Oxidative half-reaction of P2O at various temperatures and Eyring plots. The transient kinetics of the oxidative half-reaction of P2O was investigated at various temperatures (5, 10, 15, 20, 25, and 30 °C) using stopped-flow spectrophotometry. Kinetic simulations with a two-step consecutive model (dotted line traces) according to the method described in ref 18 were used for analysis of rate constants. Insets show the Eyring plots of rate constants for formation (k_1), decay of C4a−OOH (k_2), and H_2O_2 elimination (k_3). The enthalpy of activation from the Eyring plots and the activation energies from QM calculations are summarized in the table, and the values were also plotted in Scheme 3

Cys170), while the *re*-side has an empty cavity for accommodating O_2 and the resulting −OOH moiety. Therefore, the preference for the *re*-side reaction in P2O is mainly due to the steric hindrance effects on the *si*-side. Trp168 and Cys170 are thus important for directing the formation of the C4aOOH on the *re*-side in P2O.

Steps 4 and 5: H_2O_2 Elimination from C4a-Hydroperoxyflavin and TS2 (Species 5 to Species 7). There are four hydrogen-bond interactions to the −OOH moiety and the isoalloxazine ring of the C4aOOH intermediate: (1) the N^{ε} of His548 accepts a hydrogen bond from the −OOH moiety (1.57 Å), (2) the $N^{\delta}H$ of Asn593 donates a hydrogen bond to the O_p of OOH moiety (2.17 Å), (3) the O^{γ} of Thr169 accepts a hydrogen bond from the N5H of the isoalloxazine (2.01 Å), and (4) the $-O^{\gamma}H$ of Thr169 donates a hydrogen bond to the O4 of the isoalloxazine (2.06 Å) (Figure 3). Among these hydrogen bonds, the one from Asn593 in the C4aOOH intermediate (species 5) is significantly stronger (2.17 Å) than the corresponding one in species 2−4 (>2.36 Å). Thus, Asn593 is not only positioning the O_p atom of the ·OOH to be directly above the flavin C4a position to form the C4aOOH intermediate, it is also stabilizing the C4aOOH intermediate by tightening the hydrogen-bond interaction.

For H_2O_2 elimination, a direct proton transfer from the flavin N5−H to the O_p of a peroxide leaving group can occur with a calculated activation energy (from C4aOOH to TS2) of 24.9 kcal/mol (Figure 4), making it the rate-limiting step in the oxidative half-reaction of P2O. The C4aOOH has a C4a−O_p distance of 1.44 Å and an O_p−H(N5) distance of 2.66 Å. (Figure 3, Table in Figure 4). In TS2, the C4a−O_p distance is lengthened to 2.55 Å and the O_p−H(N5) distance is shortened to 1.54 Å. As the O_d−H(N5) distance is also shortened from 2.88 Å in C4a-OOH to 2.04 Å in TS2, the proton transfer from N5 to O_p of a peroxide leaving group is mediated through the N5 and O_d interaction.

The bond distance between the O^{γ} of Thr169 and the N5H of the isoalloxazine in TS2 (2.60 Å) is relatively weaker than that found in C4aOOH (2.01 Å). Thus, the hydrogen bonds from Thr169 appear to be flexible, i.e. changing from a tight interaction which stabilizes C4aOOH to a more relaxed interaction in the H_2O_2 elimination process. The loosening of the hydrogen-bond interaction between O^{γ} of Thr169 and the N5H of the isoalloxazine in TS2 is also consistent with experimental observation. Variants of Thr169, in which the interaction at the flavin N5H is absent, do not stabilize the C4aOOH intermediate.[48]

The intramolecular proton transfer step to eliminate H_2O_2 via TS2 is consistent with previous experimental data showing that H_2O_2 elimination from the C4aOOH intermediate is controlled by a single proton transfer from the flavin N5 to an O_p of a peroxide leaving group.[56] Stopped-flow experiments showed that mutation of His548, Asn593 (see results in Figure 6 and Figures S6−S8 in SI), and Thr169[48] resulted in abolishing C4a-hydroperoxyflavin formation. This is consistent with our calculations that reveal the importance of protonated His548 for proton-coupled electron transfer to activate dioxygen to form the C4aOOH intermediate and the role of hydrogen bonds from Asn593, His548 and Thr169 in stabilizing the C4aOOH intermediate.

Once the proton is transferred from the flavin N5 to a peroxide leaving group to form the FAD_{Enz}:H_2O_2 complex (species 7), the C4a−O_p distance is lengthened to 3.27 Å, confirming cleavage of the C4a−O_p bond. Overall, the process of H_2O_2 elimination results in a release of energy of −36.2 kcal/mol. The reverse reaction via TS2 needs to overcome an energy barrier of +36.3 kcal/mol. Thus, formation of H_2O_2 tends to be irreversible, and H_2O_2 departure from the active site is presumably facilitated by conformational changes of the P2O enzyme.[45,57]

Activation Energy of the Reaction of Reduced P2O with Oxygen Analyzed by the Eyring Equation. To complement our density functional calculations, reactions of reduced P2O with dioxygen at various temperatures (5−30 °C) were carried out using stopped-flow spectrophotometry to

dx.doi.org/10.1021/ja4088055 | J. Am. Chem. Soc. 2014, 136, 241−253

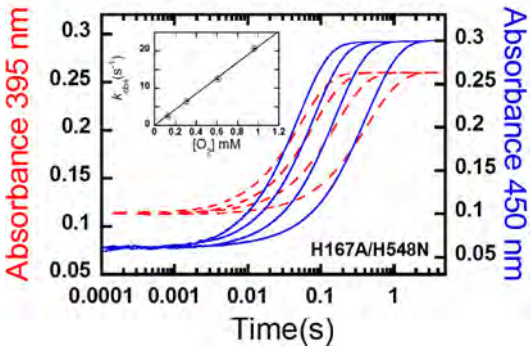

Variants	Bimolecular rate constant ($M^{-1}s^{-1}$)
H167A/H548A	58 ± 2
H167A/H548C	233 ± 3
H167A/H548S	359 ± 2
H167A/H548N	21,000 ± 8
N593H	529 ± 6

Figure 6. Kinetics of the reactions of reduced H167A/H548N variant with O_2. The data show monophasic kinetics, indicating that flavin is oxidized without forming C4a-hydroperoxyflavin. The inset shows the observed rate constants which are linearly dependent on O_2 concentrations. Summary of bimolecular rate constants of the oxidative half-reactions of N593H and H167A/H548 variants are shown in the table.

determine the enthalpy of activation ($\Delta H^{\ddagger}$) for C4aOOH formation from the reaction of $FADH^{-}_{Enz}$ and O_2 in both forward and reverse directions, and for H_2O_2 elimination (Experimental Procedures). As determined by analysis of the Eyring plot, the transient kinetics data (Figure 5, Table S4 and Figure S5) show that the enthalpy of activation for C4aOOH formation from the reaction of $FADH^{-}_{Enz}$ and O_2 in the forward direction ($\Delta H_1^{\ddagger}$) is 6.3 kcal/mol and in the reverse reaction ($\Delta H_2^{\ddagger}$) is 10.0 kcal/mol. The enthalpy for H_2O_2 elimination ($\Delta H_3^{\ddagger}$) is 14.1 kcal/mol. The calculated energy barrier is in agreement with the experimental enthalpy barrier in that the energy barrier for C4aOOH formation is lower than that for its reverse reaction ($\Delta E_1^{\ddagger}$ and $\Delta E_2^{\ddagger}$ vs $\Delta H_1^{\ddagger}$ and $\Delta H_2^{\ddagger}$) (Scheme 3, table in Figure 5). Proton abstraction from N5H was determined as the rate-determining step as the energy barrier for H_2O_2 elimination is the highest ($\Delta E_3^{\ddagger}$ and $\Delta H_3^{\ddagger}$). Since only the active site as a part of the enzyme was considered in the model studied for computational feasibility and the corrections for zero-point vibrational energy and thermal effects cannot be included in the calculation, we expect some discrepancies between the calculated energy and the experimental enthalpy to exist. A similar level of discrepancy between experimental and calculation results was also present in other works.[58] Overall, the results show that the relative activation energy ($\Delta E^{\ddagger}$) displays the same trend as the relative enthalpy of activation ($\Delta H^{\ddagger}$) derived experimentally from the Eyring plots. Specifically, this implies that the energy change for O_2 activation by P2O mainly derives from the change of electronic structures of the intermediates and transition states involved.

Transient Kinetics of Reactions of Reduced H548 and N593 Variants with Oxygen. Transient kinetic experiments for Asn593 variant (N593H), and His548 variants (H167A/H548A, H167A/H548C, H167A/H548S, and H167A/H548N) were performed to confirm the involvement of these two conserved residues in stabilization of C4a-hydroperoxyflavin. For the oxidative half-reactions of P2O(WT) and H167A variant enzymes,[18,49] the reaction shows biphasic kinetics, indicating formation of a C4a-hydroperoxyflavin intermediate (Figure 5). For His548 and Asn593 variants, the results showed only one kinetic phase, indicating that only flavin oxidation was observed (Figure 6 and Figures S6–S8 in SI). These data indicate that a C4a-hydroperoxyflavin intermediate does not form in these variants (Figure 6, Figures S6–S8 in SI), confirming the findings from QM calculations that His548 and Asn593 are important for stabilization of C4a-hydroperoxyflavin. Moreover, when the imidazole rescue experiment for His548 variants at various pHs was performed, the results were similar to those in the absence of imidazole in which no C4a-hydroperoxyflavin was detected (Table S5, SI). These results indicate that not only is a proton required, but proper geometry of the protonated His548 in the active site of the P2O enzyme is mandatory for formation of the C4a-hydroperoxyflavin intermediate.

Our previously published results for T169A, T169S, T169N, and T169G variants indicated that all of these variants also void formation of C4a-hydroperoxyflavin.[48] Therefore, the QM analysis results in which Thr169, His548, and Asn593 were identified as residues important for the stabilization of TS1 and C4a-hydroperoxyflavin are supported well by stopped-flow studies of the variant enzymes.

■ DISCUSSION

Our findings based on QM analysis and transient kinetic studies have identified the physical factors underlying the reaction of reduced flavin and dioxygen catalyzed by P2O. The data provide mechanistic insight that is different from the general model currently used for explaining the reaction of reduced flavin and oxygen.[6,9,55] The initial protonation of dioxygen by His548 of P2O that occurs in a concerted manner with an electron transfer is key for the oxygen activation process. The data obtained from QM analysis and transient kinetics indicate that the −OOH moiety of the C4a-hydroperoxyflavin is stabilized via a "face-on" configuration. The C4a-hydroperoxyflavin is stabilized by the hydrogen-bond interactions from His548, Asn593, and Thr169. H_2O_2 elimination occurs via a direct proton transfer from the flavin N5−H. The trends observed for the energy profiles based on the QM results also correlated well with the enthalpy of activation profiles obtained from the Eyring plots.

The data in Figure 2 suggest that the first step of the P2O reaction is a single electron transfer that is coupled with a proton transfer. The relative timing of proton transfer in Figure 2 is different from the current views toward the reaction of reduced flavin and oxygen in flavoenzymes which propose that a single electron is first transferred to form the flavin semiquinone and superoxide radical pair (paths a and b in Scheme 1[6,7,9]). A new model based on our results can be summarized as in Scheme 1, path C. Results from DFT calculations agree well with the experimental data because they suggest that no net proton transfer is involved in the TS1 transformation to the C4a-hydroperoxyflavin intermediate

dx.doi.org/10.1021/ja4088055 | J. Am. Chem. Soc. 2014, 136, 241−253

(Figure 3), which is consistent with the previous experiments indicating that no solvent kinetic isotope effect (SKIE) was detected for the C4a-hydroperoxyflavin formation.[56] However, with a similar calculation method, different results were obtained for the QM analysis of flavindestructase (BluB) because the first step of the BluB-catalyzed reaction is a single electron transfer from reduced flavin to dioxygen to generate the flavin semiquinone and superoxide radical pair before it collapses to form a negatively charged C4a-flavin peroxide intermediate. This intermediate is stabilized by two hydrogen bonds from the backbone amide of Gly61 and the O2 hydroxyl group of reduced FMN.[29] As the next step of BluB reaction is a cleavage of the isoalloxazine ring, it can thus be seen that protonation is not necessary for C4a-flavin peroxide in BluB catalysis. Therefore, different active site environments can influence the relative timing of electron and proton transfers differently.

The DFT analysis and transient kinetics indicate that the conserved His548 in P2O provides an internal proton for oxygen activation. This protonation process makes oxygen a better electron acceptor as the Mulliken charge of dioxygen atoms on the ·OOH molecule in the active site model (−0.480) is more negative than in the free flavin model (−0.249)—the model that describes the unprotonated His548 condition (Figure 2). The His548 and Asn593 help in aligning a ·OOH radical such that it is properly oriented for the next step in C4a-hydroperoxyflavin formation. The DFT results agree well with the experimental data because the reaction at lower pH is much faster than that at higher pH and formation of C4a-hydroperoxyflavin can only be detected at pH values lower than 8.0.[50] Moreover, results from studies of the reductive half-reaction of P2O indicate that the conserved His548, which acts as a general base during the reductive half-reaction, likely exists in the protonated form at the initial stage of the oxidative half-reaction.[53] Therefore, the functional role of His548 in P2O can be viewed as that of a general base in the reductive half-reaction and a general acid in the oxidative half-reaction (path c in Scheme 1).

In addition to P2O, many studies of other flavoenzyme oxidases have shown that positive charges near the flavin N5 are important for the oxygen activation process. For glucose oxidase, the protonated His516 is required because the pH-rate profiles showed that the $k_{cat}/K_{m(O2)}$ is 2600-fold higher at lower pH than at higher pH.[59,60] In contrast, for choline oxidase, oxygen activation is thought to be caused by the positive charge of the substrate.[16] For monomeric sarcosine oxidase, *N*-methyltryptophan oxidase, and fructosamine oxidase, mutation of Lys 256 to a neutral amino acid results in a 550−9000-fold decrease in oxygen reactivity.[13−15] More moderate effects were observed for similar mutations in polyamine oxidase and dihydroorotate dehydrogenase.[15,17] In most of these studies, the role of the positively charged residues was proposed to provide electrostatic interactions to stabilize the formation of a negatively charged superoxide radical. Our current findings suggest that quantum mechanical calculations for these enzymes should be useful for analyzing whether these positively charged residues can act as proton donors similar to what is observed in the P2O reaction.

The DFT optimized structure of C4a-hydroperoxyflavin (Figure 3) offers a molecular view of the physical and chemical interactions required for stabilization of the intermediate in a flavoenzyme. The data show that the intermediate is closely interacting with the side chains of Thr169, His548, and Asn593. Experimental evidence also confirms that these interactions are important because mutation of His548, Asn593 (Figure 6, Figures S6−S8 in SI), and Thr169 variants[48] failed to stabilize the C4a-hydroperoxyflavin intermediate. Moreover, the imidazole rescue experiment for the His548 variants could not restore the formation of C4a-hydroperoxyflavin (Table S5, SI), implying that the geometry of the general acid (His548) in relation to the flavin position is very important for stabilization of TS1 or C4a-hydroperoxyflavin. It is interesting to note that the −OOH moiety in Figure 3 is configured in a "face-on" configuration. In most of the X-ray structures of enzymes that can form C4a-hydroperoxyflavin, a cavity above the *re*-face of the flavin C4a atom is common.[6] Therefore, the "face-on" configuration can fit in active sites and may be prevalent in many enzymes.

Data in Figure 4 also confirm that the C4a-hydroperoxyflavin can undergo a unimolecular reaction to generate H_2O_2, and the relaxed H-bond interaction between the Oγ of Thr169 and the N5H of the isoalloxazine in TS2 (bond length of 2.60 Å) could be a key feature that enables this process. In previous studies, when the reduced enzyme which was specifically labeled with a single deuterium atom to give flavin N5-D reacted with dioxygen, a KIE of ∼3 for the H_2O_2 elimination was observed. The KIE is the same as that observed when the reaction was carried out in D_2O.[56] These experimental results agree well with the formation of species 5, TS2, and species 7. They also provide evidence supporting a unimolecular mechanism of H_2O_2 elimination consisting of a single proton transfer from N5-H to a peroxide leaving group. The importance of H-bond interactions at the flavin N5 in stabilization of the C4a-hydroperoxyflavin has been observed in many systems. For Thr169 variants of P2O in which a H-bond interaction at the flavin N5 is absent, the C4a-hydroperoxyflavin intermediate could not be detected.[48] In the oxygenase component of *p*-hydroxylphenylacetate hydroxylase, upon removal of the residue (Ser171) that forms hydrogen bonds with the flavin N5, the rate of H_2O_2 elimination increased by ∼1400-fold.[61] For a Baeyer−Villiger monooxygenase, the interaction between the flavin N5 and a bound $NADP^+$ is necessary in order to stabilize the C4a-hydroperoxyflavin.[62] A recent DFT calculation by Bach and Mattevi[32] suggests that in the absence of protein environment, the H_2O_2 elimination from C4a-hydroperoxyflavin is not feasible. When H_2O or CH_3OH (to model Thr or Ser) was included to serve as a proton shuttle path, the energy barrier for H_2O_2 elimination significantly decreased. Interaction of amine or amide residues with the N5 locus of C4a-hydroperoxyflavin also markedly reduces the energy barrier for H_2O_2 elimination. The interaction of Thr169 and flavin N5-locus shown in TS2 (Figure 4) may be similar to those found in the Bach and Mattevi study.[32] On the basis of our data in Figures 3−4, we propose that a more relaxed H-bond interaction to the flavin N5-H in TS2 when compared to a tighter H-bond interaction in C4a-OOH (bond length of 2.01 Å) is important for allowing H_2O_2 elimination to occur.

In summary, the combined usage of QM analysis and transient kinetics provides the theoretical basis underlying oxygen activation and the C4a-hydroperoxyflavin stabilization in P2O. Results in this report represent the chemical reaction in a flavoenzyme oxidase that uniquely stabilizes C4a-hydroperoxyflavin. It should be interesting to explore in future studies whether a similar basis holds for monooxygenases in which C4a-hydroperoxyflavin is utilized as a reactive intermediate.

dx.doi.org/10.1021/ja4088055 | *J. Am. Chem. Soc.* 2014, 136, 241−253

■ ASSOCIATED CONTENT

Supporting Information

Reaction catalyzed by P2O. Summary of the relative electronic energies by B3LYP/6-31G(d) and the relative electronic energies with solvation correction by B3LYP/6-311+G(d,p). The expectation value of the total spin angular momentum, $\langle S^2 \rangle$. Spin densities of the $FADH^-_{Free}{:}O_2$, $FADH{\cdot}_{Free}{:}{\cdot}OOH$ and $FADH{\cdot}_{Enz}{:}{\cdot}OOH$ complexes. Optimized structures and reaction energies for H_2O_2 elimination from C4aOOH on the *re*- and *si*-faces. Effects of temperature on the P2O reaction. Kinetics of the reactions of H167A/H548 variants with O_2. Bimolecular rate constants for the imidazole rescue experiments. Coordinates and calculated energies for all structures. This material is available free of charge via the Internet at http://pubs.acs.org.

■ AUTHOR INFORMATION

Corresponding Author

pimchai.cha@mahidol.ac.th

Author Contributions

‡T.W. and P.S. contributed equally to this study.

Funding

This work was supported by The Thailand Research Fund through Grants No. RTA5680001 (to P.C.), MRG5580117 (to P.S.), Development and Promotion of Science and Technology Talents Project DPST Research Grant No. 025/2555 (to P.S.), Center of Excellence for Innovation in Chemistry (PERCH-CIC), Office of the Higher Education and Commission, Ministry of Education (to P.S.), a grant from the Faculty of Science, Mahidol University (to P.C.), and National Science and Technology Development Agency (to T.W.). J.S. received support from The Thailand Research Fund (RSA5580050). N.S.S. is an EPSRC Established Career Fellow and a Royal Society Wolfson Merit Award holder.

Notes

The authors declare no competing financial interest.

■ ACKNOWLEDGMENTS

We thank Bruce A. Palfey, University of Michigan, for critical reading of the manuscript.

■ REFERENCES

(1) Fagan, R. L.; Palfey, B. A. In *Comprehensive Natural Products II: Chemistry and Biology*; Mander, L., Lui, H.-W., Eds.; Elsevier: Oxford, 2010; Vol. 7, pp 37−113.

(2) Monti, D.; Ottolina, G.; Carrea, G.; Riva, S. *Chem. Rev.* **2011**, *111*, 4111−4140.

(3) Mirzakulova, E.; Khatmullin, R.; Walpita, J.; Corrigan, T.; Vargas-Barbosa, N. M.; Vyas, S.; Oottikkal, S.; Manzer, S. F.; Hadad, C. M.; Glusac, K. D. *Nat. Chem.* **2012**, *4*, 794−801.

(4) Leisch, H.; Morley, K.; Lau, P. C. *Chem. Rev.* **2011**, *111*, 4165−4222.

(5) Fraaije, M. W.; Berkel, W. J. H. v. Flavin-Containing Oxidative Biocatalysts. In *Biocatalysis in the Pharmaceutical and Biotechnology Industries*; Patel, R. N., Ed. CRC Press, Taylor & Francis Group: Boca Raton, FL, 2006; p 181.

(6) Chaiyen, P.; Fraaije, M. W.; Mattevi, A. *Trends. Biochem. Sci.* **2012**, *37*, 373−380.

(7) Bruice, T. C. *Isr. J. Chem.* **1984**, *24*, 54−61.

(8) Eberlein, G.; Bruice, T. C. *J. Am. Chem. Soc.* **1983**, *105*, 6685−6697.

(9) Massey, V. *J. Biol. Chem.* **1994**, *269*, 22459−22462.

(10) Klinman, J. P. *Acc. Chem. Res.* **2007**, *40*, 325−333.

(11) Kommoju, P. R.; Chen, Z. W.; Bruckner, R. C.; Mathews, F. S.; Jorns, M. S. *Biochemistry* **2011**, *50*, 5521−5534.

(12) Jorns, M. S.; Chen, Z. W.; Mathews, F. S. *Biochemistry* **2010**, *49*, 3631−3639.

(13) Zhao, G.; Bruckner, R. C.; Jorns, M. S. *Biochemistry* **2008**, *47*, 9124−9135.

(14) Bruckner, R. C.; Winans, J.; Jorns, M. S. *Biochemistry* **2011**, *50*, 4949−4962.

(15) McDonald, C. A.; Fagan, R. L.; Collard, F.; Monnier, V. M.; Palfey, B. A. *J. Am. Chem. Soc.* **2011**, *133*, 16809−16811.

(16) Gadda, G. *Biochemistry* **2012**, *51*, 2662−2669.

(17) Henderson Pozzi, M.; Fitzpatrick, P. F. *Arch. Biochem. Biophys.* **2010**, *498*, 83−88.

(18) Sucharitakul, J.; Prongjit, M.; Haltrich, D.; Chaiyen, P. *Biochemistry* **2008**, *47*, 8485−8490.

(19) Wongnate, T.; Chaiyen, P. *FEBS J.* **2013**, *280*, 3009−3027.

(20) van der Kamp, M. W.; Mulholland, A. J. *Biochemistry* **2013**, *52*, 2708−2728.

(21) Groenhof, G. *Methods Mol. Biol.* **2013**, *924*, 43−66.

(22) Siegbahn, P. E.; Himo, F. *J. Biol. Inorg. Chem.* **2009**, *14*, 643−651.

(23) Senn, H. M.; Thiel, W. *Angew. Chem., Int. Ed.* **2009**, *48*, 1198−1229.

(24) Polyak, I.; Reetz, M. T.; Thiel, W. *J. Am. Chem. Soc.* **2012**, *134*, 2732−2741.

(25) Mata, R. A.; Werner, H. J.; Thiel, S.; Thiel, W. *J. Chem. Phys.* **2008**, *128*, 025104.

(26) Ridder, L.; Mulholland, A. J.; Rietjens, I. M.; Vervoort, J. *J. Mol. Graphics Modell.* **1999**, *17*, 163−175 and p 214.

(27) Tian, B.; Strid, A.; Eriksson, L. A. *J. Phys. Chem. B* **2011**, *115*, 1918−1926.

(28) Tian, B.; Tu, Y.; Strid, A.; Eriksson, L. A. *Chemistry* **2010**, *16*, 2557−2566.

(29) Wang, X. L.; Quan, J. M. *J. Am. Chem. Soc.* **2011**, *133*, 4079−4091.

(30) Prabhakar, R.; Siegbahn, P. E.; Minaev, B. F. *Biochim. Biophys. Acta* **2003**, *1647*, 173−178.

(31) Hernández-Ortega, A.; Lucas, F.; Ferreira, P.; Medina, M.; Guallar, V.; Martínez, A. T. *Biochemistry* **2012**, *51*, 6595−6608.

(32) Bach, R. D.; Mattevi, A. *J. Org. Chem.* **2013**, *78*, 8585−8593.

(33) Frisch, M. J.; Trucks, G. W.; Schlegel, H. B.; Scuseria, G. E.; Robb, M. A.; Cheeseman, J. R.; Scalmani, G.; Barone, V.; Mennucci, B.; Petersson, G. A.; Nakatsuji, H.; Caricato, M.; Li, X.; Hratchian, H. P.; Izmaylov, A. F.; Bloino, J.; Zheng, G.; Sonnenberg, J. L.; Hada, M.; Ehara, M.; Toyota, K.; Fukuda, R.; Hasegawa, J.; Ishida, M.; Nakajima, T.; Honda, Y.; Kitao, O.; Nakai, H.; Vreven, T.; Montgomery, J. A.; Peralta, J. E.; Ogliaro, F.; Bearpark, M.; Heyd, J. J.; Brothers, E.; Kudin, K. N.; Staroverov, V. N.; Keith, T.; Kobayashi, R.; Normand, J.; Raghavachari, K.; Rendell, A.; Burant, J. C.; Iyengar, S. S.; Tomasi, J.; Cossi, M.; Rega, N.; Millam, J. M.; Klene, M.; Knox, J. E.; Cross, J. B.; Bakken, V.; Adamo, C.; Jaramillo, J.; Gomperts, R.; Stratmann, R. E.; Yazyev, O.; Austin, A. J.; Cammi, R.; Pomelli, C.; Ochterski, J. W.; Martin, R. L.; Morokuma, K.; Zakrzewski, V. G.; Voth, G. A.; Salvador, P.; Dannenberg, J. J.; Dapprich, S.; Daniels, A. D.; Farkas, O.; Foresman, J. B.; Ortiz, J. V.; Cioslowski, J.; Fox, D. J. *Gaussian 09*, Revision C.01. Gaussian, Inc.: Wallingford CT, 2010

(34) Becke, A. D. *J. Chem. Phys.* **1993**, *98*, 5648−5652.

(35) Lee, C.; Yang, W.; Parr, R. G. *Phys. Rev. B* **1988**, *37*, 785−789.

(36) Stephens, P. J.; Devlin, F. J.; Chabalowski, C. F.; Frisch, M. J. *J. Phys. Chem.* **1994**, *98*, 11623−11627.

(37) Siegbahn, P. E.; Borowski, T. *Acc. Chem. Res.* **2006**, *39*, 729−738.

(38) Bauschlicher, C. W. Jr.; Ricca, A.; Partridge, H.; Langhoff, S. R. In *Recent Advances in Density Functional Methods, Part II*; Chong, D. P., Ed.; World Scientific Publishing Co.: Singapore, 1997; Vol. 1, pp 165−228.

(39) Hariharan, P. C.; Pople, J. A. *Theor. Chim. Acta* **1973**, *28*, 213−222.

(40) Petersson, G. A.; Al-Laham, M. A. *J. Chem. Phys.* **1991**, *94*, 6081.

(41) Petersson, G. A.; Bennett, A.; Tensfeldt, T. G.; Al-Laham, M. A.; Shirley, W. A.; Mantzaris, J. *J. Chem. Phys.* **1988**, *89*, 2193.
(42) Barone, V.; Cossi, M. *J. Phys. Chem. A* **1998**, *102*, 1995−2001.
(43) Adamo, C.; Barone, V. *J. Chem. Phys.* **1999**, *110*, 6158−6170.
(44) Hallberg, B. M.; Leitner, C.; Haltrich, D.; Divne, C. *J. Mol. Biol.* **2004**, *341*, 781−796.
(45) Kujawa, M.; Ebner, H.; Leitner, C.; Hallberg, B. M.; Prongjit, M.; Sucharitakul, J.; Ludwig, R.; Rudsander, U.; Peterbauer, C.; Chaiyen, P.; Haltrich, D.; Divne, C. *J. Biol. Chem.* **2006**, *281*, 35104−35115.
(46) Isobe, H.; Yamanaka, S.; Kuramitsu, S.; Yamaguchi, K. *J. Am. Chem. Soc.* **2008**, *130*, 132−149.
(47) Prongjit, M.; Sucharitakul, J.; Wongnate, T.; Haltrich, D.; Chaiyen, P. *Biochemistry* **2009**, *48*, 4170−4180.
(48) Pitsawong, W.; Sucharitakul, J.; Prongjit, M.; Tan, T. C.; Spadiut, O.; Haltrich, D.; Divne, C.; Chaiyen, P. *J. Biol. Chem.* **2010**, *285*, 9697−9705.
(49) Sucharitakul, J.; Wongnate, T.; Chaiyen, P. *Biochemistry* **2010**, *49*, 3753−3765.
(50) Prongjit, M.; Sucharitakul, J.; Palfey, B. A.; Chaiyen, P. *Biochemistry* **2013**, *52*, 1437−1445.
(51) Eyring, H. *J. Chem. Phys.* **1935**, *3*, 107.
(52) Winzor, D. J.; Jackson, C. M. *J. Mol. Recognit.* **2006**, *19*, 389−407.
(53) Wongnate, T.; Sucharitakul, J.; Chaiyen, P. *ChemBioChem* **2011**, *12*, 2577−2586.
(54) Tan, T. C.; Pitsawong, W.; Wongnate, T.; Spadiut, O.; Haltrich, D.; Chaiyen, P.; Divne, C. *J. Mol. Biol.* **2010**, *402*, 578−594.
(55) Mattevi, A. *Trends Biochem. Sci.* **2006**, *31*, 276−283.
(56) Sucharitakul, J.; Wongnate, T.; Chaiyen, P. *J. Biol. Chem.* **2011**, *286*, 16900−16909.
(57) Tan, T. C.; Haltrich, D.; Divne, C. *J. Mol. Biol.* **2011**, *409*, 588−600.
(58) Tian, B.; Strid, A.; Eriksson, L. A. *J. Phys. Chem. B* **2011**, *115*, 1918−1926.
(59) Su, Q.; Klinman, J. P. *Biochemistry* **1999**, *38*, 8572−8581.
(60) Roth, J. P.; Klinman, J. P. *Proc. Natl. Acad. Sci. U.S.A.* **2003**, *100*, 62−67.
(61) Thotsaporn, K.; Chenprakhon, P.; Sucharitakul, J.; Mattevi, A.; Chaiyen, P. *J. Biol. Chem.* **2011**, *286*, 28170−28180.
(62) Orru, R.; Pazmiño, D. E.; Fraaije, M. W.; Mattevi, A. *J. Biol. Chem.* **2010**, *285*, 35021−35028.

■ NOTE ADDED AFTER ASAP PUBLICATION

Scheme 3 and Figure 2 contained errors in the version published ASAP December 24, 2013; the correct version reposted December 26, 2013.

MedChemComm

RSC Publishing

CONCISE ARTICLE

View Article Online
View Journal | View Issue

Cite this: *Med. Chem. Commun.*, 2013, **4**, 1590

Flavans from *Desmos cochinchinensis* as potent aromatase inhibitors†

Vilailak Prachyawarakorn,*[a] Suwannee Sangpetsiripan,[a] Panida Surawatanawong,[b] Chulabhorn Mahidol,[a] Somsak Ruchirawat[acd] and Prasat Kittakoop*[acd]

Received 13th June 2013
Accepted 21st September 2013

DOI: 10.1039/c3md00166k

www.rsc.org/medchemcomm

Flavans from the roots of *Desmos cochinchinensis* exhibited potent aromatase inhibitory activity at nanomolar levels, and could be leads for the development of anti-aromatase drugs. In addition, these aromatase inhibitors did not show pronounced cytotoxic activity. Flavans exert their inhibitory activity through binding, as revealed by molecular docking studies, with aromatase at Arg115, Met374, and Leu477; the C-7 hydroxyl (or methoxyl) forms hydrogen bonds with Met374 and Arg115 of aromatase.

Introduction

In 2013, it is estimated that breast cancer is one of the three most commonly diagnosed types of cancer among women in the United States, accounting for 29% of all new cancer cases in women.[1] In 2012, it was estimated that breast cancer was one of the most common causes of female mortality in Europe.[2] Among breast cancer in post-menopausal women, around 75% are estrogen-dependent, and post-menopausal women could produce estrogen by non-ovarian tissues (*i.e.*, breast tissue).[3,4] Elevated estrogen levels in tissues is one of the causes of breast cancer. Estrogens are normally biosynthesized from androgens by the aromatization of the A ring of a steroidal skeleton, and such reactions are catalyzed by the enzyme aromatase (also known as cytochrome P450 aromatase or CYP19). The reduction of the estrogen level by inhibiting aromatase activity is one of the therapeutic approaches for breast cancer; both steroidal and non-steroidal aromatase inhibitors have been intensively explored to date.[5–9] The non-steroidal aromatase inhibitors clinically used are anastrozole and letrozole (azole-type compounds), while examples of steroidal aromatase inhibitor drugs are formestane and exemestane.

Natural products have a long history as human medicines, and they currently play important roles in both traditional[10] and modern medicine.[11,12] There are many natural products which act as aromatase inhibitors,[13,14] however only few compounds have been reported to exhibit potent aromatase inhibitory activity with IC_{50} values at nanomolar levels.[15–17] Plants of the genus *Desmos* are used in Chinese traditional medicines.[18] Previously, we reported that hybrid flavan-chalcones and flavonoids from the leaves of *Desmos cochinchinensis* were aromatase inhibitors with IC_{50} values of 0.8–3.3 μM.[19] Later, we found that the root extract of *D. cochinchinensis* was more potent than the leaf extract; chemical exploration of the root extract led to the identification of flavans **1–6** and flavanones **7** and **8** (Fig. 1), which inhibited aromatase at nanomolar levels. In the present work, we report the isolation, characterization and aromatase inhibitory activity of flavans from the roots of *D. cochinchinensis*. Moreover, a molecular docking study of these aromatase inhibitors is also discussed.

Results and discussion

Isolation and structure elucidation of flavans

An extract of the air-dried roots of *D. cochinchinensis* was separated by size exclusion Sephadex LH-20 column chromatography, preparative TLC and C_{18} reversed phase HPLC to yield

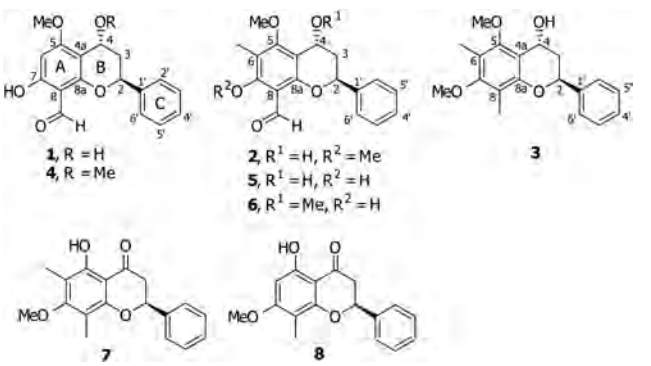

Fig. 1 Aromatase inhibitors isolated from the roots of *D. cochinchinensis*.

[a]*Chulabhorn Research Institute, Kamphaeng Phet 6 Road, Laksi, Bangkok 10210, Thailand. E-mail: vilailak@cri.or.th; prasat@cri.or.th; Tel: +66 869755777*

[b]*Department of Chemistry and Center of Excellence for Innovation in Chemistry, Mahidol University, 272 Rama VI Road, Ratchathewi, Bangkok 10400, Thailand*

[c]*Chulabhorn Graduate Institute, Chemical Biology Program, Kamphaeng Phet 6 Road, Laksi, Bangkok 10210, Thailand*

[d]*Center of Excellence on Environmental Health and Toxicology (EHT), CHE, Ministry of Education, Thailand*

† Electronic supplementary information (ESI) available: NMR spectra of new compounds; molecular docking study of androstenedione, formestane, **2**, and **3**. See DOI: 10.1039/c3md00166k

flavans **1–6** and flavanones **7** and **8**. Flavans **1–4** were new compounds, while **5–8** were known metabolites. The structures of the new flavans **1–4** were elucidated by analysis of the spectroscopic data, and the absolute configuration was addressed by analysis of the CD spectra. The spectroscopic data of known compounds **5–8** was identical to those reported in the literature.[20–23]

Compound **1** was obtained as a colourless oil, with $[\alpha]_D^{26}$ −62.8 (*c* 0.78, $CHCl_3$). Its molecular formula was determined as $C_{17}H_{16}O_5$, according to APCI-TOF MS. The IR spectrum of **1** showed the presence of a hydroxy (3435 cm^{-1}) and an aldehyde (1630 cm^{-1}) group. The ^1H NMR spectrum of **1** showed signals of a monosubstituted benzene ring at δ_H 7.36–7.48 (5H, m, H-2′-H-6′), a hydroxyl proton at δ_H 12.53 (1H, s, 7-OH), an aldehyde proton at δ_H 10.11 (1H, s, 8-CHO) and a methoxy group at δ_H 3.92 (3H, s, 5-OMe). The presence of an –$OCHCH_2CHO$– unit (H-2/H_2-3/H-4) in **1** was supported by the ^1H–^1H COSY spectrum. The two oxygenated methines resonated at δ_H 5.27 (1H, dd, J = 12.3 Hz, 1.8 Hz, H-2) and δ_H 4.96 (1H, br dd, J = 3.7 Hz, 1.9 Hz, H-4), while non-equivalent methylenes were at δ_H 2.01 (1H, ddd, J = 14.5 Hz, 13.4 Hz, 3.4 Hz, H-3_{ax}) and δ_H 2.30 (1H, dt, J = 14.5 Hz, 1.7 Hz, H-3_{eq}); these resonances are typical for H-2/H_2-3/H-4 in flavan-4-ol molecules. The downfield shift of 7-OH (δ_H 12.53) was a result of hydrogen bonding of the hydroxyl proton with 8-CHO. The HMBC correlations from the H-6 proton to C-5 and C-7, 7-OH to C-6, C-7 and C-8, 8-CHO to C-8 and C-7, and 5-OMe to C-5, in combination with the NOESY cross peak between the 5-OMe protons and the H-6 aromatic proton, assisted the assignment of the H-6 position and the other substituents on the aromatic ring A of compound **1**. HMBC correlations from H-2 to C-1′ and C-2′ (or C-6′), H-3 to C-4a, and H-4 to C-4a, C-5 and C-8a were observed, connecting ring B with the aromatic rings A and C. On the basis of these spectroscopic data, compound **1** was identified as 5-methoxy-8-formyl-4,7-dihydroxyflavan. The proton and carbon resonances for **1** were assigned by analysis of the 2D NMR data (Table 1). The coupling constants of H-2 ($J_{2ax,3ax}$ ∼ 12.0 Hz) and H-4 ($J_{3ax,4eq}$ ∼ 3.7 Hz and $J_{3eq,4eq}$ ∼ 2.0 Hz) revealed a *trans* configuration of H-2 and H-4 in **1**. Normally, the absolute configuration of flavanones can be established by the circular dichroism (CD) technique.[24,25] However, the CD method could not be applied directly for the 2,4-*trans*-flavan-4-ol moiety in **1**. Accordingly, compound **1** was transformed to the flavanone **1a** by oxidation with Dess–Martin periodinane (DMP) (Fig. 2). The absolute configuration at C-2 of the flavanone **1a** was assigned as *2S*, since the CD spectrum of **1a** exhibited positive and negative Cotton effects at 344 nm and 269 nm, respectively (a characteristic for (2*S*)-flavanones).[24] Therefore, the *trans* configuration of H-2 and H-4 readily indicated the *R* configuration of C-4 in **1**.

Compound **2** possessed a molecular formula of $C_{19}H_{20}O_5$, as deduced from the APCI-TOF MS. The ^1H and ^{13}C NMR spectra of compound **2** were similar to those of flavan **1**, except the signals relating to the substitutions on the aromatic ring A. Compound **2** had the additional signals of a methoxy (δ_H 3.82, 7-OMe) and a methyl (δ_H 2.18, 6-Me) group. The HMBC spectrum of **2** indicated that H-6 in **1** was replaced by a methyl group (6-Me) in **2**, showing a correlation from 6-Me to C-5, C-6, and C-7. The 7-OH group (δ_H 12.53) in **1** was replaced by 7-OMe (δ_H 3.82) in **2**, and the HMBC correlation from 7-OMe to C-7 established the methoxy position in **2**. Thus, compound **2** was identified as 5,7-dimethoxy-8-formyl-4-hydroxy-6-methylflavan, which was a 7-methoxy derivative of **5**.[20] The assignments for ^1H and ^{13}C in compound **2** are in Table 1. The coupling constants revealed a *trans* configuration of H-2 and H-4. The absolute configuration of **2** was defined in the same manner as for **1**. The oxidation of **2** with DMP gave the corresponding ketone derivative **2a** (Fig. 3), whose CD absorptions exhibited a positive Cotton effect at 353 nm and a negative Cotton effect at 319 nm, suggesting the *2S* configuration for **2a**.[24] It should be noted that the flavanone **2a** has CD absorptions *ca.* 20–25 nm higher than normal absorptions for flavanones, which absorb at 320–330 nm and 270–290 nm.[24] Although compound **5** is a known flavan,[20] its absolute configuration has not been defined to date. Flavan **5** was transformed to the flavanone **2a** by DMP oxidation and methylation (Fig. 3). Compound **2a**, from the transformation of **5**, displayed the same CD spectrum as that from the oxidation of compound **2**, suggesting that **5** had the same *2S* configuration as **2**.

Compound **3** had the molecular formula of $C_{19}H_{22}O_4$ (by APCI-TOF MS). The ^1H and ^{13}C NMR spectra of **3** shared a great deal of similarities to those of **2**; the 8-CHO (δ_H 10.42; δ_C 188.3) in **2** was replaced by 8-Me (δ_H 2.15; δ_C 8.9) in **3**. The position of 8-Me in **3** was assigned by the HMBC correlation (8-Me to C-7, C-8, and C-8a) and the NOESY cross peak of 7-OMe and 8-Me. Thus, **3** was identified as 5,7-dimethoxy-4-hydroxy-6,8-dimethylflavan. Both **2** and **3** exhibited a negative optical rotation, meaning they should share the same absolute configuration. The ^1H and ^{13}C resonances for compound **3** were assigned by analysis of the 2D NMR data (Table 1).

Compound **4** had the molecular formula of $C_{18}H_{18}O_5$ (by APCI-TOF MS). The ^1H and ^{13}C NMR spectra of **4** and **1** could almost be superimposed. Analysis of the ^1H, ^{13}C and MS data

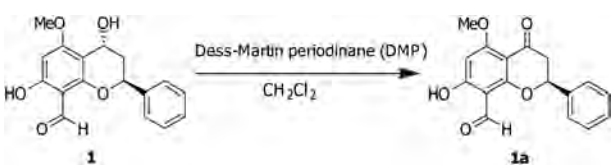

Fig. 2 Oxidation of **1** to the flavanone **1a**.

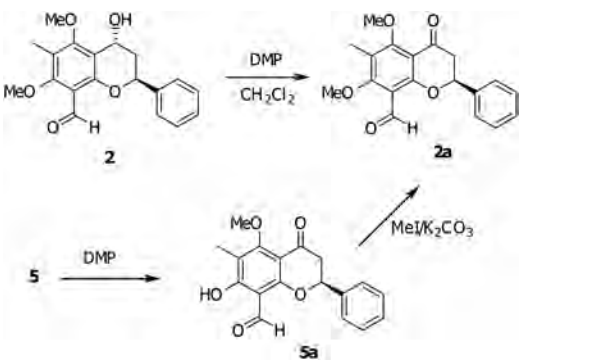

Fig. 3 Transformation of flavans **2** and **5** to the flavanone **2a**.

Table 1 ^{1}H and ^{13}C NMR spectral data ($CDCl_3$) for flavans **1–4**

Position	**1**[a]		**2**[a]		**3**[b]		**4**[a]	
	δ_H, m (*J*, Hz)	δ_C	δ_H, m (*J*, Hz)	δ_C	δ_H, m (*J*, Hz)	δ_C	δ_H, m (*J*, Hz)	δ_C
2	5.27, dd (12.3, 1.8)	74.2	5.29, dd (12.2, 1.6)	73.6	5.17, d (11.1)	72.9	5.31, dd (12.5, 2.0)	74.1
3	2.01, ddd (14.5, 13.4, 3.4, H-3_{ax}); 2.30, dt (14.5, 1.7, H-3_{eq})	37.2	2.03, ddd (14.5, 12.3, 3.8, H-3_{ax}); 2.35, dt (14.5, 2.1, H-3_{eq})	37.4	2.00, ddd (14.4, 12.3, 3.9, H-3_{ax}); 2.30, dt (14.4, 1.9, H-3_{eq})	38.0	1.88, ddd (14.4, 12.5, 3.0, H-3_{ax}); 2.37, dt (14.4, 2.3, H-3_{eq})	34.0
4	4.96, dd (3.7, 1.9)	58.5	5.03, dd (3.8, 2.1)	59.3	5.03, dd (3.7, 1.9)	60.0	4.48, t (2.7)	66.7
4a	—	104.7	—	114.6	—	113.8	—	102.5
5	—	165.8	—	163.5	—	155.7	—	166.2
6	6.06, s	91.8	—	117.3	—	115.8	6.05, s	91.7
7	—	166.0	—	161.8	—	158.2	—	166.2
8	—	105.4	—	115.2	—	115.4	—	105.2
8a	—	158.3	—	157.0	—	151.9	—	158.6
1′	—	140.0	—	140.2	—	141.5	—	140.2
2′/6′	7.36–7.48, m	126.0	7.50, m	125.9	7.50, br d (7.5)	126.0	7.34–7.47, m	126.1
3′/5′	7.36–7.48, m	128.6	7.41, m	128.6	7.41, t (7.5)	128.4	7.34–7.47, m	128.6
4′	7.36–7.48, m	128.2	7.35, m	128.0	7.34, t (7.4)	127.7	7.34–7.47, m	128.2
4-OMe	—	—	—	—	—	—	3.48, s	56.3
5-OMe	3.92, s	56.1	3.92, s	61.4	3.86, s	61.2	3.91, s	56.1
6-Me	—	—	2.18, s	8.9	2.20, s	9.3	—	—
7-OMe	—	—	3.82, s	62.0	3.72, s	60.1	—	—
7-OH	12.53, s	—	—	—	—		12.56, s	—
8-CHO	10.11, s	192.0	10.42, s	188.3	—		10.11, s	192.0
8-Me	—	—	—	—	2.15, s	8.9	—	—

[a] 400 MHz for ^{1}H and 100 MHz for ^{13}C. [b] 600 MHz for ^{1}H and 150 MHz for ^{13}C.

revealed that **4** was a methoxy derivative of **1**. The ^{13}C NMR resonance at C-4 (δ_C 66.7) of **4** was *ca.* 6–7 ppm further downfield than those (δ_C 58.5–60.0) of flavans **1–3**, suggesting that an additional methoxy group was located at the C-4 of **4**. The HMBC correlation from 4-OMe to C-4 finally confirmed the position of 4-OMe in **4**. On the basis of these data, **4** was identified as 4,5-dimethoxy-8-formyl-7-hydroxyflavan. Compound **4** showed a similar negative optical rotation to **1**, implying that **4** had the same absolute configuration as **1**. The assignment of the protons and carbons in **4** was achieved by analysis of the 2D NMR data (Table 1).

Inhibition of aromatase and the cytotoxicity of flavans

The isolated flavonoids **1–8** were subjected to an aromatase inhibitory assay. Compounds **1–6** and **8** inhibited the aromatase enzyme, and among the compounds tested, flavans **1**, **4**, and **5** exhibited potent aromatase inhibitory activity with IC_{50} values of 40.0, 90.0 and 80.0 nM, respectively (Table 2). Compounds **2**, **3**, **6** and **8** displayed inhibitory activity with respective IC_{50} values of 1010, 10 700, 150 and 600 nM (Table 2). The cytotoxicity of flavans **1–6** and the flavanone **7** was evaluated against the A549 (human lung carcinoma), HuCCA-1 (human cholangiocarcinoma), MOLT-3 (acute lymphoblastic leukemia) and HepG2 (human hepatocellular liver carcinoma) cancer cell lines (ESI, Table S1†). The flavan aromatase inhibitors **1–6** were inactive or showed only weak cytotoxic activity against the HepG2, A549 and HuCCA-1 cell lines, with IC_{50} values ranging from 99.6 to 146.6 μM (Table S1†). Compounds **1–6** exhibited weak cytotoxic activity towards the MOLT-3 cell line, with IC_{50} values of 24.3–63.5 μM. It is worth mentioning that in our laboratory, the MOLT-3 cell line is sensitive to the compounds tested. Our results revealed that flavans **1**, **4**, and **5** not only inhibit aromatase at nanomolar levels (IC_{50} values of 40.0, 90.0 and 80.0 nM, respectively), they also have low cytotoxic activity. Therefore, they could be leads for aromatase inhibitor drugs.

Table 2 Inhibition of aromatase by flavans **1–8**

Compound	Inhibition of aromatase IC_{50} (nM), mean ± s.d. ($n = 3$)
1	40.0 ± 20.0
2	1010 ± 40.0
3	10 700 ± 200
4	90.0 ± 30.0
5	80.0 ± 10.0
6	150 ± 30.0
7	>12 500
8	600 ± 100
Letrozole[a]	1.1 ± 0.2

[a] The reference compound was letrozole.

Molecular docking study

As flavans **1–6** are non-steroidal inhibitors, they should inhibit aromatase *via* the competitive mechanism. We employed Autodock Vina for the molecular docking study to estimate the relative binding energies of the flavans in comparison to the natural substrates, and to give insights into how these flavans

bind to aromatase. In recent years, Autodock Vina has served as a tool to study molecular docking.[26–29] Mishra and co-workers showed that although Autodock Vina tends to overestimate the absolute binding energy, especially for low affinity binders, it still gives more accurate binding energies than other docking software.[30]

In this study, the aromatase structure was taken from the crystallographic structure 3EQM.[31] The binding energies of the flavans were compared with that of the natural substrate, androstenedione, and its C-4 hydroxyl analog, formestane, the first steroidal aromatase inhibitor clinically used.[1] We explored both flexible and rigid docking and found that, overall, the flexible docking gave binding energies in better agreement with the experimental aromatase inhibitory activity than the rigid docking (ESI, Table S2†). Thus, we focused on flexible docking, as described in the Experimental section. B3LYP/6-31G(d)-optimized structures of the aromatase inhibitors were used in the docking study. The binding energy of the androstenedione from the B3LYP optimization is -13.7 kcal mol^{-1}, only slightly higher than that of the androstenedione from the crystal structure (-14.1 kcal mol^{-1}) (ESI, Table S2†). The binding energy of the formestane (-13.4 kcal mol^{-1}) is slightly higher than that of the androstenedione. The binding positions of both androstenedione and formestane showed that the steroidal ring can fit into the binding pocket of the aromatase active site, and the C-17 carbonyl can donate a hydrogen bond to Met374 (1.9–2.0 Å) (ESI, Fig. S1†). This hydrogen bond is significant for the inhibition of aromatase activity, according to the previous study.[6] Among the aromatase inhibitors **1–6**, flavans **2** and **3** have higher binding energies (-7.3 kcal mol^{-1} and -8.0 kcal mol^{-1} respectively) than compound **6** (-8.3 kcal mol^{-1}), while the potent inhibitors **1**, **4**, and **5** have the lowest binding energy (-8.5 kcal mol^{-1}).

Flavan **1** and its 4-OMe derivative **4** inhibit aromatase at relatively the same magnitude (Table 2). The lowest energy position of the inhibitor **1** has a binding energy of -8.5 kcal mol^{-1}. The C-7 hydroxyl of **1** donates two hydrogen bonds to Met374 (2.11 Å) and Arg115 (2.58 Å) (Fig. 4A), whereas the C-4 hydroxyl and the C-8 aldehyde do not play a role in forming hydrogen bonds. Thus, the substitution of the C-4 hydroxyl in **1** by a methoxyl in **4** has no effect on the lowest energy position (Fig. 4B). The C-7 hydroxyl of **4** donates a weaker hydrogen bond to Met374 (2.48 Å), and donates a stronger hydrogen bond to Arg115 (2.22 Å) (Fig. 4). Therefore, the binding energy of **4** is the same as that of **1** (-8.5 kcal mol^{-1}). The IC_{50} values of **1** (40.0 nM) and **4** (90.0 nM) are in the same order of magnitude, which is in agreement with the same calculated binding energy.

Flavan **5** exhibits more potent aromatase inhibitory activity than its 4-OMe derivative **6** (Table 1). Although a C-6 methine proton of **1** is substituted by a larger methyl group in **5**, the inhibitor **5** can still fit into the binding pocket with the same binding position as **1** and **4**. Although the two hydrogen bonds of the C-7 hydroxyl of **5** with Met374 (2.34 Å) and Arg115 (2.64 Å) are relatively weaker than those of **1** and **4** (Fig. 5A), a C-4 hydroxyl of **5** can accept a weak hydrogen bond from Ser478 (2.80 Å). Therefore, the binding energy of **5** is as low as those of **1** and **4** (-8.5 kcal mol^{-1}), corresponding to an IC_{50} value in the same range (80.0 nM). The inhibitor **6** has a methoxyl substituted in place of the C-4 hydroxyl of **5**. The lowest energy position also has the C-7 hydroxyl of **6** donating two hydrogen bonds to Met374 (2.32 Å) and Arg115 (2.57 Å) (Fig. 5B). Unlike the inhibitor **5**, the C-4 methoxyl of **6** can not accept a hydrogen bond from Ser478. Thus, the binding energy of **6** is slightly higher than that of **5** (-8.3 kcal mol^{-1}), and the IC_{50} value of **6** (150 nM) is slightly higher than that of **5** (80.0 nM).

Compound **2** has a methoxyl group substituted in place of the C-7 hydroxyl group of **5**. The lowest energy position has the C-4 methoxyl of **2** donating a hydrogen bond to Thr310 (1.83 Å) (ESI, Fig. S2A†). Compound **3**, with a methyl group substituted in place of the C-8 aldehyde of **2**, has a similar binding position to that of **2** (Fig. S2B†). The C-4 methoxyl of **3** also donates a hydrogen bond to Thr310 (2.26 Å) (Fig. S2B†). Compared to the inhibitors **1**, **4**, **5** and **6**, with the presence of both the C-6 methyl and the C-7 methoxyl groups, the fused ring of **2** and **3** can not fit into the binding pocket of Arg115, Met374 and Leu477. Thus, hydrogen bonds between the C-7 methoxyl and Met374 and Arg115 are not established. Correspondingly, the binding energies of **2** (-7.3 kcal mol^{-1}) and **3** (-8.0 kcal mol^{-1}) are higher than those of the inhibitors **1**, **4**, **5** and **6** which have better aromatase inhibitory activity.

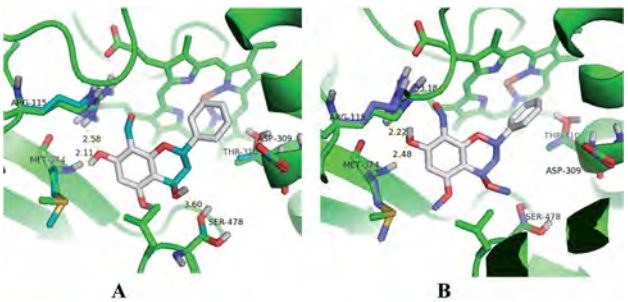

Fig. 4 Lowest energy positions of the aromatase inhibitors **1** (A) and **4** (B), within the aromatase binding site. The crystal structure is in bright green. The flexible residues are Met374, Arg115, Thr310, Ser478 and Asp309. Due to the flexible docking, some atoms change from their starting positions (shown in cyan and in purple). The ligand structures were optimized by B3LYP/6-31G(d).

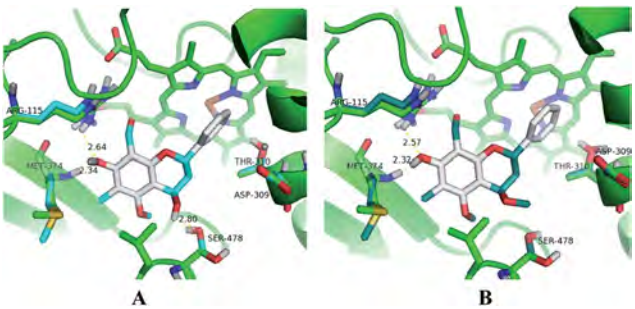

Fig. 5 Lowest energy positions of the aromatase inhibitors **5** (A) and **6** (B), within the aromatase binding site. The crystal structure is in bright green. The flexible residues are Met374, Arg115, Thr310, Ser478 and Asp309. Due to the flexible docking, some atoms change from their starting positions (shown in light cyan and in bright cyan). The ligand structures were optimized by B3LYP/6-31G(d).

The key features for flavan-based aromatase inhibitors to show inhibitory activity are (i) the ability to fit the fused ring into the binding pocket of Arg115, Met374 and Leu477, and (ii) the presence of a hydrogen bond donating group (*i.e.*, hydroxyl or methoxyl) at the C-7 to establish strong hydrogen bonds with Met374 and Arg115.

Conclusions

Flavans from the roots of *D. cochinchinensis* were found to be potent aromatase inhibitors. These inhibitors were inactive or showed only weak cytotoxic activity, and they could therefore be leads for the development of anti-aromatase drugs. Molecular docking studies revealed that these flavans have the ability to bind with aromatase in the pocket of Arg115, Met374 and Leu477, and that the C-7 hydroxyl (or methoxyl) has hydrogen bonds with Met374 and Arg115 of aromatase, enhancing the inhibitory activity.

Experimental section

Plant material

Roots of *D. cochinchinensis* were collected from Tai Rom Yen National Park, Surat Thani Province, Thailand (October 2008). The plant was identified by P. Charoenchai, and a specimen (no. CRI 526) was deposited at the Laboratory of Natural Products, Chulabhorn Research Institute, Thailand.

Extraction and isolation

The powder of the air-dried roots of *D. cochinchinensis* was extracted with CH_2Cl_2 three times at room temperature to give a crude extract (4 g). The extract was fractionated by Sephadex LH-20 column chromatography (CC) and eluted with CH_2Cl_2–MeOH (50 : 50), to provide thirteen fractions (A1 to A13). Fraction A5 was further subjected to Sephadex LH-20 CC and eluted with MeOH, to provide nine fractions (B1 to B9). Fraction B4 was then subjected to silica gel CC, and eluted with hexane with increasing proportions of EtOAc, then with EtOAc with increasing proportions of MeOH, and finally with MeOH, to provide eleven fractions (C1–C11). Fraction C4 was compound **5** (415 mg). Fraction C1 was separated by preparative C_{18} reversed phase HPLC and eluted with MeOH–H_2O (78 : 22, flow rate of 10 mL min^{-1}), to give **7** (19 mg). Fraction C2 was further separated by preparative TLC, developed with hexane–EtOAc (94 : 6), followed by C_{18} reversed phase HPLC (MeOH–H_2O (80 : 20), flow rate of 10 mL min^{-1}), to give **6** (32 mg). Fraction C3 was separated by C_{18} reversed phase HPLC (MeOH–H_2O (70 : 30), flow rate of 8 mL min^{-1}), providing compounds **3** (6 mg) and **4** (42 mg). Fraction C5 was separated by C_{18} reversed phase HPLC and eluted with MeOH–H_2O (70 : 30, flow rate of 10 mL min^{-1}), to give compounds **1** (113 mg) and **2** (42 mg). Fraction B5 was purified by C_{18} reversed phase HPLC (MeOH–H_2O (75 : 25), flow rate of 10 mL min^{-1}), to give compounds **8** (7 mg) and **2** (4 mg).

5-Methoxy-8-formyl-4,7-dihydroxyflavan (1)

Colourless oil; $[\alpha]_D^{26}$ −62.8 (*c* 0.78, $CHCl_3$); UV (MeOH) λ_{max} (log ε) 215 (4.38), 228 (4.20), 294 (4.24) nm; CD (MeOH, *c* 113.3 μM) λ nm ($\Delta\varepsilon$) 227 (+3.46), 322 (−3.58); IR (UATR) ν_{max} 3435, 2926, 1630, 1440, 1366, 1331, 1286, 1232, 1204, 1149, 1114, 1047, 907, 874, 839, 812, 760, 700 cm^{-1}; ^1H and ^{13}C NMR data see Table 1; APCI-TOF MS *m*/*z* 301.1083 $[M + H]^+$ (calcd for $C_{17}H_{17}O_5$, 301.1070).

5,7-Dimethoxy-8-formyl-4-hydroxy-6-methylflavan (2)

Yellow solids, mp 115–116 °C; $[\alpha]_D^{26}$ −64.70 (*c* 1.99, $CHCl_3$); UV (MeOH) λ_{max} (log ε) 208 (3.55), 272 (3.05), 327 (2.70) nm; CD (MeOH, *c* 97.6 μM) λ nm ($\Delta\varepsilon$) 232 (+6.64), 268 (−3.91), 316 (−3.15), 352 (−3.32); IR (UATR) ν_{max} 3450, 2938, 1684, 1580, 1455, 1430, 1305, 1192, 1133, 1115, 1053, 981, 875, 753, 700 cm^{-1}; ^1H and ^{13}C NMR data see Table 1; APCI-TOF MS *m*/*z* 329.1388 $[M + H]^+$ (calcd for $C_{19}H_{21}O_5$, 329.1383).

5,7-Dimethoxy-4-hydroxy-6,8-dimethylflavan (3)

Pale yellow viscous liquid; $[\alpha]_D^{26}$ −20.04 (*c* 0.31, $CHCl_3$); IR (UATR) ν_{max} 3421, 2923, 1599, 1455, 1433, 1375, 1191, 1127, 1105, 1053, 994, 875, 754, 698 cm^{-1}; ^1H and ^{13}C NMR data see Table 1; APCI-TOF MS *m*/*z* 314.1503 $[M]^+$ (calcd for $C_{19}H_{22}O_4$, 314.1513).

4,5-Dimethoxy-8-formyl-7-hydroxyflavan (4)

Colourless solids, mp 108–109 °C; $[\alpha]_D^{26}$ −78.66 (*c* 1.02, $CHCl_3$); UV (MeOH) λ_{max} (log ε) 212 (3.40), 228 (3.23), 293 (3.21) nm; CD (MeOH, *c* 63.7 μM) λ nm ($\Delta\varepsilon$) 205 (+5.75), 224 (+3.23), 236 (+2.6), 262 (−0.41), 325 (−3.20); IR (UATR) ν_{max} 2927, 1630, 1439, 1366, 1349, 1329, 1286, 1230, 1203, 1150, 1112, 1076, 1022, 957, 898, 797, 757, 699 cm^{-1}; ^1H and ^{13}C NMR data see Table 1; APCI-TOF MS *m*/*z* 315.1232 $[M + H]^+$ (calcd for $C_{18}H_{19}O_5$, 315.1227).

5-Methoxy-8-formyl-4,7-dihydroxy-6-methylflavan (5)

$[\alpha]_D^{26}$ −80.45 (*c* 0.99, $CHCl_3$); CD (MeOH, *c* 104.2 μM) λ nm ($\Delta\varepsilon$) 227 (+2.66), 307 (−0.52), 344 (−1.83).

Preparation of flavanones 1a, 2a, and 5a

A solution of each flavanonol (**1**, **2**, and **5**; 1 equiv.) and DMP (2 equiv.) in dry CH_2Cl_2 was stirred at room temperature for 1 h. The reaction mixture was evaporated and purified using preparative TLC to give flavanones **1a** (70%), **2a** (92%) and **5a** (49%).

5-Methoxy-7-hydroxy-8-formylflavanone (1a)

CD (MeOH, *c* 54.5 μM) λ nm ($\Delta\varepsilon$) 214 (+9.69), 269 (−7.27), 344 (+0.81); ^1H NMR (300 MHz, $CDCl_3$) δ_H 12.92 (1H, s, 7-OH), 10.15 (1H, s, 8-CHO), 7.45 (5H, br s, C-ring), 6.10 (1H, s, H-6), 5.56 (1H, dd, J = 13.0 Hz, 3.2 Hz, H-2), 3.98 (3H, s, 5-OMe), 3.08 (1H, dd, J = 16.6 Hz, 13.0 Hz, H-3a), 2.89 (1H, dd, J = 16.6 Hz, 3.2 Hz, H-3b); APCI-TOF MS *m*/*z* 299.0916 $[M + H]^+$ (calcd for $C_{17}H_{15}O_5$, 299.0914).

5-Methoxy-6-methyl-7-methoxy-8-formylflavanone (2a)

CD (MeOH, *c* 110.4 μM) λ nm ($\Delta\varepsilon$) 319 (−4.27), 353 (+2.86). ^1H NMR (300 MHz, $CDCl_3$) δ_H 10.42 (1H, s, 8-CHO), 7.51–7.39 (5H,

m, C-ring), 5.56 (1H, dd, J = 12.4 Hz, 3.5 Hz, H-2), 3.92 (3H, s, 5-OMe), 3.89 (3H, s, 7-OMe), 3.07 (1H, dd, J = 17.0 Hz, 12.4 Hz, H-3a), 2.96 (1H, dd, J = 17.0 Hz, 3.5 Hz, H-3b), 2.15 (3H, s, 6-Me); APCI-TOF MS m/z 327.1229 $[M + H]^+$ (calcd for $C_{19}H_{19}O_5$, 327.1227).

7-Hydroxy-5-methoxy-6-methyl-8-formylflavanone (5a)

CD (MeOH, c 96.2 μM) λ nm ($\Delta\varepsilon$) 279 (−0.81), 354 (+1.21). ^{1}H NMR (400 MHz, $CDCl_3$) of **5a** was identical to that of the desmosflavanone II;[32] δ_H 12.99 (1H, s, 7-OH), 10.24 (1H, s, 8-CHO), 7.47–7.41 (5H, m, C-ring), 5.55 (1H, dd, J = 13.1 Hz, 3.1 Hz, H-2), 3.91 (3H, s, 5-OMe), 3.06 (1H, dd, J = 17.0 Hz, 13.1 Hz, H-3a), 2.88 (1H, dd, J = 17.0 Hz, 3.1 Hz, H-3b), 2.09 (3H, s, 6-Me); APCI-TOF MS m/z 313.1072 $[M + H]^+$ (calcd for $C_{18}H_{17}O_5$, 313.1071).

Methylation of flavanone 5a

Flavanone **5a** (14.6 mg) and K_2CO_3 (30 mg) was dissolved in 1 mL of acetone, and then 1 mL of MeI was added. The reaction mixture was refluxed for 24 h. The reaction mixture was purified by preparative TLC, developed with 20% acetone in hexane, to provide flavanone **2a** (14 mg, 92%). The ^{1}H NMR and CD spectra of the obtained flavanone were identical to those of flavanone **2a** which was prepared from **2**.

Assays for biological activities

The inhibition of aromatase was evaluated using the method reported by Stresser and co-workers.[33] The reference compound was letrozole (Table 2). The cytotoxicity for adhesive cell lines, including the HuCCA-1, HepG2, and A549 cancer cell lines, was evaluated with the MTT assay,[34,35] while the cytotoxicity for the non-adhesive MOLT-3 cell line was assessed using the XTT assay.[36] Doxorubicin and etoposide were used as the reference drugs; doxorubicin exhibited cytotoxic activity against HuCCA-1 and A549 cells with IC_{50} values of 1.10 and 0.90 μM, respectively, while etoposide displayed respective IC_{50} values of 22.11 and 0.03 μM towards the HepG2 and MOLT-3 cell lines (ESI, Table S1†).

Molecular docking calculation

The X-ray crystal structure of human aromatase was taken from the PDB (code 3EQM.pdb).[31] All of the water and phosphate molecules were removed from the crystal structure. Hydrogen atoms were added by AutoDock Tools.[37] To prepare for the docking study, a molecule of androstenedione was removed from the crystal structure. The inhibitor structures were optimized with the Gaussian09 program.[38] All of the structures were fully optimized with the default convergence criteria, and frequencies were calculated to ensure that there was no imaginary frequency for the minima. The B3LYP[39–41] density functional and 6-31G(d)[42–44] basis set were used for all of the ligand geometry optimizations and frequency calculations. The docking calculations were performed by AutoDock Vina.[45] The inhibitors were docked to the binding site of aromatase. Rigid and flexible dockings were performed. Rigid docking has a rigid receptor and only the rotational torsion angles of the ligands can freely rotate. Within 10 Å around the C-9 of androstenedione, there are five residues which contain hydrogen bond donors and acceptors, Met374, Arg115, Thr310, Ser478 and Asp309. For flexible docking, all of the rotatable torsion angles of these side chain residues were allowed to freely rotate. A grid box size of 25 × 25 × 25 Å was used. The grid was centered at the position of C-9 of androstenedione, at x, y, z coordinates of 86.174, 53.912, 45.811. PyMol[46] was used for the graphical presentation of the data.

Acknowledgements

P. K. is supported by The Thailand Research Fund and the Center of Excellence on Environmental Health and Toxicology, Science & Technology Postgraduate Education and Research Development Office (PERDO), Ministry of Education. P. S. is financially supported by the Thailand Research Fund (Grant No. MRG5580117), Development and Promotion of Science and Technology Talents Project (DPST), the Center of Excellence for Innovation in Chemistry (PERCH-CIC), Office of the Higher Education Commission, Ministry of Education, and by the Faculty of Science, Mahidol University. We thank Chulabhorn Research Centre, Institute of Molecular Biosciences, Mahidol University, for partial financial support for this project. We thank S. Sitthimonchai for the aromatase inhibition assay, and P. Intachote, S. Sengsai, and B. Saimanee for the cytotoxicity testing.

References

1 R. Siegel, D. Naishadham and A. Jemal, *Ca-Cancer J. Clin.*, 2013, **63**, 11–30.
2 J. Ferlay, E. Steliarova-Foucher, J. Lortet-Tieulent, S. Rosso, J. W. Coebergh, H. Comber, D. Forman and F. Bray, *Eur. J. Cancer*, 2013, **49**, 1374–1403.
3 J. M. Grodin, P. K. Siiteri and P. C. MacDonald, *J. Clin. Endocrinol. Metab.*, 1973, **36**, 207–214.
4 J. S. O'Neill, R. A. Elton and W. R. Miller, *Br. Med. J.*, 1988, **296**, 741–743.
5 D. Ghosh, J. Lo, D. Morton, D. Valette, J. Xi, J. Griswold, S. Hubbell, C. Egbuta, W. Jiang, J. An and H. M. Davies, *J. Med. Chem.*, 2012, **55**, 8464–8476.
6 C. Varela, E. J. Tavares da Silva, C. Amaral, G. Correia da Silva, T. Baptista, S. Alcaro, G. Costa, R. A. Carvalho, N. A. Teixeira and F. M. Roleira, *J. Med. Chem.*, 2012, **55**, 3992–4002.
7 F. Stauffer, P. Furet, A. Floersheimer and M. Lang, *Bioorg. Med. Chem. Lett.*, 2012, **22**, 1860–1863.
8 J. McNulty, J. J. Nair, N. Vurgun, B. R. Difrancesco, C. E. Brown, B. Tsoi, D. J. Crankshaw and A. C. Holloway, *Bioorg. Med. Chem. Lett.*, 2012, **22**, 718–722.
9 S. Gobbi, C. Zimmer, F. Belluti, A. Rampa, R. W. Hartmann, M. Recanatini and A. Bisi, *J. Med. Chem.*, 2010, **53**, 5347–5351.
10 M. Jiang, J. Yang, C. Zhang, B. Liu, K. Chan, H. Cao and A. Lu, *Planta Med.*, 2010, **76**, 2048–2064.

11 D. J. Newman and G. M. Cragg, *J. Nat. Prod.*, 2012, **75**, 311–335.
12 A. D. Kinghorn, L. Pan, J. N. Fletcher and H. Chai, *J. Nat. Prod.*, 2011, **74**, 1539–1555.
13 M. J. Balunas and A. D. Kinghorn, *Planta Med.*, 2010, **76**, 1087–1093.
14 M. J. Balunas, B. Su, R. W. Brueggemeier and A. D. Kinghorn, *Anti-Cancer Agents Med. Chem.*, 2008, **8**, 646–682.
15 R. Monteiro, H. Becker, I. Azevedo and C. Calhau, *J. Agric. Food Chem.*, 2006, **54**, 2938–2943.
16 T. K. Lee, D. I. Kim, J. Y. Han and C. H. Kim, *Immunopharmacol. Immunotoxicol.*, 2004, **26**, 315–327.
17 R. Monteiro, A. Faria, I. Azevedo and C. Calhau, *J. Steroid Biochem. Mol. Biol.*, 2007, **105**, 124–130.
18 J. H. Wu, X. H. Wang, Y. H. Yi and K. H. Lee, *Bioorg. Med. Chem. Lett.*, 2003, **13**, 1813–1815.
19 S. P. Bajgai, V. Prachyawarakorn, C. Mahidol, S. Ruchirawat and P. Kittakoop, *Phytochemistry*, 2011, **72**, 2062–2067.
20 S. X. Liao, G. Y. Han, Y. R. Zhang, Q. T. Zheng and C. H. He, *Acta Pharm. Sin.*, 1989, **24**, 110–113.
21 M. J. Mao, J. L. Qian and B. Jiang, *Chin. Chem. Lett.*, 2005, **16**, 1056–1058.
22 R. Mayer, *Phytochemistry*, 1990, **29**, 1340–1342.
23 L. T. Byrne, J. R. Cannon, D. H. Gawad, B. S. Joshi, B. W. Skelton, R. F. Toia and A. H. White, *Aust. J. Chem.*, 1982, **35**, 1851–1858.
24 D. Slade, D. Ferreira and J. P. Marais, *Phytochemistry*, 2005, **66**, 2177–2215.
25 E. J. Carcache-Blanco, Y. H. Kang, E. J. Park, B. N. Su, L. B. Kardono, S. Riswan, H. H. Fong, J. M. Pezzuto and A. D. Kinghorn, *J. Nat. Prod.*, 2003, **66**, 1197–1202.
26 Z. Feng, D. Chakraborty, S. B. Dewell, B. V. Reddy and S. F. Brady, *J. Am. Chem. Soc.*, 2012, **134**, 2981–2987.
27 C. Kishor, R. Gumpena, R. Reddi and A. Addlagatta, *Med. Chem. Commun.*, 2012, **3**, 1406–1412.
28 A. Somoza, M. Terrazas and R. Eritja, *Chem. Commun.*, 2010, **46**, 4270–4272.
29 J. A. Friest, Y. Maezato, S. Broussy, P. Blum and D. B. Berkowitz, *J. Am. Chem. Soc.*, 2010, **132**, 5930–5931.
30 S. K. Mishra, J. Adam, M. Wimmerová and J. Koča, *J. Chem. Inf. Model.*, 2012, **52**, 1250–1261.
31 D. Ghosh, J. Griswold, M. Erman and W. Pangborn, *Nature*, 2009, **457**, 219–223.
32 J. H. Wu, S. X. Liao, S. L. Mao, H. Q. Liang, Y. L. Wang and Z. W. Su, *J. Chin. Pharm. Sci.*, 1997, **6**, 119–120.
33 D. M. Stresser, S. D. Turner, J. McNamara, P. Stocker, V. P. Miller, C. L. Crespi and C. J. Patten, *Anal. Biochem.*, 2000, **284**, 427–430.
34 J. Carmichael, W. G. DeGraff, A. F. Gazdar, J. D. Minna and J. B. Mitchell, *Cancer Res.*, 1987, **47**, 943–946.
35 T. Mosmann, *J. Immunol. Methods*, 1983, **65**, 55–63.
36 A. Doyle and J. B. Griffiths, *Mammalian cell culture: essential techniques*, John Wiley & Sons, Chichester, UK, 1997.
37 G. M. Morris, R. Huey and A. J. Olson, *Current Protocols in Bioinformatics*, John Wiley & Sons, Inc., 2002.
38 M. J. Frisch, G. W. Trucks, H. B. Schlegel, G. E. Scuseria, M. A. Robb, J. R. Cheeseman, J. J. A. Montgomery, T. Vreven, K. N. Kudin, J. C. Burant, J. M. Millam, S. S. Iyengar, J. Tomasi, V. Barone, B. Mennucci, M. Cossi, G. Scalmani, N. Rega, G. A. Petersson, H. Nakatsuji, M. Hada, M. Ehara, K. Toyota, R. Fukuda, J. Hasegawa, M. Ishida, T. Nakajima, Y. Honda, O. Kitao, H. Nakai, M. Klene, X. Li, J. E. Knox, H. P. Hratchian, J. B. Cross, C. Adamo, J. Jaramillo, R. Gomperts, R. E. Stratmann, O. Yazyev, A. J. Austin, R. Cammi, C. Pomelli, J. W. Ochterski, P. Y. Ayala, K. Morokuma, G. A. Voth, P. Salvador, J. J. Dannenberg, V. G. Zakrzewski, S. Dapprich, A. D. Daniels, M. C. Strain, O. Farkas, D. K. Malick, A. D. Rabuck, K. Raghavachari, J. B. Foresman, J. V. Ortiz, Q. Cui, A. G. Baboul, S. Clifford, J. Cioslowski, B. B. Stefanov, G. Liu, A. Liashenko, P. Piskorz, I. Komaromi, R. L. Martin, D. J. Fox, T. Keith, M. A. Al-Laham, C. Y. Peng, A. Nanayakkara, M. Challacombe, P. M. W. Gill, B. Johnson, W. Chen, M. W. Wong, C. Gonzalez and J. A. Pople, *Gaussian 03, Revision B.4, B.5, and C.1*, Gaussian, Inc., Pittsburgh, PA, 2003.
39 A. D. Becke, *J. Chem. Phys.*, 1993, **98**, 5648–5652.
40 C. Lee, W. Yang and R. G. Parr, *Phys. Rev. B: Condens. Matter Mater. Phys.*, 1988, **37**, 785–789.
41 P. J. Stephens, F. J. Devlin, C. F. Chabalowski and M. J. Frisch, *J. Phys. Chem.*, 1994, **98**, 11623–11627.
42 P. C. Hariharan and J. A. Pople, *Theor. Chim. Acta*, 1973, **28**, 213–222.
43 G. A. Petersson and M. A. Al-Laham, *J. Chem. Phys.*, 1991, **94**, 6081–6090.
44 G. A. Petersson, A. Bennett, T. G. Tensfeldt, M. A. Al-Laham, W. A. Shirley and J. Mantzaris, *J. Chem. Phys.*, 1988, **89**, 2193–2218.
45 O. Trott and A. J. Olson, *J. Comput. Chem.*, 2010, **31**, 455–461.
46 http://pymol.org/pymol.

